Activity, Mud Migration, and Formation Mechanisms of Helgoland and Dvurechenskii Mud Volcanoes, Black Sea

Dissertation

Zur Erlangung des
Doktorgrades der Naturwissenschaften
(Dr. rer. nat.)

Im Fachbereich der Geowissenschaften
der Universität Bremen

vorgelegt von
Tingting Wu

Bremen, July 2015

Gutachter:

1. Prof. Dr. Gerhard Bohrmann

2. Prof. Dr. Tilo von Dobeneck

Table of Contents

Table of Contents

List of Abbreviations

AC	Active Center
AOM	Anaerobic Oxidation of Methane
AUV	Autonomous Underwater Vehicle
BGHSZ	Base of the GHSZ
BSR	Bottom Simulating Reflector
CIL	Cold Intermediate Layer
COF	Central Dobroea-Capidava-Ovidiu Fault
CTD	Oceanography Instrument for Conductivity, Temperature, and Depth of the Ocean
DAPC	Dynamic Autoclave Piston Corer
DGPS	Differential Global Positioning System
DMV	Dvurechenskii Mud Volcano
DSF	Down-Sag Fault
DVL	Doppler Velocity Logger
GBS	Gas Bubble Sampler
GC	Gravity Corer
GeoB	Geosciences, University of Bremen, Sample or Profile Numbers
GH	Gas Hydrate
GHSZ	Gas Hydrate Stability Zone
GIS	Geographic Information System
GPS	Global Positioning System
GUI	Graphic User Interface
HD	High Definition
HMMV	Håkon Mosby Mud Volcano
HMV	Helgoland Mud Volcano
I.S.E.	International Submarine Engineering
IC	Inner Crest
IM	Inner Moat
LAN	Local Area Network
M	The German Research Vessel: *R/V* METEOR
MARUM	Zentrum für MARine UMweltwissenschaften
MBES	Multibeam Echosounder
mbsf	Meters below sea-floor
mbsl	Meters below sea-level
MIC	Minicorer
MPW	Mission Planning Workstation
MSM	The German Research Vessel: *R/V* MARIA S. MERIAN
MTL	Miniature Temperature Logger
MV	Mud Volcano
OC	Outer Crest
OM	Outer Moat
OS	Operating System

PC	Personal Computer
PCC	Payload Control Computer
PCF	Pechenega-Camena Fault
PHF	Primary High Frequency (of single beam echosounder)
PHINS	An Inertial Navigation System
PTconditions	Pressure and Temperature Conditions
QNX	Unix-like Real-time Operating System
RF	Radio Frequency
ROV	Remotely Operated Vehicle
SCC	Surface Control Computer
SLF	Secondary Low Frequency (of single beam echosounder)
SVP	Sound Velocity Profile
TTR	Training Through Research
USBL	Ultra-Short Base Line
VCC	Vehicle Control Computer

Abstract

Submarine mud volcanoes are positive and/or negative geological seafloor structures from which mud and fluid (water, brine, gas, and oil) flow or erupt. The source of these expulsions can be traced to several kilometers below the seafloor, thus this material provides important information about regional tectonics and geology, and the presence of potential hydrocarbon reservoirs. Although mud volcanoes occur globally, there is still insufficient knowledge concerning their numbers, distribution, development and activity. Their significance as contributors to slope instability, the global methane flux and carbon cycle and thus to climate change, is also unclear.

With the development and advancement in marine hydro-acoustic instrumentation, submarine mud volcanoes therefore became a focal point of deep-sea research during the past four decades. However, the research was constraint by the technical limitation of the traditional ship-mounted and towed acoustic devices, which could not satisfy the demand for high resolution mapping. As a result, a state-of-the-art, near-to-seafloor, Autonomous Underwater Vehicle (AUV) and Remotely Operated Vehicle (ROV) were developed to provide high resolution micro-bathymetry maps, backscatter maps and, high definition (HD) seafloor imaging.

One of the main motivations of this study was therefore, to use these new near-to-seafloor remotely-operated instruments to obtain detailed information on the morphology, sedimentology and gas emissions of two neighboring mud volcanoes; the Dvurechenskii Mud Volcano (DMV) and the Helgoland Mud Volcano (HMV) located in the Sorokin Trough, northern Black Sea at water depths of >2,000 mbsl. The resulting deep marine data sets include high resolution micro-bathymetry and backscatter data of the mud volcanoes and the surrounding seafloor, sediment and water column temperatures, sediment samples, and *in-situ* HD-photographic imaging. This allowed us to obtain new insights into the factors controlling mud volcanoes I) formation and development, II) activity, including horizontal and vertical mud migration processes, III) the inter-relationship of neighboring diapir- and fault-formed mud volcanoes and, IV) mud volcano gas emissions.

First study concentrates on the HMV. The micro-bathymetric map obtained from the AUV shows that, the HMV is a double-ringed seafloor structure consisting of two depressions (Inner Moat and Outer Moat), two positive reliefs (Inner Crest and Outer

Crest) and one Active Center. Elevated water temperature anomalies indicate that additional heat is brought up to the surface through the upward migration of mud from a deep sub-surface source (diapir) via the central conduit. A NW-SE aligned fault across the HMV that correlates with the high water temperature anomalies, as seen in the micro-bathymetric and high resolution side-scan sonar maps, suggest that the HMV's activity might also be fault controlled which could result in more violent eruption. The data indicates that the HMV has experience at least two phases of mud eruptions, accompanied by gravity-driven sediment movement from the northwest. A circular depression is found around the northern part of the HMV, seen in the micro-bathymetric and backscatter maps and some faults or fractures are shown on the sub-bottom profiles. They all indicate a circular shaped fault around the mud volcano which is interpreted to be related to down-sag tectonics. Gas emissions from the Active Center, observed both indirectly from the hydro-acoustic parasound system and, directly from the camera mounted on the ROV, were seen to migrate ≥800 m in the water column. This methane, then dissolves and oxidizes very fast without its hydrate skin (outside the Gas Hydrate Stability Zone) therefore it is potentially impossible that it reaches the sea surface. We infer that the methane emitted from the HMV would thus not effect atmospheric methane concentration and as a consequence, have very limited impact on climate change.

The second study concentrates on morphological signatures and processes for mud movement of the DMV and addresses its time of formation. Evaluations of the vertical and horizontal mudflow, mud temperatures and velocities are made. The data shows distribution variations in the DMV's mud temperature gradients which range from 0.336 - 0.468°C/m on the margins and 5.884°C/m in the center. High temperature anomalies of up to 23°C at 75 mbsf in the center of the DMV plateau were also observed together with ubiquitous concentric ridges that radiate out from the summit. These findings might be the internal and surficial manifestation for cyclic mud eruption processes. This also suggests that the DMV is experiencing a relatively active period. Vertical and horizontal mud flow velocities of 0.22 m/day and 0.19 - 0.22 m/day, respectively, could be inferred from either real *in-situ* data (sediment temperature profiles) recorded with a gravity core mounted T-mooring (long-term temperature measurement instrument) and/or theoretical models (a Radial Model and a Contour-based Model). Based on a simplified model that utilizes the estimated vertical and horizontal velocities it was feasible to approximate the time of the DMV's formation. Estimates suggest that the DMV is ≃22 - 26 yrs old. However, these age

estimates may be erroneous due to some factors not integrated into the model e.g. mud consolidation, cyclic mud eruptions and seafloor erosion via deep water currents. These state-of-the-art data acquisition methods have therefore provided information on the DMV's mud migration characteristics and allowed for an evaluation of vertical and horizontal mud flow patterns and velocities and thus helped improve our understanding of MV activity and evolution.

In the third study we evaluate the fault-induced inter-relationship of neighboring diapir-formed mud volcanoes (the DMV and HMV). Through the analyses of the micro-bathymetric and backscatter data it was possible to build I) a geological evolution model for the DMV and II) a fault-induced inter-relationship model for the DMV and HMV. The main findings verify the presence of down-sag faults for both mud volcanoes. The fault-induced inter-relationship was confirmed by surficial evidence for the presence of ≃north-south orientated normal faults across both the DMV and HMV. These faults are the surficial corroboration of down-sag faults emanating from the neighboring mud volcano i.e. from the HMV and DMV, respectively. The affirmation that gas flare release sites occur in the vicinity of faults, through the margin-active gas flare, could support the theory that the activity of gas and mud expulsion migrates to be released from the margin of mud volcanoes when overburden pressure in the central areas stops gas and fluid discharge.

In summary, the state-of-the-art, near-to-seafloor, Autonomous Underwater Vehicle (AUV) and Remotely Operated Vehicle (ROV) can provide detailed information on deep sea submarine mud volcanoes and satisfy our research demands. Thanks to this data, the studies on the two neighboring mud volcanoes has allowed us to obtain new insights into the morphology of mud volcanoes and the factors controlling I) their formation and development, such as normal and down-sag faults II) their activity, including horizontal and vertical mudflow temperatures and migration processes, III) the inter-relationship of neighboring diapir- and fault-formed mud volcanoes and, IV) mud volcano gas emissions. In addition, the inter-relationship model between these two neighboring mud volcanoes, suggests and provides us with a new perspective to look at the formation of mud volcanoes.

Chapter 1 Introduction

1.1 Introduction to Mud Volcanoes

1.1.1 Definition

Mud volcanoes are geological structures formed by a combination of mud eruption, gas emission, and water seepage from the subsurface at both the earth's terrestrial surface and the seafloor (Fig. 1-1)(Milkov, 2000; Dimitrov, 2002; Kopf, 2002). Water, gas, and fine-grained muddy sediment in semi-liquid form are forced by tectonic compressions to migrate up through fissures or narrow openings in the crust and produce an outflowing mass of mud on the earth's surface (Dimitrov, 2003).

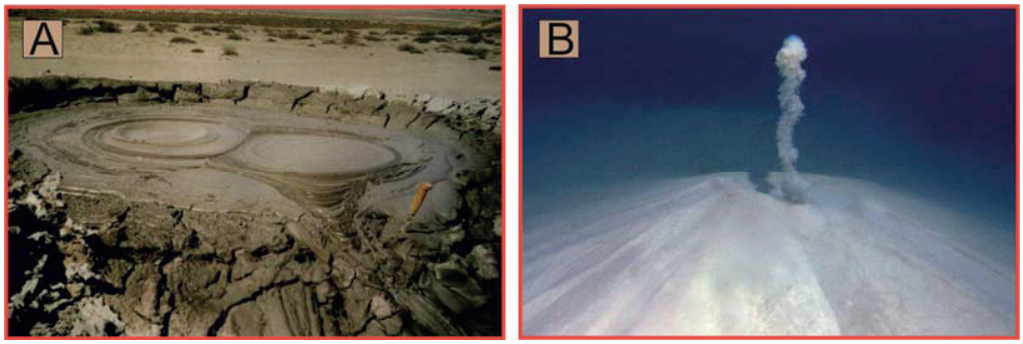

Figure 1-1: Photos of terrestrial and submarine mud volcanoes. A: Terrestrial mud volcano cone in Azerbaijan (Hovland et al., 1997). B: Submarine mud volcano in the Gulf of Mexico taken with a ROV (http://flowergarden.noaa.gov/image_library/volcanoimages.html).

1.1.2 History and Technical Development

Terrestrial mud volcanoes have a long research history due to their wide distribution and accessibility. Mud volcanoes have therefore attracted the attention of geoscientists for centuries. Scientific reports date back to the early 17th century, but people have known about them and described them for even longer, e.g. Pliny in his *NaturalisHistoria* (77 AD). Up till the start of the 21 century, mud volcanoes where only known to exist on land and in very shallow water. Furthermore, they were thought to only have a limited global distribution (Yakubov et al., 1971; Ali-Zade et al., 1984). By 2002, ≃800 mud volcanoes were known to exist worldwide (Dimitrov,

2002).

Higgins and Saunders were the first to systematically examine the abundance of mud volcanoes on a broad scale (Higgins and Saunders, 1974). Their work primarily concentrated on terrestrial mud volcanoes and research on the relationships between mud volcanism, hydrocarbons, and regional tectonics using industry drill-hole data. The formation mechanism and the important role of mud volcanoes for petroleum prospecting are the main research focus today (Hedberg, 1974; Barber et al., 1986; Rhakmanov, 1987).

Since the 1970s, numerous submarine mud volcanoes have been discovered at water depths of 500 to 5,000 meters in areas of the Black Sea, the Mediterranean Ridge, the Gulf of Cadiz, the Barbados Accretionary Wedge, and other submarine locations around the globe (Dimitrov, 2002). This progress in marine mud volcano research is due to the wide use of new, advanced equipment for underwater research, such as seismic exploration, seafloor imagery, side-scan sonar, and the increased accuracy of the positioning of bottom samplers (Milkov, 2000). Using this geophysical data and *in-situ* samples, researchers can further understand mud volcanoes, including their mechanics, driving forces, and the evolution of their features (Barber et al., 1986; Brown, 1990), as well as their activity, emission products, and the geohazards that may result from their activity (Robertson, 1996; Kopf, 1999). As a result of extensive exploration of the deep ocean, the total number of known submarine mud volcanoes is increasing every year (Milkov, 2000; Holland et al., 2003; Martinelli and Panahi, 2006).

Although comprehensive studies of submarine mud volcanoes have been made using newly advanced equipment in recent decades, the full imaging or recording of submarine mud volcano activity is still difficult. Most of the time, the features of the mud volcano are identified by a combination of geophysical and geological methods. Two criteria have been proposed for identifying submarine mud volcanoes: I) recovered sediment and II) local topographic morphology (Milkov, 2000). The mud breccias that have erupted from mud volcanoes should contain a range of different sediments in terms of for example, age, composition and structure. Moreover, the *in-situ* morphology can be identified using side-scan sonar records and seismic sections, in addition to underwater photographic and video surveys (Milkov, 2000). Although the two criteria are sometimes not so dependable (they may be confused with volcanic

structures), evidence for submarine mud volcanoes is still summarized by Milkov (2000) as follows:

1. Sub-circular structures from tens to several kilometers in diameter that are elevated above or below the surrounding seafloor and which can be identified on the bathymetric map.

2. Fluid expulsion or gas emission observed on hydro-acoustic profiles (PARASOUND), or recorded by underwater video cameras.

3. Higher backscatter than for surrounding areas on a side-scan sonar map.

4. Visible diapir structure in the subsurface seismic profiles.

5. Mud breccias from various formations of the sedimentary piles can be recovered from the sediment sampling.

6. Gas hydrate is recovered by sediment-sampling the core.

1.1.3 Classification

1.1.3.1 Size and Shape

Mud volcanoes vary in size, from a few meters to several hundreds of meters in height, and from several meters up to tens of kilometers in diameter. The geometry of their seafloor expression is also variable. The extruded material, which is called mud breccias (water, gas, oil, and mud), can originate from several kilometers' depth and form different shapes (Kopf, 2002). Many mud volcanoes have a cone shape, forming as conically shaped mountains or hills (Dimitrov, 2002). Other shapes, such as flat-topped cones, domes or mushroom-like shapes, depressions, or calderas, have also been discovered (Bohrmann et al., 2003; Somoza et al., 2003). On land, some large and complex mud volcanoes often contain both active and inactive smaller volcano structures such as clusters of cones and elevated pools (Hovland et al., 1997). Although many factors can affect the shape and size of a mud volcano, there are still some basic simple rules that we can use (Dimitrov, 2002): "The higher the pore-fluid pressure, the more violent the eruption; the more frequent the activity, the larger the structure; the lower the viscosity, the larger and flatter the body."

1.1.3.2 Frequency of Mud Volcano Activity

The activity of mud volcanoes represents regular, distinct cyclic changes, including catastrophic events with strong mud eruptions and gas emissions, and relative quiescent periods, which are characterized by moderate activity. The frequency of mud volcano activity can range from weeks to tens of years, and this is controlled by more than one external agent, which influences the local pressure regime within the mud volcanoes themselves (Deville and Guerlais, 2009).

Before the 1970s, statistics about mud volcano activity were only available for a very limited number of areas, such as Panama, Trinidad (Ridd, 1970), southern Sakhalin Island (Sirik, 1968), and the Kerch and Taman Peninsulas (Gubkin and Feodorov, 1940). The most complete and long-term observations were carried out at the Azerbaijan mud volcanoes (Yakubov et al., 1971; Ali-Zade et al., 1984). Between 1840 and 1967, 122 eruptions occurred at 32 mud volcanoes in the eastern Azerbaijan region. The average time periods for the eruptions of mud volcanoes were from about 6 to 12 and 25 to 26 years (Yakubov et al., 1971). The real frequency of eruptions however, varies from less than one year to more than 65 years. Between 1810 and 2001, 287 eruptions of 76 (from a total of about 300) mud volcanoes onshore and offshore in Azerbaijan were documented (Guliyev et al., 1996). Thus, without the remote and short-term eruptions, as mentioned by Bagirov et al. (1996), the average frequency of recorded mud volcano eruptions in Azerbaijan is 1.51/yr. It has been estimated that approximately 60 - 65 eruptions have occurred worldwide each year, spread across a total of about 1,950 mud volcanoes (Dimitrov, 2003). Comparing the number of terrestrial mud volcanoes with the number of offshore ones, between 34 - 37 eruptions occur on land and in adjacent shallow waters, while the remainders take place in deep-sea regions (Dimitrov, 2003).

Researchers have used astronomical cycles to explain the frequency of the relatively steady mud volcano activity (Huseynov and Guliyev, 2004). This relationship was made because astronomical cycles, such as the orbital forces, affect temperature and pressure conditions (PTconditions) in the atmosphere and hydrosphere, as well as PTconditions in the sediment. From a study of mud volcanism in the South Caspian Basin Huseynov and Guliyev (2004) inferred that approximately 60% of all eruptions take place during either new or full moons. Moreover, Graue (2000) suggested a relationship between the cycle of the sun's activity (11 years) and the frequency of

mud volcano eruptions. Other geological tectonic mechanisms, such as faults, earthquakes, and tectonic compression, have been used to explain rather frequent, more irregular eruptions of mud volcanoes (Tinivella and Giustiniani, 2012).

1.1.3.3 Types of Mud Volcanoes

Based on the variable morphological expression and the active characteristics of mud volcanoes, Kalinko (1964) grouped them in three main types:

I class—Lokbatan type

This type of mud volcano has a strong, explosive character, always accompanied by the ignition of the emitted gases. Activity periods are short and separated by long, passive periods. Because the extruded mud breccias are usually of low viscosity, this type of mud volcano forms the well-formed steep conical shape.

II class—Chikishlyar type

In contrast to Lokbatan volcanoes, Chikishlyar mud volcanoes are characterized by calm, relatively weak, and continuous activity. Gases are continuously released in more or less uniform quantities, and numerous vents eject small amounts of gassy mud and water. These volcanoes usually form very low, flat domes, which merge with the surrounding plane, or plate-shaped depressions that are often filled with water.

III class—Schugin type

Schugin mud volcanoes are transitional ones, sharing qualities with the other two types. Eruptive periods are intermittently replaced by periods of continuous weak activity. This type of mud volcano has the widest global distribution and is characterized by a wide variety of forms, though they typically build composite craters.

No relationship has been found between mud volcano types and their distribution. All the known mud volcano belts can contain each of these three types. The types are mainly dependent on the local lithological and tectonic framework of the host sediments (Dimitrov, 2002).

1.2 Major Terminologies

1.2.1 Edifices on Land and on the Seafloor

Mud volcanoes can be considered as topographically expressed edifices on land and on the seafloor that result from fluid mud (water, brine, gas, oil) expulsion. Although their morphology may vary significantly, two main morphological groups can be summarized: I) an internal feeder system group and II) an external edifice group (Dimitrov, 2002).

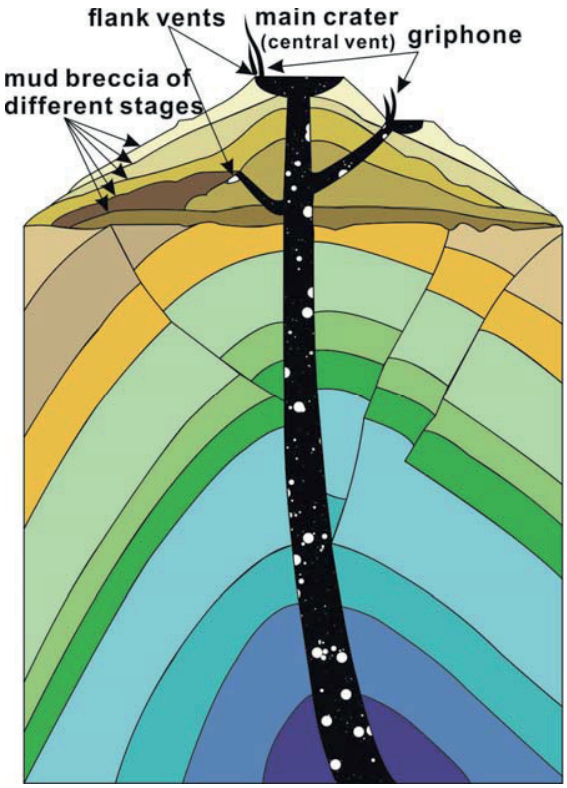

Figure 1-2: Basic structure and main elements of a conical mud volcano as initially described by Dimitrov (2002). Gryphones are small secondary vents shorter than 3 m, which may form around the craters and in many places on the mud volcano body. These commonly emit gas, mud and water are characterized by the complete absence of solid rock fragments. Modified after Tinivella and Giustiniani (2012).

For a conically shaped mud volcano, the basic structure and main elements are described in figure 1-2 (Tinivella and Giustiniani, 2012). Mud volcano breccias are usually extruded from a central funnel, which is called a *feeder channel* or *conduit*. This feeder channel or conduit may be either cylindrical, irregularly shaped, or a slit (i.e., a fracture, fault, etc.) (Kopf, 2002) and it is possible for it to split off into a smaller flank or lateral pipes on its way to the surface. When the main conduit appears at the surface, the seafloor elevation (usually the summit of a mud volcano) will form, this is known as the *crest* or *main vent*. If the crest or main vent is present as a

depression with a circular shaped rim, it is called a *caldera-type crater* or *central crater*. If the crater is filled with fluidized mud, it is termed a *mud pool*. The main conduit formed crater can also be referred to as a *pingo* or *cauldron* (Portuguese for caldera) (Kopf, 2002). Splays of the main conduit can result in small craters, known as *satellite*, *parasite*, *salses,* or *secondary craters* and are located somewhere off the center. Numerous small *secondary vents*, or *gryphons*, may form around the craters. The mud breccias extruded from the main crater or the satellite crater, will spill out and form fan-shaped or tongue-like mud flows, which may be up to several hundred meters wide and several kilometers long (Yakubov et al., 1971). The mudflows, which consist of mobilized sediments that originated from different lithologies, build up the body of the mud volcano. Slumps and slides often form in mud volcano areas (Dimitrov, 2002). When a submarine mud volcano is located within a gas hydrate stability zone, gas hydrate may form just below or at the seafloor surface.

1.2.2 Subsurface Features

In order to understand the subsurface features of a mud volcano, it is important to recognize the differences between a mud volcano and a diapir. All mud volcanoes are associated with diapirs, but not vice versa (Milkov, 2000). A diapir is a kind of structure that rises from the deep subsurface, sometimes piercing the seafloor or terrestrial surface, but sometimes not. However, mud volcanoes can be defined as floor-piercing diapirs. The feeder channel is usually on top of a diapir or originates from a diapir.

1.2.3 Geometric Constraints on the Mechanism of Eruption

A great deal of research into the relationship between the surface expression of mud volcanoes and the processes occurring within the subsurface has taken place in recent years. Studies have focused on how mechanisms control the growth and evolution of large (500 m diameter) mud volcano edifices over time (Evans et al., 2008). The shape and size of the edifices on the terrain floor or seafloor may be associated with the physical properties of the extruded mud breccias, and may also reflect the width of the conduit that facilitated the eruption (Kopf, 2002). The viscosity and consolidation of the extruded mud breccias control the shape of the edifices. Low porosity mud forms high-elevation mud domes or ridges above the seafloor, while high-porosity mud creates mud pies (Lance et al., 1998). The size of the feature is mainly controlled

by the size of the conduit and the driving force in the area around the mud volcano. Wide conduits and effective triggers at depth, tend to form large-sized features. In addition, laboratory models have shown that wide feeders yield flat mud pies, while narrow feeders create cones when using the same material (Lance et al., 1998). Steadily expulsed mud is moreover, an important factor that affects the height of a mud volcano.

1.3 Formation Mechanisms

1.3.1 Tectonic Compression and High Sedimentation Rates

Although mud volcanoes are distributed in many places both onshore and offshore with various tectonic settings, a major variety of mud volcanoes are found along tectonic compression zones, such as neat accretionary complexes and thrust and overthrust belts e.g. the Mediterranean Ridge, Nankai, Barbados, and Southern Caribbean Thrust Belts, and Banda accretionary complexes, which coincide with active plate boundaries (Dimitrov, 2002). The mud volcanoes found outside tectonic compression zones are observed in areas with high sedimentation rates such as in modern fan systems or in areas with an intensive development of diapirism. Therefore, rapid sedimentation and convergent tectonic compression are considered two of the main mechanical reasons for the formation of mud volcanoes (Milkov, 2000; Tinivella and Giustiniani, 2012). For all mud volcanoes, there should be suitable source layers of muddy sediments in the deeper part underneath the mud volcano. This source usually consists of fine-grained, soft material of low density which is covered by at least 1 - 1.5 km of thick sedimentary sequences. When the mud volcano is located at the forearc and outer orogenic basins, such thick sediment may be caused by thrusting and overthrusting (Tinivella and Giustiniani, 2012). When it suffers from compressive tectonic forces, the deep over-pressurized muds and fluids in the deep subsurface will flow through high permeability conduits, such as faults, fractures, and diapirs to earth's surface (Foucher et al., 2010). This process may also happen along passive continental margins with little tectonic compression but fluidized overpressuring and compression from the rapid sedimentation of large amounts of (argillaceous) sediments (Graue, 2000; Milkov, 2000). Furthermore, thermal and/or biogenically formed hydrocarbon gases can significantly increase under these conditions.

In 2000, Milkov reported that mud volcanoes formed by muddy or gaseous material

are either created I) on top of a seafloor-piercing diapir or, II) due to a rise of fluidized sediments along newly formed faults or fractures (see Fig. 1-3) (Hovland et al., 1997; Graue, 2000; Milkov, 2000; Dimitrov, 2002; Kopf, 2002).

To understand the two mechanisms, we should first distinguish between diapirs and mud volcanoes. Diapirs are usually dome shaped and are produced by the flow of fine-grained sediments originating from the very deep subsurface. Sometimes, they rupture the overlying rocks. When a diapir reaches the seafloor surface, it can be called a mud volcano, otherwise, when it has only risen to a depth beneath the surface of the seafloor, it cannot be called a mud volcano (Dimitrov, 2002).

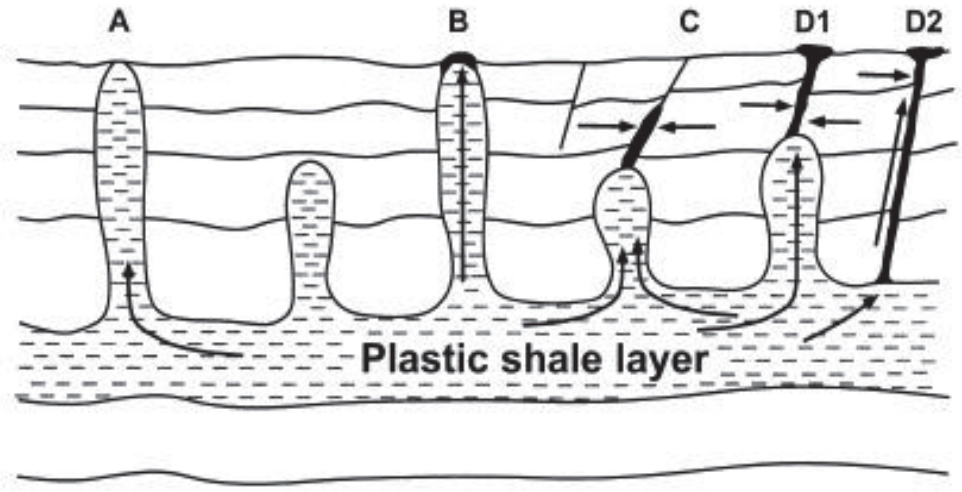

Figure 1-3: Cartoon showing submarine mud volcanoes formed by two basic mechanisms: (A) a seafloor-piercing shale diapir without a mud volcano; (B) a mud volcano formed on top of a seafloor-piercing shale diapir; (C) a seafloor seepage; (D1, D2) mud volcanoes formed due to the rise of fluidized sediments along faults. Arrows show the migration paths of fluids (Milkov, 2000).

The first formation mechanism is in the case that a mud volcano is formed directly on top of a seafloor-piercing shale diapir as a result of fluid migration along the diapir-formed conduit. Typical diapir-formed submarine mud volcanoes are found in the Caspian Sea (Ginsburg and Soloviev, 1994), in the Mediterranean Sea (Ivanov et al., 1996), and in the Sorokin Trough of the Black Sea (Krastel et al., 2003). The second (and more common) mechanism for the formation of mud volcanoes is due to the rise of fluidized sediments along faults or fractures. The material migration pathway is either directly connected to the source layer, or is connecting to a diapir that is below the mud volcano but has not pierced the seafloor. Typical examples of these types of

mud volcanoes are found in the Gulf of Mexico (Prior et al., 1989) and in the Black Sea (Woodside et al., 1997).

1.3.2 Driving Force

Although two formation mechanisms have been described in the previous section, the question still remains as to what causes deeply buried muddy sediment to rise to the seafloor surface? Buoyancy plays a significant role in the diapiric formation stage; however, the power provided by this buoyancy is not enough, therefore an additional force, pore-fluid pressure, is believed to be the main driving force for mud volcano formation.

Table 1-1: Causes for Overpressure, distinguished by Origin, Mechanism, and Corresponding Geological Setting from Kopf (2002).

Origin	*Mechanism*	*Environment*	*Significance*	*Selected References*
Burial	sedimentary loading, compaction/settling	any sedimentary setting (i.e., deltas and active and passive margins)	major in such settings	*Braunstein and O'Brien* [1968] *Morgan et al.* [1968] *Moon and Hurst* [1984]
	slumping, sliding	marine slopes of active and passive margins	major on slopes	*Hovland and Judd* [1988]
Tectonic	tectonic loading	any compressional margin, thrust zones, and wedges	major in such settings	*Shipley et al.* [1990] *Westbrook and Smith* [1993]
	deep level ducting	accretionary complexes	major in such settings	*Moore* [1989]
	smectite dehydration	accretionary complexes	can be major	*Fitts and Brown* [1999]
Thermogenic	opal/quartz reactions	any setting with biosilica	usually minor	*Kastner* [1981]
	smectite dehydration	any setting with abundant clay deposition	can be major	*Schoonmaker* [1987] *Colten-Bradley* [1987]
	other diagenesis	deeper subduction zone	minor?	*Moore and Saffer* [2001]
	metamorphism	deep subduction zones and other collision zones	usually minor, but locally important	*Bebout et al.* [1999]
	methanogenesis/hydrocarbon generation	any setting and reservoirs	can be locally important	*Ridd* [1970] *Hedberg* [1974]
	thermal expansion; hydrothermal pressuring	magmatic arcs and ridges	can be locally important	*Barker and Horsfield* [1982]
Biogenic	methanogenesis	shallow marine settings and accretionary prisms	can be very important	*Ritger et al.* [1987] *Suess et al.* [1999]
Other	osmosis	clay-bearing sedimentary environments	very minor	*Fertl* [1976]

[a]Table is modified from *Clennell* [1992].

Several factors affect the development of high pore-fluid pressure (Dimitrov, 2002):

1. The active tectonic setting of folding creates high accreting and overthrusting sedimentation rates.

2. Because of the high burial rate, the remaining water content of the sedimentation material and the overburden on top, which results in them being undercompacted, leads to an increase in the pore-fluid pressure.

3. Biogenic and thermogenic gases formed by the post-depositional transformation are other factors that create the internal overpressured, undercompacted environment.

4. The tectonic force of compression also results in high pore-fluid pressure.

5. Other factors also help to form high pore-fluid pressure, such as the diagenetic phenomena (the dehydration of expandable clays through mineralogical transformation), secondary precipitation of cementing materials (creating sealing barriers and/or decreasing pore space), thermodynamic effects, and biochemical effects (two- to threefold volume increases caused by the breakdown of hydrocarbon molecules).

1.3.3 Triggering Events for Mud Volcano Formation

Triggering events are necessary for the formation of mud volcanoes, but the formation may be self-induced. After the pore-fluid pressure reaches a high enough value, vertical hydraulic fracturing may occur. Tectonic compression can also be a triggering event. It increases the pore-fluid pressure, resulting in high levels of seismicity and creating faults. Tectonic compression not only provides a pathway but also breaks the fragile metastable conditions of the over-pressured subsurface material and initiates the movement. Regional extension can also play a role in triggering mud volcano formation, because it can fracture the overburden and make the overburden sediment thin (Jackson and Vendeville, 1994).

The eruption of some mud volcanoes is also associated with the astronomical cycles of the moon and sun, because the semi-liquid nature of mud breccia is provoked by their gravitational forces (Guliyev et al., 1996) and can therefore, triggering the formation of mud volcanoes.

1.4 Global Distribution

1.4.1 Geographical Location and Numbers

Mud volcanoes have a worldwide distribution (Fig. 1-4) and can be found in both terrestrial and marine environments. They have been discovered in 44 onshore

(Martinelli and Panahi, 2006) and 27 offshore areas (Milkov, 2000). Submarine mud volcanoes are inferred from indirect geological and geophysical evidence, as well as deep-sea observations by remotely operated cameras.

① Aleutian trench, Alaska Margin: Copper River Basin
② British Columbia, Canada
③ Cascadia (Oregon, Washington)
④ California, Nevada
⑤ Mexico, Gulf of Mexico
⑥ Texas, Mississippi, Lousiana
⑦ Lake Michigan
⑧ Costa Rica
⑨ Columbia
⑩ Ecuador
⑪ Barbados
⑫ Venezuela and Trinidad
⑬ Greeland, North Atlantic
⑭ Morocco/North Africa
⑮ Spain
⑯ Barents Sea, North Sea, Baltic Sea
⑰ Alboran Sea
⑱ Western Alps, Appennines/Italy
⑲ Sicily
⑳ Peleponnensus/Greece, Adriatic Sea
㉑ Aegean Sea
㉒ Eastern Mediterranean Sea
㉓ Roumanla
㉔ Tanzanla/East Africa
㉕ Black Sea, Kerch and Crimea Peninsulas
㉖ Caucasus (Taman, Georgia, Azerbaijan)
㉗ Caspian Sea
㉘ Iran, Turkmenistan
㉙ Makran and Pakistan
㉚ India
㉛ Burma
㉜ Sumatra, Java
㉝ Borneo, Brunei, Sabah/Malaysia
㉞ Central Australia (Gosses Bluff)
㉟ Timor-Ceram Arc
㊱ Irian Raya, Papua New Guinea
㊲ Taiwan
㊳ Ryukyu Trench, Nankai, Janpan Trench, Japan
㊴ Sakhalin Island/Sea of Ochotsk
㊵ Marianas
㊶ Australia
㊷ New Zealand
㊸ Lybian Dessert, Egypt
㊹ Netherlands

Figure 1-4: Global occurrence of mud volcanoes (Kopf, 2002).

Based on the long history of the terrestrial mud volcano research, many areas of mud volcanism have been observed, such as; in Alaska, Azerbaijan, the Barbados Ridge, the Black Sea region, Borneo, the Caspian Sea region, China, Ecuador, Georgia,

Greece, Greenland, India, Iran, Italy, Java, Kyrgyzstan, Mexico, the Mississippi Delta, Myanmar, The Netherlands, New Guinea, New Zealand, Pakistan, Panama, Romania, Russia and its Sakhalin region, Spain, Sumatra, Taiwan, Tanganyika, Tanzania, Timor, Trinidad, Tunisia, Turkmenistan, Ukraine, the United Kingdom, and Venezuela (Martinelli and Panahi, 2006).

It is widely known that seas and oceans cover about two thirds of the earth's surface, and evidence suggests that submarine mud volcanoes are present in all oceans (Milkov, 2000). However, due to technical limitations, a comprehensive investigation of submarine mud volcanoes has only occurred during the past 30 years. The development of hydro-acoustic instruments and deep-ocean sampling instruments has made research on submarine mud volcanoes possible. The already-known areas with submarine mud volcanoes include: Barbados Island, the Gulf of Mexico, the Norwegian Sea, offshore Greece, offshore Crete, offshore Cyprus, the Black Sea, offshore Nigeria, and the Caspian Sea (Martinelli and Panahi, 2006).

Although research on mud volcanoes has been conducted for decades, the total number of these formations is still not precisely known, and new submarine mud volcanoes are being discovered every year due to the continuous investigation of the abyssal seafloors using more advanced techniques. Dimitrov, in his 2003 paper, proposed that about 1,100 terrestrial or shallow-water mud volcanoes are known. Approximately 150 prominent mud-piercing structures are confirmed, and about 700 submarine mud volcanoes are inferred in the deep oceans (Dimitrov, 2003). Milkov (2000) speculates on the number of submarine mud volcanoes based on observations of a mud volcano's density, estimating that 1,000 - 100,000 submarine mud volcanoes may exist worldwide (Judd, 2005; Tinivella and Giustiniani, 2012). Another estimation shows that the total number of submarine mud volcanoes is between 7,000 and 1 million. However, when comparing current data from Kopf (Kopf, 2002) to the compilation by Higgins and Saunders (1974), twice the number of mud volcanoes is now known. This number is certain to increase in the future with continuing research.

1.4.2 The Tectonic Environment

The two major reasons for the formation of mud volcanoes are I) high sedimentation rates and II) tectonic compression. As a result, it can be inferred that the geological environment strongly controls the geographic distribution of mud volcanoes. In fact,

they occur in various tectonic settings (Fig. 1-5), however, a large majority of them are located within compressional zones, such as accretionary complexes, thrust and overthrust belts, the forelands of Alpine orogenic structures, and zones of dipping noncompensating sedimentary basins, all of which coincide with the active areas of the plate boundaries (Tinivella and Giustiniani, 2012). A few mud volcanoes can be found in zones with high sedimentation rates, such as in modern submarine fan systems. Moreover, there are still some mud volcanoes reported within areas with thin sediments, for example, in the Baltic Sea where mud volcanoes have occurred where the sediment is only 10 m thick (Söderberg and Flodén, 1991 and1992).

Mud volcanoes are irregularly clustered in separate areas along convergent plate margins with thick sedimentary sequences. The main mud volcano-forming belts around the world include the Alpine-Himalayan belt, the Pacific orogenic belt, and the Atlantic Ocean-Caribbean orogenic belt. Moreover, a number of mud volcanoes are also situated at some submarine deltaic and fan complexes (Hovland et al., 1997; Kopf et al., 2001; Delisle et al., 2002; Dimitrov, 2002; Etiope et al., 2002; Deville et al., 2003; Yassir, 2003; Shakirov et al., 2004; Stewart and Davies, 2006).

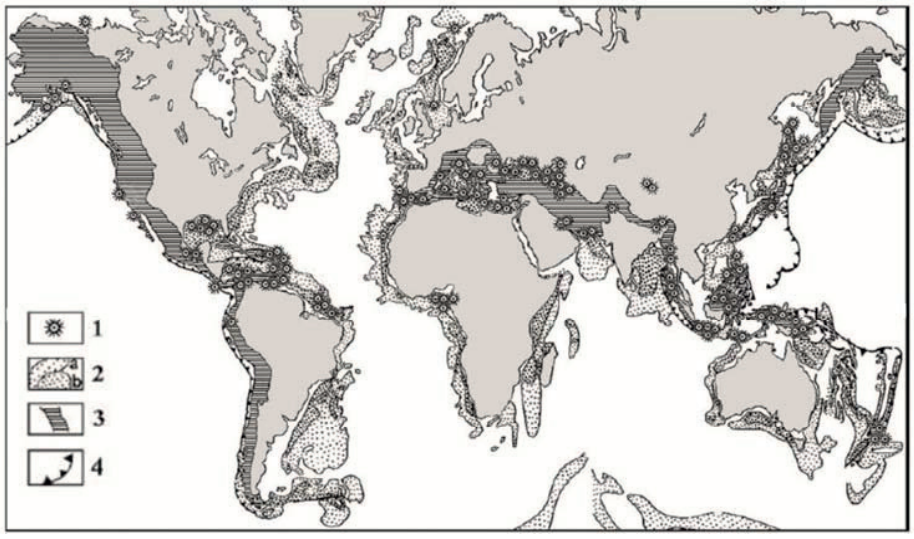

Figure 1-5: World geographical distribution of mud volcanoes. (1) single mud volcanoes, separated mud volcano areas and mud volcano belts; (2) sediment thickness in the areas away from continental shelves: a) 1-4 km, b) >4 km; (3) some of the main areas of industrial petroleum production; (4) subduction zones; (5) active compressional areas (Dimitrov, 2002).

More than half of all mud volcanoes are related to the Alpine-Himalaya active belt.

The largest cone-shaped mud volcanoes occur in this region, with approximately 650 terrestrial and more than 470 offshore prominent mud volcanoes (Dimitrov, 2003). The world's most active terrestrial mud volcano area is in the Baku region of eastern Azerbaijan, on the Caspian Coast. The greatest number of mud volcanoes in the world is also along this belt. The Alpine-Himalayas mud volcano belt begins at the Mediterranean Ridge (Limonov et al., 1996) and its adjacent inland area, including Albania and southern, central, and northern Italy (Martinelli and Judd, 2004). This belt extends east and passes through the forelands of the Eastern Carpathians in Romania, the Kerch and Taman Peninsulas (Arhangelski, 1932; Gubkin and Feodorov, 1940), the forelands of the Great Caucasus (Gubkin and Feodorov, 1940) and the Black Sea (Ivanov et al., 1996). Then the belt turns southward into the area of the Southern Caspian Sea, which consists of the Azerbaijan (Yakubov et al., 1971), the Turkmenistan (Yakubov et al., 1971; Guliyev et al., 1996), the South Caspian Basin (Ginsburg and Soloviev, 1994), and Gorgon Plain in Iran (Mazzini et al., 2014). To the east, the belt continuous through the Makran coast of Pakistan (Higgins and Saunders, 1974). Furthermore, this belt passes through the southern Himalayas (India and China) and Burma. It continues south, into the most NE part of the Indian Ocean on and around numerous forearc islands, which are situated along the Indonesia and Banda Arcs (Barber et al., 1986), Indonesia– Australia accretion and collision complexes (Williams et al., 1984), and the Banda accretionary complex offshore (Barber et al., 1986).

About 150 terrestrial mud volcanoes and a large number of submarine mud volcanoes are located in the Pacific Ocean's mud volcano belt (Dimitrov, 2002). This belt is situated along the ocean's eastern and western edges. The western branch can be traced to begin at Sakhalin Island in the Sea of Ochotsk. After that, it passes through Hokkaido Island and bifurcates in the southernmost islands of Japan, circling the East China Sea along the Okinawa islands and the Nankai Trough to Taiwan (Shih, 1967). It turns eastward to Melanesia and then runs southwest to Samoa and Australia, where it ends on the north island of New Zealand (Ridd, 1970). A relatively small number of mud volcanoes are found along the eastern branch of the Pacific Ocean mud volcano belt. They are mainly concentrated near Southern Alaska (Motyka et al., 1989), offshore of the Aleutian accretionary complex, offshore California, in the subduction zones off Costa Rica and southern Panama, the Ecuadorean coast, and inland in Peru (Dimitrov, 2003).

Several hundreds of both onshore and offshore mud volcanoes have been identified in the Atlantic Ocean mud volcano belt. This belt runs through the eastern- and western-central parts of the ocean and, the southern Caribbean Sea (Dimitrov, 2003). Most of the mud volcanoes occur along the Caribbean thrust belts and within the Barbados accretionary complex. Small groups of mud volcanoes are found in the Amazon and Niger Deltas (Graue, 2000; Dimitrov, 2003), along the Gulf of Cadiz (Mazurenko et al., 2002), in the southern Canary basin, offshore Portugal and Morocco, and in the Alboran Basin (Pérez-Belzuz et al., 1997).

In addition to mud volcanoes associated with the three mud-volcano belts described above, mud volcanoes are also found in the Mississippi Delta (Hovland et al., 1997), Lake Michigan (Kopf, 2002), Greenland (Kopf, 2002), the North Sea (Vogt et al., 1997), and The Netherlands (Paine, 1968), and in salt diapirism areas such as in the Gulf of Mexico (Neurauter and Roberts, 1994), Buzachi Peninsula (the northeastern Caspian Sea), and the Alboran basin in the Western Mediterranean (Pérez-Belzuz et al., 1997).

1.5 Emission Products

Gas (Fig. 1-6), water, fluid, and mud are the primary components that form the structure of a mud volcano and contribute to its activity. The quantities and the exact qualitative properties of these components are varied and are usually controlled by the

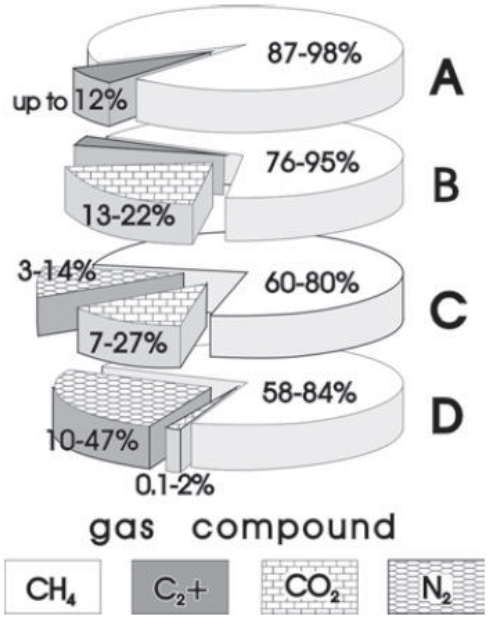

Figure 1-6: Average composition of characteristic gases emitted from mud volcanoes of (A) the South Caspian Basin, (B) the Baku area of Azerbaijan, (C) the South Sakhalin Island and Kerch and Taman peninsulas, and (D) the Cooper River Basin, Alaska (Dimitrov, 2003).

in-situ geological character and the volcano's own forming process (Tinivella and Giustiniani, 2012).

1.5.1 Gas Emissions

1.5.1.1 Origins of Gas: Biogenic and Thermogenic Gas

Gases (methane, ethane, carbon dioxide, nitrogen, hydrogen sulfide, argon, helium, etc.) are one of the components of mud volcanoes, and they play an important role in their formation and activity. Among these gases, methane is always the dominant component, and it accounts for about 58 - 98% of the total volume (see Fig. 1-6). These gases either come from deep source sediments (clays, shales, mudstones, siltstones, and marls), or shallow deposited muddy layers. As a result, the generation of these gases is constrained in these areas by three kinds of origins. (1) *Biogenic gases* maybe generated by a bacterial decay process during which organic matter in marine and freshwater sediments is broken down (Claypool and Kaplan, 1974). Such biochemical gases can occur at a shallow sediment surface (Allen et al., 1969; Friedman et al., 1971) or at depths of up to 1,200 - 2,000 m. (2) *Thermogenic gases* can also be the thermal alteration of organic matter, which generates methane and higher order hydrocarbons by catagenesis in the deeper sediment (Kvenvolden, 1985). (3) The *recycling of gases* means that gas may be generated during the process of hydrate dissociation that accompanies sedimentation (Paull et al., 1994). Sometimes, gases can be mixed in origin (e.g., biogenic and thermogenic gases can mix to form the released gas of a mud volcano). Gases of thermogenic origin can also accompany oil leakage, as is seen with the mud volcano areas of Azerbaijan, Romania, Columbia and Mexico (MacDonald et al., 2000).

As the major component of the gases, methane of biogenic and thermogenic origins can be distinguished using chemical and isotopic methods. Relative to thermogenic methane, biogenic methane is depleted in C13 (Whiticar, 1999). The ratio of methane (C1) to heavier hydrocarbons, usually expressed as the sum of ethane and propane (C2 + C3), can also be used to discriminate the methane source. The ratio of the biogenic gas [C1/ (C2 + C3)] is usually greater than 10^3. However, in thermogenic gas, this ratio is usually less than 100 (Bernard et al., 1976). Elemental and isotopic analyses of hydrate samples indicate that the methane in most oceanic hydrate is derived from microbial sources. The typical areas where gas hydrates are found are

the Blake Ridge (Dickens et al., 1997), Hydrate Ridge (Suess et al., 2001), Nankai Trough (Takahashi et al., 2001), Congo-Angola Basin (Ginsburg et al., 1993; Charlou et al., 2004), and the Sea of Okhotsk (Ginsburg et al., 1993). Hydrates formed with thermogenic methane have been recovered from the Gulf of Mexico (Brooks et al., 1984) and the Caspian Sea (Ginsburg et al., 1992). However, for mud volcanoes, thermogenic methane forms the most abundant part of the released gas (see Fig. 1-7).

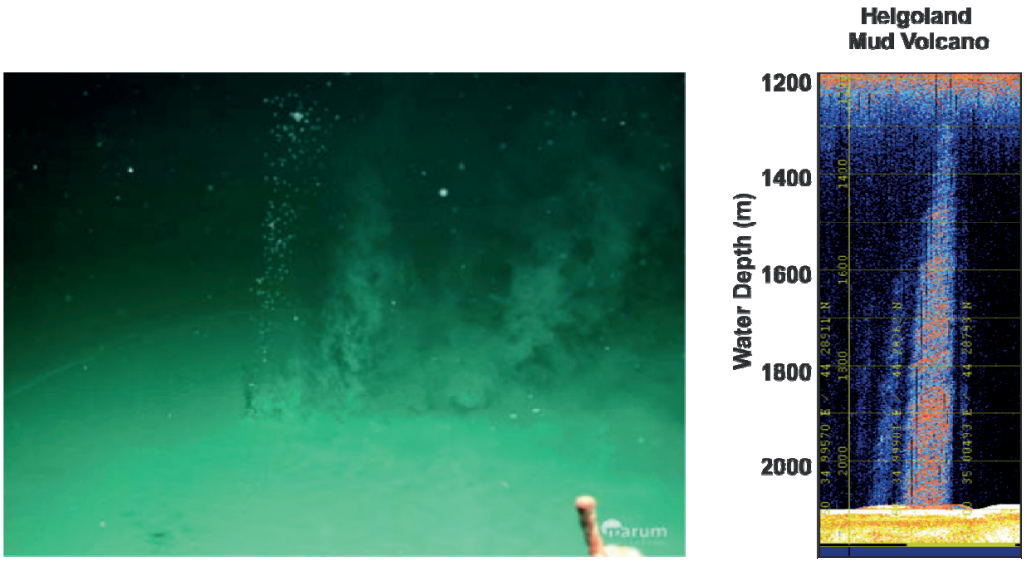

Figure 1-7: An *in-situ* photo of a bubble emission site at the Helgoland mud volcano in the Sorokin Trough (Black Sea) (Bohrmann, 2011a). The echogram of the gas flare records of the Helgoland Mud Volcano (right).

1.5.1.2 Fate of Gas

After being released from mud volcanoes, gases can take three paths: (I) when the gas is released within the gas hydrate stability zone it may form gas hydrate in contact with water, (II), it may emit and dissolve into the water column, and (III), it can emit directly into the atmosphere.

1.5.1.2.1 Gas Hydrates

Gas hydrate, also known as clathrate, is a crystalline solid structure composed of water and gas (Fig. 1-8). The water (H_2O) molecules form the main structural molecules that form a rigid lattice of cages (the host). The gas molecules (guests) are trapped in the cages (Fig. 1-9) to form the clathrates (Max, 2003). Typical natural gas molecules in the clathrate are methane, ethane, propane, and carbon dioxide (Sloan Jr

and Koh, 2007). Previous research has shown that most natural gas hydrates consist of more than 99% methane and are also known as methane hydrates (Sloan, 1998; Kvenvolden and Lorenson, 2001).

Figure 1-8: Gas hydrate recovered from marine sediment (from MARUM, Bremen; https://www.marum.de/Allgemeine_Geologie_-_Marine_Geologie.html)

Three different crystal structures have been recognized in nature (Fig. 1-9); they are referred to as structures I, II, and H (Sloan, 1998; Max, 2003). Which of these three

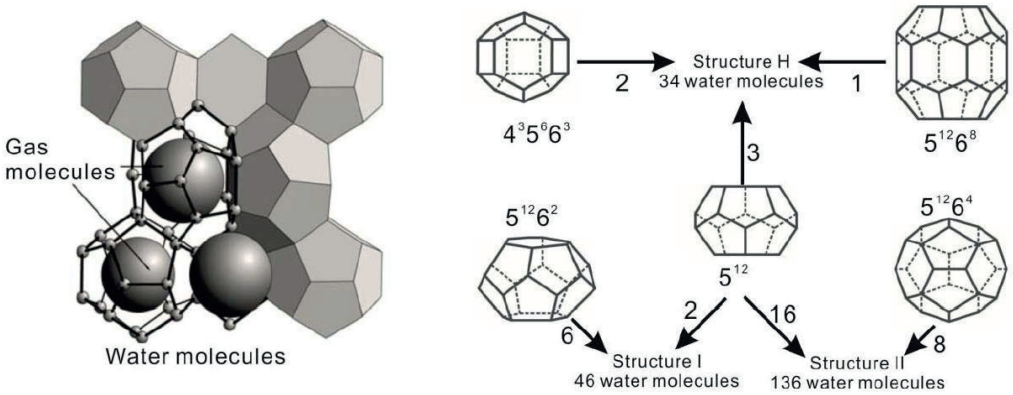

Figure 1-9: The molecular structure of gas hydrate and three variable crystal structures (Bohrmann and Torres, 2006).

structures form, depends on the cage made by the water molecule and the size of the trapped gas molecules? Structure I is most common among marine sediments. The cages of a structure I crystal form a body-centered, packed cubic crystallographic system and can contain natural gases with small molecule sizes, including methane,

ethane, and other gas molecules of similar diameter, such as carbon dioxide and hydrogen sulfide (CO_2 and H_2S respectively) (Sloan, 1998). Structure II crystals feature diamond packing in the cubic system and are formed with large enough cages that they can include not only methane and ethane, but also gas molecules as large as propane and isobutane. Structure H is least common in nature; it is present in the hexagonal crystallographic system and has larger cages than those found in structure II. Mixtures of small molecules (such as methane, nitrogen, or carbon dioxide) and very large ones, such as metylcyclohexane, are all included in Structure H (Sloan, 1998).

It is notable that methane hydrate is observed worldwide (Kvenvolden, 1995). Methane is usually composed of a more than 99% hydrocarbon gas mixture thus, these almost pure methane hydrates are likely structure I specimens (Max, 2003). Under standard conditions, one volume of methane hydrate can translate into 164 volumes of methane (Davidson et al., 1978). Structure II hydrates are often found in the Gulf of Mexico (Brooks et al., 1984) and the Caspian Sea (Ginsburg et al., 1992). Methane, accompanied by significant amounts of ethane and propane, is found in such gas hydrates. Structure H gas hydrates have also been found in the Gulf of Mexico (Sassen and MacDonald, 1994) and at the Cascadia Margin (Lu et al., 2007).

The formation of gas hydrate requires a specific environment. It usually occurs at relatively high pressures, low temperature conditions, and in the presence of many gases (Kvenvolden, 1993; Sloan, 1998). Moreover, water salinity and the presence of other gases such as CO_2, H_2S, and higher hydrocarbons also have an effect on the formation of gas hydrates. At a given pressure, the maximum stability temperature will increase with the presence of CO_2, H_2S, and higher hydrocarbons. Conversely, at that pressure, the maximum stability temperature will decrease with higher salinity conditions. For example, at that given pressure, the dissociation temperature of methane hydrate shifts about 1.1°C, with a seawater salinity of 33.5%, when compared to a fresh water system (Dickens and Quinby-Hunt, 1994).

Gas hydrate only occurs in a very thin sediment layer that runs parallel to the land or seabed surface, both in permafrost regions and in the oceans. This zone is constrained by gas hydrate stability zones (GHSZ) (Fig. 1-10). The lower boundary of the gas hydrate stability zone is called the base of gas hydrate stability (BGHSZ). It could be marked by a bottom-simulating seismic reflector (BSR) and follows an isotherm line,

which is almost parallel or sub-parallel to the morphology of the seafloor (Hyndman and Davis, 1992; Hyndman and Spence, 1992). High heat flow originating from the subsurface will make the GHSZ even thinner; for example, near mud volcanoes, pockmarks, and gas seep sites. The upper depth limit for methane hydrate in Polar Regions is about 150 m below the surface, with surface temperatures below 0°C (Max, 2003). In oceanic continental slope sediments, gas hydrate is found where bottom-water temperatures approach 0°C and the water depth exceeds roughly 300 mbsl.

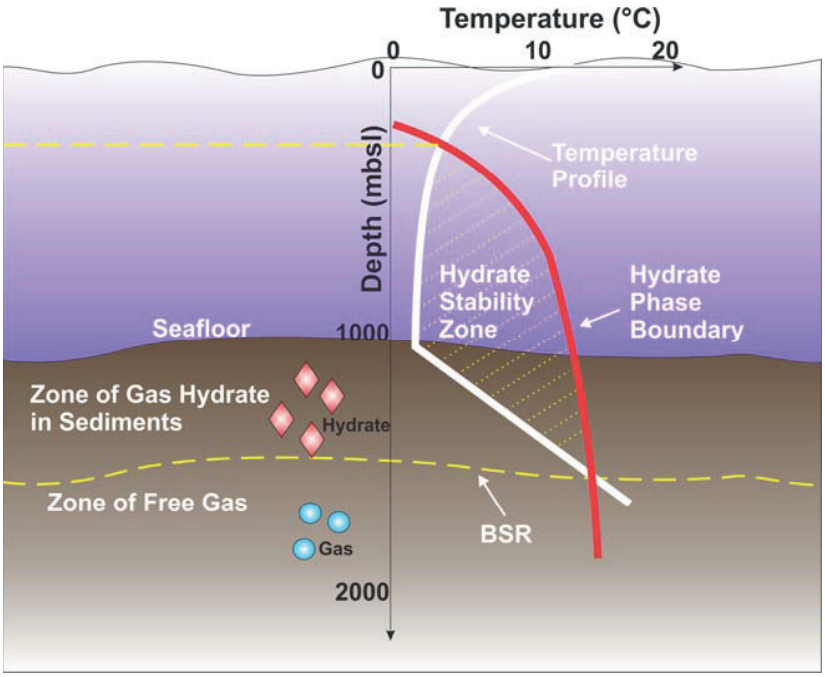

Figure 1-10: Gas hydrate stability zone in the oceans.

Gas hydrates are often found in deep-water mud volcanoes. Since first being noted in 1984, they have been reported in many areas, such as the Caspian Sea (Ginsburg and Soloviev, 1994), the Black Sea (Ginsburg et al., 1990; Limonov et al., 1994; Woodside et al., 1997; Bohrmann et al., 2003), the Mediterranean Sea (Woodside et al., 1997, 1998), Norwegian Sea (Vogt et al., 1997; Ginsburg et al., 1999), offshore Barbados (Martin et al., 1996), offshore Nigeria (Sultan et al., 2007), and the Gulf of Mexico (Slope, 1998). At standard temperatures and pressures, the global methane accumulation of gas hydrates associated with mud volcanoes is inferred to be about 10^{10}–10^{12} m^3 (Milkov, 2000). The gas hydrates recovered from mud volcanoes can be thermogenic, biogenic, or mixed in origin and are usually white or grayish-white in color. Sometimes they have plate-like habits and are randomly oriented in sediments.

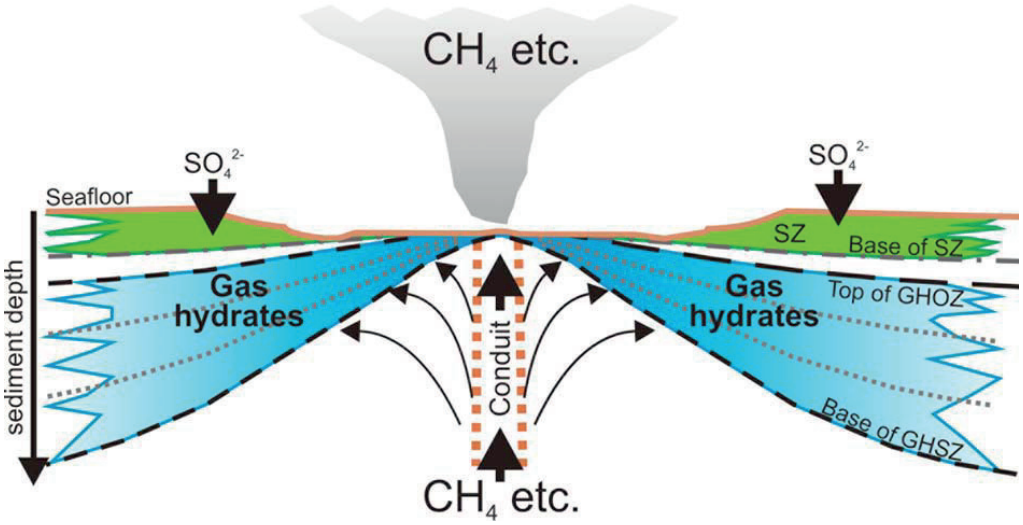

Figure 1-11: Cross section illustrating typical gas hydrate (GH) distributions in shallow deposits of submarine mud volcanoes (modified after Bohrmann and Torres [2006]) indicating temperature isolines, the base of the gas hydrate stability zone (BGHSZ), and the top of the gas hydrate occurrence zone (GHOZ). Hydrocarbons including methane along with heat ascend through a central conduit toward the seafloor. Within the sulfate zone (SZ), methane is microbially consumed, which affects the relative position of the top of the GHOZ (Pape et al., 2011).

A model to explain the formation and distribution of gas hydrates in mud volcanoes was based on research from the Haakon Mosby Mud Volcano in the Norwegian Sea (Fig. 1-11). Gas hydrate accumulates at the mud volcanoes' concentric-zone and is controlled by the ascending flow of warm fluids (Ginsburg et al., 1999). At the very center of the model, where hot mud and fluid flow out, no gas hydrate can form because of the high temperatures. Around the central area, however, the rising fluid provides enough gas for its formation. When it cools down around the central area, gas hydrate will form at the shallow subsurface (Zatsepina and Buffett, 1997). The reactants (water and gas) for forming gas hydrate come from the deep, external fluid that filters through volcanic mud sediments. This process is similar to the conventional low-temperature hydrothermal process of mineral formation (Tomkeieff et al., 1983). At the peripheral areas of the mud volcano, the gas used for gas hydrate formation comes from the diffusion of gas that has erupted in the central area and the local biochemical gas that formed in the sediment. The water that participates in the reaction comes from the local sediment. As soon as oversaturated methane comes in contact with the water, gas hydrate is formed. The presence of methane hydrate depends on the stability field of gas hydrate which is primarily determined in mud

volcanoes by the temperature distribution (Fig. 1-11).

1.5.1.2.2 Alternative Gas Fates

In addition to forming gas hydrates, the destinations of the gas released from the mud volcanoes include:

1) *Microbial oxidation with oxygen*. When gas is emitted from a mud volcano, some components of the gas (e.g., methane) may be oxidized by microbes in the shallow subsurface sediment or in water column.

2) *Water column dissolution*. Methane, ethane, and other gas components are in higher concentrations in the gas bubbles than in the surrounding water column which leads to gas dissolution in the water column (De Angelis et al., 1993).

3) *Atmospheric emission*. Under specific conditions, gas may migrate through the sediment and ambient water column without being reabsorbed to be expelled, directly into the atmosphere.

Which fate the gases experience depends on a variety of controlling factors that include I) bubble size, II) rising velocity, III) initial water depth, and IV) whether bubbles are coated by gas hydrate or oil. The larger the bubble size the greater the potential for methane, that has not been totally consumed by dissolution or microbes, to be released into shallow water (MacDonald et al., 2002). An increased rising velocity and shallower initial water depth also increases the potential of gas migration to the surface waters, and ultimately to the atmosphere (Leifer and Patro, 2002). This also applies to gas hydrates and oil-coated bubbles that are more easily emitted to the water's surface (Rehder et al., 2002; De Beukelaer et al., 2003; Heeschen et al., 2003; MacDonald et al., 2003; Greinert et al., 2006; Sauter et al., 2006).

1.5.2 Fluid Flux

Higher fluid flux is another important feature of an active mud volcano. Liquid seepage usually occurs in some petroleum fields where higher hydrocarbons coexist in the ascending mud (White, 1955; Humphrey, 1963). However, liquid seepages are more often observed in submarine mud volcanoes. Liquids may include hydrothermal waters that have migrated through deep-seated faults (Slack et al., 1998) or, may be brines (Robertson, 1996), freshened waters from mineral dehydration reactions, gas

hydrate dissociation (De Lange and Brumsack, 1998), or lateral meteoric water influx. The source of the fluid and source depth can usually be inferred from the fluid's signature (Mottl, 1992; Martin et al., 1996). The fluids in mud volcanoes may either be trapped or migrate to the surface. Low permeability material or gas hydrate formation in mud volcanoes may hinder the outflow of the fluid. An increase in lithostatic pressure nonetheless, will result in a usually violent eruption and sudden release, as evidenced by hydro fractured clasts (Robertson and Kopf, 1998). Tectonic activity and earthquakes are also important mechanisms for facilitating the rapid pressure release and vigorous mud volcano activity.

Fluid from mud volcanoes is an important food for the evolution of specialized chemosynthetic faunal assemblages. This chemosynthetic biomass of tube warms vesicomyids, mytilid, and solemyid bivalves, and sulfur-oxydizing bacteria are associated with seeps and are well know globally (Olu et al., 1996). Large specimens of the sponge Cladorhizida have been found offshore Barbados in association with such fluids (Ser, 1996; Olu et al., 1997). Previous research shows that mud volcanoes provide a great number of sub-seafloor habitats for microbes and the biogenic degradation of organic matter, which is an important part of the seafloor surface life.

1.5.3 Mud Expulsion

One essential activity of mud volcanoes is mud expulsion. The semi-liquid material (mud) that is expulsed from the main conduit and the gryphon is called mud breccia, or diapiric mélange, and it is the main material for the formation of mud volcanoes. Mud breccia from mud consists of the mud matrix, which supports a variable quantity of chaotically distributed angular to rounded rock clasts, fluid mud, and ash. The size of the mud matrix can range from a few millimeters to several meters in diameter (Hovland et al., 1997; Deville et al., 2003). Mud clasts may be of various lithologic types and provenances, derived from the rocks of the parent beds (or, sometimes, as source layers or mud reservoirs). They pass through the conduit or fractures to the terrestrial surface or the seafloor (Dimitrov, 2002; Kopf, 2002; Tinivella and Giustiniani, 2012).

The morphology of mud volcanoes is affected by the physical properties of the mud breccias. Most commonly, mud volcanoes have a central crater from which the mudflow is expulsed to form the edifice. Moreover, the slumps, slides, and the

sedimentary flow also affect the structure of a mud volcano. The viscosity and consolidation of the extruded material are the major reason for the shape of the edifice. Muds with low porosities form mud domes or ridges, while muds with high porosity create mud pies (Lance et al., 1998). Based on backscatter research of the Mediterranean Ridge features, it is clear that steep cones correspond to strong reflectivity (i.e., indurated material), while flat mud pies are hardly recognizable against the unconsolidated sediment apron of the wedge (Kopf et al., 2001). The mud breccia of the highly reflective domes contains up to 65% lithified clasts, based on a sediment sampling analysis (Flecker and Kopf, 1996). It is believed that mud volcanoes that are composed of the largest amount of mélange-type deposits are the longest-lived (Robertson, 1996) and can resist erosion, even when undergoing intense deformation. However, if no clasts exist in the extruding mud, the size of the conduit will control the geometry of the feature.

Since muds that are expulsed from the mud volcanoes are composed of rock clasts from the parent bed and some overlying rock fragments, research on mud breccias' matrices could make a contribution to *in-situ* regional geological and lithological investigations. The marker particles of mud breccias may indicate thermal maturation, diagenetic alteration, or dating information of the parent bed (Cita et al., 1981). Sediment that enters a subduction zone in accretionary margins can therefore be estimated from the mud breccias of the mud volcanoes that are situated along the accretionary margins. An example where classical methods for identifying the parent bed were carried out is, where the mud breccias of the Olimpi field mud volcanoes were related to the regional geology around the Mediterranean Ridge accretionary complex (Cita et al., 1981). Multidisciplinary investigations (e.g., seismics and microfossil assemblages) were applied to constrain the possible parent bed.

1.6 Climatic, Economic and Social Significance of the Mud Volcanoes

Mud volcanoes are globally, widely distributed geological structures. They can affect the global climate and the marine environment and therefore are of significance to mankind. Research in this field is thus important. Some aspects of mud volcano research that still needs attention can be summarized as follows:

1. Greenhouse gases such as methane and carbon dioxide, that are generated and emitted into the atmosphere from mud volcanoes, cause climate change. Exact figures on gas released from mud volcanoes during their periods of activity are hard to estimate, because the total number of mud volcanoes, their eruption frequency, and quantities of the released gas are all unknown and difficult to investigate. However, some preliminary estimations, have shown a total of 10.3 to 12.6 Tg methane (CH_4) is emitted into the atmosphere by quiescent and eruptive mud volcano activity every year (Dimitrov, 2002). This is enough to affect global climate and therefore requires further research.

2. Oil seepage within mud volcanoes indicates evidence for high petroleum potential in the deep subsurface. This is a valuable natural energy resource. In addition, gas hydrates formed in the shallow sediments of mud volcanoes serve as a "newer" potential energy resource which could satisfy human energy requirements (Kvenvolden, 1993; Collett, 2002). These natural resources associated with mud volcanoes thus needs further attention.

3. The analysis of the mud volcanoes' mud breccias provides useful information about the *in-situ* lithology. The origin and some geological characteristics can be inferred from this data. Thus work on mud volcano expulsion products is important.

4. Mud Volcano research also provides a possibility for a better understanding of hidden deep structural and diagenetic processes, such as the formation of gas hydrates, mineral dissolution and transformation, the degradation of organic material, and high pressure and temperature reactions.

5. Mud volcanoes can also be classified as geo-hazards. Marine mud volcanoes form indirect hazards through e.g. their role in the collapse of continental margins. Terrestrial mud volcanoes, in contrast, have a more direct impact on humans. A recent example of this is the eruption of the Lusi Mud Volcano on 29 May 2006, which is located in the sub-district of Porong, Sidoarjo on East Java Island. Within a few weeks, several villages were covered by boiled mud and thousands of families lost their homes. It is still active to date (May, 2015), and after an initial discharge of 180,000 cubic meters of mud per day, it now discharges 10,000 cubic meters per day. Therefore, a better understanding of mud volcanoes will help in future risk management research.

1.7 Main Objectives of This Study

The main objective of this PhD study is to focus on mapping deep-sea mud volcanoes using a more recently developed, high resolution, hydro-acoustic instrument Autonomous Underwater Vehicle (AUV). In combination with data sets from other deep-sea instruments (e.g. a PARASOUND and a gravity corer) information will be obtained about sediment temperature, the sedimentology, and subsurface structures of mud volcanoes. Gas flares, water column temperatures and seafloor photos will also be obtained with an ROV. The goal of this project is to improve our understanding of the tectonic mechanism, activity, structure formation, and mud migration process of the Helgoland and Dvurechenskii Black Sea submarine mud volcanoes using information from gas-releasing sites, mud eruption sites, seafloor structures, subsurface structures, and *in-situ* thermal structures. Some scientific research has already been carried out on the Dvurechenskii Mud Volcano (DMV) since 1997 when the DMV flare was first discovered in the northern part of the Black Sea. However, the DMV is located at a water depth of 2,000 mbsl, and past technical limitations constrained a detailed morphological investigation. Thus, to date, scientific research into the formation process and tectonic mechanism was also limited. The development of the new AUV satisfied the demand for detailed morphological research and helped fill the gaps between the ship-mounted hydro-acoustic instruments and ROV direct seafloor observations. The AUV data, combined with other scientific findings, therefore, provides excellent datasets for our investigations.

All the results here will service to resolve three main questions which are also the main subjects of the three manuscripts:

1. What is the formation process of the HMV, and which factors control its activity?

2. What is the mud movement process of the DMV and its movement velocities, both vertically and horizontally?

3. How does the development and activity of the neighboring Dvurechenskii and Helgoland mud volcanoes affect each other's formation?

In addition, the specific objectives of this study focus on the following aims:

- To map the Dvurechenskii and Helgoland mud volcanoes and their gas

seepages, together with correlated water column temperatures, sediment temperatures, and an evaluation of subsurface structures.

- To study the gas/fluid migration pathway and the related tectonic mechanism.

- To analyse the *in-situ* taken seafloor images and determine the relationship between the bathymetry-identified seafloor morphology and the real seafloor structure.

- To evaluated the water columns' thermal structures and find a possible relationship between the gas/fluid releasing site and the seafloor structures.

- To determine the mud movement processes of the DMV on both a vertical and horizontal scale and prove the mud movement's continuity.

- To research reasons for the HMV formation and calculate its time of formation.

- To build a geological evolution model for the DMV and analyze the mutual influence between the DMV and HMV during their formation.

The main datasets used in this study were collected during three cruises on-board the *R/V* METEOR and *R/V MARIA S. MERIAN* to the Black Sea. AUV-mounted multibeam data and the side-scan sonar data were the base datasets. In addition, the PARASOUND, the ROV, the temperature logger, and a gravity corer also provided complimentary datasets. They provided information on detailed seafloor morphological features, subsurface information, thermal structure, and sediment information. The instruments and methods used are described in detail in Chapter 3.

1.8 My Contribution to the Manuscripts

There are three manuscripts in this thesis that form Chapters 4, 5, and 6. For each manuscript, at the start, I discussed the scientific questions to be addressed, with my co-authors and supervisor, Prof. Bohrmann. Then, I outlined the data processing, analyse, and interpretation work independently. After I finished a preliminary version of each manuscript, the co-authors and my supervisor (Prof. Bohrmann) helped to review them.

In addition to the introduction sections of this thesis, details of the work I contributed to each manuscript are as follows:

In the first manuscript (Chap. 4), I processed the AUV bathymetry and side-scan sonar maps, analyzed the water column temperature data, did all the interpretation work on the sub-bottom profiles and the micro-bathymetry and side-scan map, and built a model. Yann Marcon provided the mosaic of the ROV seafloor photos. Thomas Pape did the gas composition work.

In the second manuscript (Chap. 5), I processed the AUV bathymetry and side-scan sonar maps, completed the analysis on the micro-bathymetry, built the mathematical-based mud movement model, conducted the temperature analysis, and drew the interpretation model.

In the third manuscript (Chap. 6), I compiled existing data and provided new high resolution micro-bathymetry data, hydro-acoustic gas flare data, and proposed an inter-relationship model for the formation of two neighboring mud volcanoes. I also carried out the interpretation work on sub-bottom profiles.

Chapter 2 Study Area

2.1 The Black Sea

2.1.1 Tectonic Evolution and Basin Morphology

The Black Sea is generally interpreted as a back-arc basin that opened during the Cretaceous period behind the Rhodope-Pontide volcanic arc and in continuity with the now closed Srednogorie Zone in Bulgaria (Robertson and Dixon, 1984; Görür, 1988; Okay et al., 1994). Its formation is related to the north-dipping subduction of the Tethys beneath Europe. The evolution of the basin is mainly controlled by compression from the collision between the Arabian, Anatolian, and Eurasian plates (Fig. 2-1) and subsidence (Nikishin et al., 2003). As a result, the Black Sea is separated into two sub-basins by the mid-Black Sea Ridge-the Andrusov Ridge (Nikishin et al., 2003).

The reasons for the Black Sea formation and the process that lead to the formation of the two sub-basins have been described by Okay et al. (1994):

> "The east-west-oriented west Black Sea basin opened as a back-arc rift in the Cretaceous by tearing a Hercynian continental sliver, the Istanbul zone, from the present-day Odessa shelf. The Istanbul zone, which was initially contiguous with the Moesian platform in the west, moved south during the Late Cretaceous-Paleocene with respect to the Odessa shelf along two transform faults, the dextral west Black Sea, and the sinistral west Crimean faults. It collided in the early Eocene with a Cimmeride zone in the south, thereby ending the extension in the western Black Sea and deactivating both the west Black Sea and the west Crimean faults as strike-slip faults. The east Black Sea basin opened as a result of the counterclockwise rotation of an east Black Sea block around a rotation pole located north of the Crimea. This block was bounded by the west Crimean fault, the southern margin of the eastern Black Sea, and the southern frontal thrusts of the Greater Caucasus. The rotation of the east Black Sea block was contemporaneous with the rifting of the west Black Sea basin but lasted until the Miocene, resulting in continuous compression along the Greater Caucasus (Fig. 2-1)."

The Black Sea is now in a compression environment that has been proven by modern stress field observations (Reilinger et al., 1997; Nikishin et al., 2003).

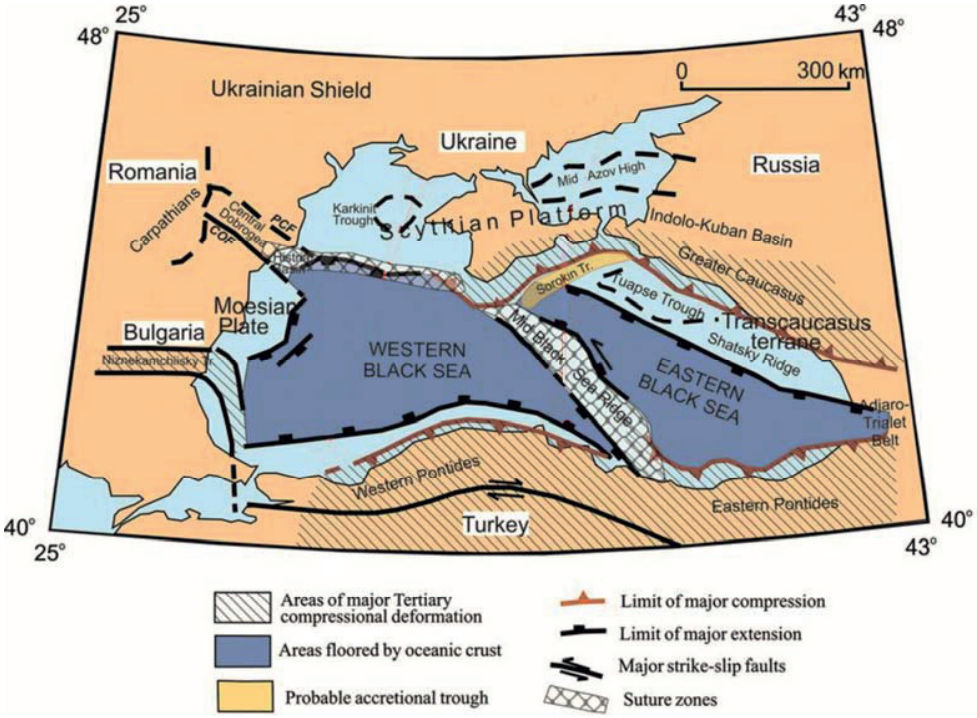

Figure 2-1: Tectonic scheme of the Black Sea area (after Robinson et al. 1995 with modifications). Abbreviations COF and PCF shows location of the fault zones confining the Central Dobroea-Capidava-Ovidiu and Pechenega-Camena fault zones, respectively.

2.1.2 Sedimentation Cover

The west and east sub-basins show different structural features on the multichannel seismic data, gravity, and magnetic records (Letouzey et al., 1977; Tugolesov et al., 1985). The western sub-basin is underlain by oceanic to sub-oceanic crust with a sediment cover of ≃19 km thickness (Tugolesov et al., 1985). The sediment is flat-lying and undisturbed and dates from the Cretaceous to Holocene periods - inferred from the age of initial rifting of the Black Sea in the Aptian to Ce-nomanian interval (Görür, 1988). It is separated from the western sub-basin by the Andrusov Ridge, which is north-west-trending and overlays the continental crust with 5 - 6 km of sediments (Nikishin et al., 2003).

Unlike the western sub-basin, the eastern sub-basin is underlain by a thin continental crust with sediment cover of ≃10 - 12 km thickness (Tugolesov et al., 1985). The

eastern sub-basin has more complex structural features than the western sub-basin. Numerous faults are intersected in the geological structure. The West Crimean fault is the west boundary of the eastern sub-basin, and a complex network of transform and extension faults form its southern margin. Plenty of south-vergent folds and thrusts are located in the northeastern compressional boundary of the eastern sub-basin. In the late Eocene period, these folds and thrusts were forming when the Slate-Diabase Ocean closed (Khain, 1975), and they continued growing into the Quaternary (Okay et al., 1994).

2.1.3 Sediment Lithology

The general features of the laminated sediments of the Black Sea were widely known after the *Atlantis II* Cruise in 1969 (Ross et al., 1970; Degens and Ross, 1972; Ross and Degens, 1974). The stratigraphy of the Black Sea from the Pleistocene to Holocene as described by Bohrmann (2011a) is shown in figure 2-2.

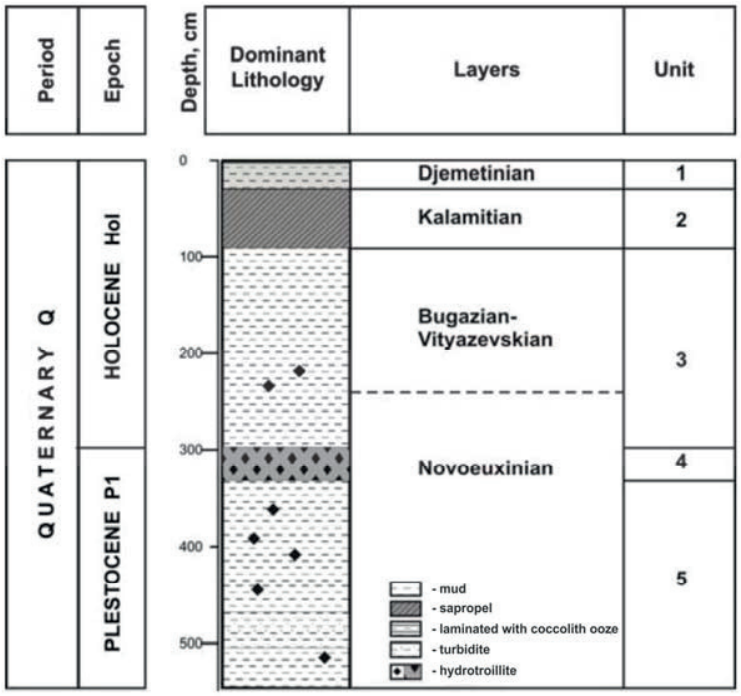

Figure 2-2: The essential stratigraphy of Pleistocene to Holocene Black Sea sediments (Bohrmann, 2011a).

Five main lithological units are contained in the Typical Black Sea sedimentary stratigraphy. Unit 1 is a fine-laminated (typically less than 1 mm) sequence of alternating white coccolith-rich laminae, sapropelic mud, and pale-grey mud. Unit 2 is characterized by sapropels and sapropelic mud, interbedded with very soft, pale-

greenish grey mud. Below the sapropel, a series of laminated moderately calcareous clays, with turbidite intercalations, which is characterized by low organic carbon content (≃0.6%), forms Unit 3. Unit 4 comprises of black to dark grey mud which is very rich in reduced iron, or hydrotroillite. The last unit, Unit 5, is characterized by finely bedded gray mud with occasional fine silt laminate and spots of black hydrotroillite (Bohrmann, 2011a). This typical Black Sea sequence can be used to determine the age of any recovered sediment.

2.1.4 Cold Seep Methane and Gas Hydrates

The methane budget of the Black Sea is supported by several sources: 1) a majority of methane is released from cold seeps, mud volcanoes, or pock marks, which originate from underlying deep sediment reservoirs. 2) Methane also derives from the decomposition of gas hydrates which are already proven to exist in the Black Sea. 3) Methane is also generated by microbial methanogenesis in shelf and slope sediments (Kessler et al., 2006) and the water column (Ivanov et al., 2002) of the Black Sea.

The underlying deep sediment reservoirs that supply methane or oil originate from the Late Oligocene-Lower Miocene Maikopian Complex, which is composed of a thick organic rich clay layer 4 - 5 km below the seafloor. Under high pressure and/or a tectonic trigger, such as a fault, the methane gas is released from surficial structures such as the mud volcanoes, pockmarks and gas emission sites which do not have significant seabed morphologies. Such methane-rich gas emission sites have been documented a gas flare in hydro-acoustic data from the Central Black Sea (Ivanov et al., 1996; Limonov et al., 1997), on the Bulgarian, Romanian, and Ukrainian shelf and slope (Ivanov et al., 1998; Naudts et al., 2006; Artemov et al., 2007), in the Sorokin Trough southeast of the Crimean Peninsula (Greinert et al., 2006) and on the slope offshore Georgia and Turkey (Klaucke et al., 2006).

Gas hydrate is one of the producers of methane. Its formation usually requires relatively high pressure and low temperature the availability of appropriate gases and water (Bohrmann and Torres, 2006). These conditions for gas hydrate formation are found in the gas hydrate stability zone (GHSZ) and in seafloor structures such as mud volcanoes. In the Black Sea, the upper boundary of the GHSZ was calculated at around 700 mbsl for pure methane conditions (Bohrmann et al., 2003). Gas hydrates have been recovered from the Black Sea since 1974. The 1974 sample was “the first

proof for natural gas hydrates in marine sediments around the world (Efremov and Zhizhchenko, 1974).” By using acoustic methods, gas hydrate accumulations are often indicated by a ‘Bottom Simulating Reflector’ (BSR) which is always parallel to the seabed and marks the bottom boundary of the GHSZ. In the Black Sea, such subsurface structures are found in the northwestern Black Sea west of the Dnepr Canyon (Lüdmann et al., 2004; Zillmer et al., 2005), offshore Georgia in the southeastern Black Sea (Bohrmann and Pape, 2007). However, gas hydrates are also recovered from areas without a typical BSR, for example in the mud volcanoes of the Sorokin Trough (Ivanov et al., 1998; Bohrmann et al., 2003).

Microbial methanogenesis also supplies methane to the Black Sea through bacterial decay processes which decompose the organic matter in water column or in marine and freshwater sediments (Claypool and Kaplan, 1974). It is either produced by CO_2 reduction with hydrogen (Chemical Reaction I)

(I) $$CO_2 + 4H_2 \rightarrow CH_4 + 2H_2O$$

Or by acetate fermentation (Chemical Reaction II)

(II) $$CH_3COO^- + H_2O \rightarrow CH_4 + HCO_3^-$$

Both these processes occur in the shelf and slope sediments and the water column. However, it is reported microbial methanogenesis is a minor contributor to the methane budget when compared to methane release from subsurface deep lying reservoirs and the decomposition of gas hydrate (Kessler et al., 2006; Pape et al., 2008).

2.1.5 Oceanography of the Black Sea

The Black Sea is a marginal basin. It has a relatively large surface area (423,500 km^2) and water volume (537,000 km^3). Moreover, the Black Sea is the largest anoxic body of water in the world (Kideys, 2002). The anoxic water depth is below 100 - 150 m, and the deep waters do not mix with the upper layers. Because its maximum water depth is ≃2 - 2.2 km, 90% of the Black Sea water is anoxic (Robinson, 1997; Finetti et al., 1988; Rangin et al., 2002; Nikishin et al., 2003).

The Black Sea is connected to the Sea of Azov, through the Strait of Kerch, in the north. Water exchange with the Atlantic Ocean occurs via the Mediterranean Sea and the Aegean Sea and various straits. e.g. it connects with the Sea of Marmara through the Bosphorus Strait, and then the Strait of the Dardanelles further connects it to the Aegean Sea region of the Mediterranean.

Eurasian fluvial systems provide fresh river water to the Black Sea from the northwestern/northern region of the sea. The most significant three rivers-the Danube, the Dnieper, and the Dniester, are responsible for about 85% of total riverine input to the Black Sea (about 340 km^3/year; Kideys, 2002). However, the circulation patterns of the Black Sea are controlled both by basin topography and fluvial inputs.

The inflow and outflow, which happened at the Bosphorus and Dardanelles Straits, are very important for water transfer in the Black Sea. The outflow from the Black Sea, which is the product of the fluvial input, has a low salinity and low density, while the inflow from the Mediterranean has a higher salinity and density. As a result, the inflow mostly occurs at the bottom of the basin while the outflow occurs near the surface. This flow pattern forms a classical estuarine circulation (Oguz et al., 1995). Usually the outflow volume is about twice that of the inflow. Because both the Bosphorus and Dardanelles Straits are narrow and shallow (only 33 and 70 m, respectively), the speeds of the inflow and outflow currents are high. This leads to a significant vertical shear and turbulent mixing of the two layers. The result of this mixing is a change in the salinity of the outflow which increases from 17 psu to 34 psu, while the inflow decreases from 38.5 psu to about 34 psu (Talley et al., 2011).

The surface circulation is cyclonic. The main surface circulation is around the perimeter of the Black Sea and is classified as the Rim Current. Within this current, two small cyclonic circulations appear at the eastern and western sub-basins (Talley et al., 2011). They are well-organized in Winter, but dissipate into a series of interconnected eddies in the Summer and Fall. Outside the Rim Current, numerous quasi-permanent coastal eddies are formed due to upwelling around the coastal apron and "wind curl" mechanisms active. Seasonal atmospheric and fluvial variations also play a control factor in the surface circulation (Korotaev et al., 2003).

A halocline exists between water depths of 50 - 100 meters and stops at the Cold Intermediate Layer (CIL) which is composed of cool, salty surface waters. It is the result of localized atmospheric cooling and decreased fluvial input during Winter

months and its base is marked by a major pycnocline at 100 - 200 meters (Talley et al., 2011).

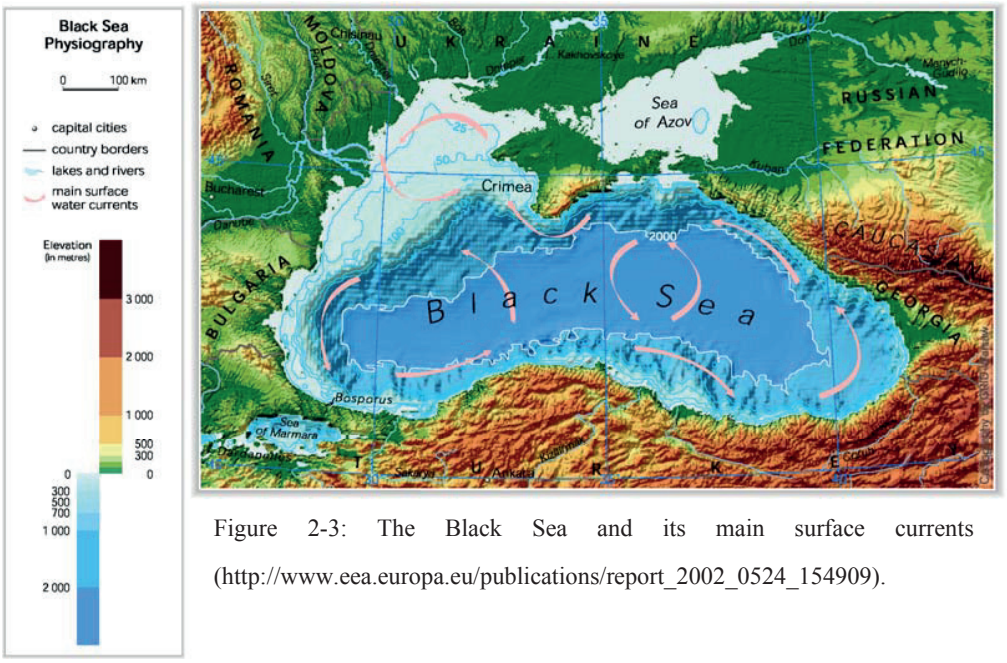

Figure 2-3: The Black Sea and its main surface currents (http://www.eea.europa.eu/publications/report_2002_0524_154909).

Below this pycnocline is the Deep Water Mass. Salinity rises to 22.3 psu and temperatures increase to around 9°C. Through hydrochemical processes these waters became anoxic. In addition, a very thick convective bottom layer was formed by weak geothermal heating and a long residence time (Korotaev et al., 2003).

2.2 Mud Volcano Fields of the Sorokin Trough

The mud volcanoes we studied, Dvurechenskii and Helgoland, belong to the Sorokin Trough mud volcano chain. The Sorokin Trough mud volcanoes are located at a water depth of 1,500 to 2,200 m and in a SE–NW direction compressional regime that was created by the movement of the Shatsky Ridge and Tatyaev Rise (Krastel et al., 2003). Sometimes, they appear associated with methane seepages. Seismic profiles show that diapirs are the main formation tectonics of the Sorokin Trough mud volcanoes (Woodside et al., 1997; Milkov, 2000).

The Dvurechenskii mud volcano is also seen to be on top of a diapir on the seismic profile (Milkov, 2000; Krastel et al., 2003), Krastel et al. (2003) calculated the source of this diapir to have originated from a depth of ≃4,000 mbsf. Based on geochemical research, however, it is calculated to be at ≃3,000 mbsf (Aloisi et al., 2004). The

upward overpressure fluid that results from tectonic compression is calculated as the reason for the diapirs (Krastel et al., 2003). Gas flares have been observed in both the DMV and HMV areas (Fig. 2-4). They appear to be time-dependent, and at different times, the strength and the height of the flares vary (Greinert et al., 2006). Using the ship-mounted hydro-acoustic instrument, we know that the DMV is a flat-topped mud volcano about 1,000 m in diameter and 25 m in height, while the HMV shows little structure. The backscatter shows the old and new mud flows of the DMV (Krastel et al., 2003), and the recovered sediment cores provide information that both the DMV and HMV have very soft and high viscosity sediment and, gas hydrate recovery (Bohrmann et al., 2003; Feseker et al., 2009). High thermal gradients are found at the central summit area of the DMV, and relatively low thermal gradients are found in the more peripheral areas (Feseker et al., 2009).

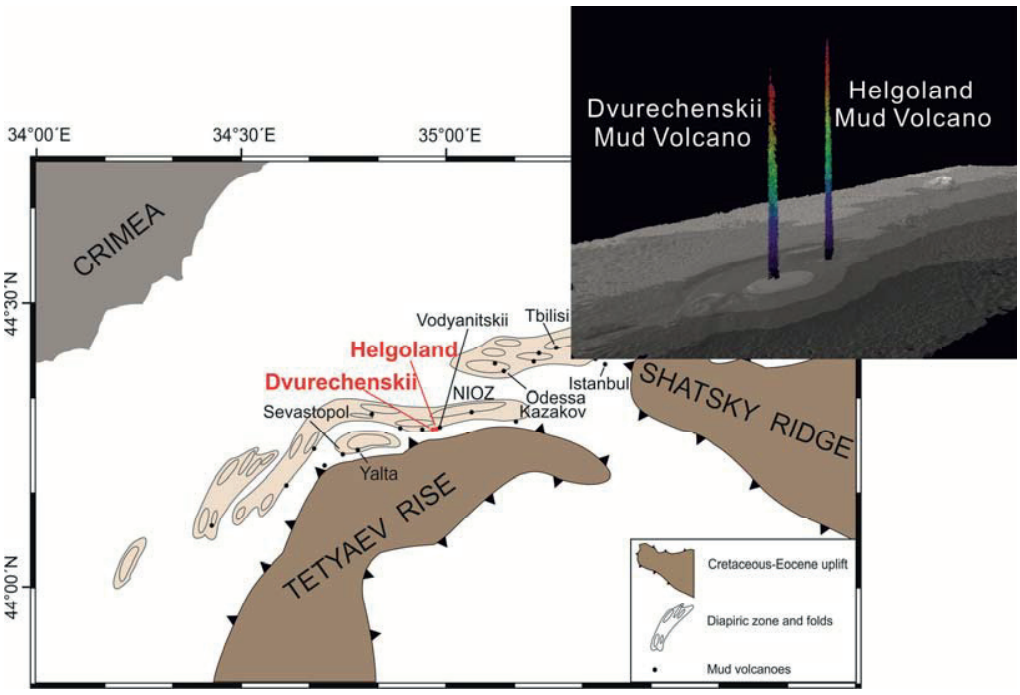

Figure 2-4: The location of the DMV and HMV in the mud volcano field of the Sorokin Trough (modified after Krastel et al. [2003]) are marked in red. The inset map shows the 3D viewed strong gas emissions related to Dvurechenskii and Helgoland mud volcanoes.

During this study, micro-bathymetry and side-scan maps of the two mud volcanoes were obtained from the AUV. More detailed information on these two mud volcanoes is available for interpretation, thus a more comprehensive result of their formation

mechanism, mud migration process, and mutually influence have been achieved. Details please see Chapters 4, 5, and 6.

Chapter 3 Instruments and Methods

3.1 Correlated Hydro-Acoustic Theory

Theoretically, sunlight could penetrate 1,000 meters into the oceans, but after 200 m depth, there is hardly any significant light left because most of it has been absorbed and converted into heat (Johnsen and Sosik, 2004). Thus, the intuitive visible methods of large-area seafloor observation are not practical. Acoustic waves, which travel very long distances in the water with very little attenuation, are therefore used to research the deep-ocean floor. Acoustic waves can reach the whole depth range of the seafloor, from a few centimeters to 11 km (maximum depth of the Mariana Trench, the deepest point in the world's oceans). They provide information about the seabed type, obstacles, and marine life/habitats. Only during the last few decades, have these acoustic instruments (sonar) become well enough developed to investigate the deep seafloor. Sonar measures the seafloor by transducing an acoustical signal and receiving its back signal.

Although a wide variety of instruments are available now, we can summarize sonar mapping systems into three types: I) single-beam echo sounders, II) multibeam echo sounders, and III) side-scan sonar (Blondel, 2009). The single-beam echo sounders are the simplest and most widely used, they look directly beneath the ship. They employ low-frequency signals (20 kHz) transmitted in short pulses (2 ms). Multibeam echo sounders transmit several beams (some transmit hundreds) at one time and cover a wide swath of the seafloor. The beams are narrower than single beams, which improves accuracy. Side-scan sonar covers even larger regions and provides higher resolution imagery of the seafloor. It transmits beams on two sides of the sonar (shown in Fig. 3-6) and achieves high-resolution maps (from 60 m down to 1 cm) with various frequencies (from 6.5 kHz to 1 MHz) (Blondel, 2009). Detailed information on sonar is given in the following sections.

3.2 Autonomous Underwater Vehicle (AUV)

3.2.1 Basic Settings and Operation

High-resolution micro-bathymetry and side-scan sonar data of the research area

Dvurechenskii and Helgoland mud volcanoes were acquired during Cruise MSM15/2 of the *R/V* MARIA S. MERIAN (Bohrmann, 2011a). Data was collected using the Autonomous Underwater Vehicle (AUV) MARUM Seal 5000. This AUV was designed as a modular sensor-carrying platform to meet the increasing demand for deep-sea information. It is capable of carrying various types of instruments and working in deep-sea areas.

The AUV was built in Canada in 2006, by International Submarine Engineering (I.S.E. http://www.ise.bc.ca/) and delivered to MARUM in June 2007. The vehicle body is torpedo-shaped and made of glass-reinforced plastic. It is approximately 5.75 m in length, 74 cm in diameter, and has a weight of about 1.3 tons (Fig. 3-1). The maximum diving depth is 5,000 m. Its power is provided by a series of dry Li-ion cells that supply about 15.6 kWh of power. This capacity can provide an overall operating time of about 19 hours with a standard payload or about 100 km travel distance (also with a standard payload). The speed of the AUV ranges from 0.6 m/sec to 2.4 m/sec, but its standard speed is 1.5 m/sec.

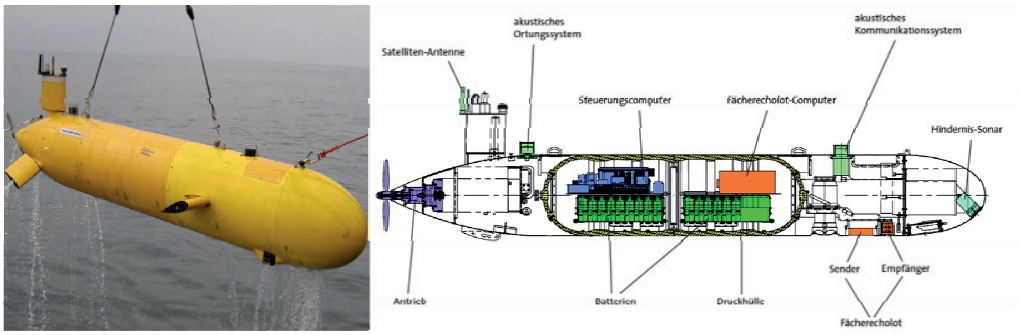

Figure 3-1: The layout of the AUV Seal 5000 from MARUM Institute (https://www.marum.de/Fahrzeug_2.html).

The AUV consists of three main components (Fig. 3-1): a modular atmospheric pressure housing made of anodized aluminum, a forward dome, and an afterward dome. The pressure housing has two sections and is the main buoyancy supporter of the AUV. The Vehicle Control Computer (VCC), the Payload Control Computer (PCC), the battery packs, and other dry-environment electronics of the payload are located here. The IXSEA inertial navigation system PHINS and the RESON multibeam processor are also installed in the dry payload area.

Auxiliary instruments and some of the navigation tools were placed in the afterward

dome of the AUV. This material included the Ultra-Short Base Line (USBL) system, RF radio, flashlight, IRIDIUM antenna, Differential Global Positioning System (DGPS) antenna, and the pressure sensors. The scientific payload was located in the forward dome. The standard payload of the forward dome is the RESON MBES 7125-B multibeam sonar, which has 512 beams and works at 400 kHz. Other, optional, scientific payload items included the KONGSBERG pencil beam (675kHz), the BENTHOS dual-frequency (100/400kHz) side-scan sonar, the IXSEA Echoes 5000 sub-bottom profiler (2 - 7 kHz), the Seabird SBE 49 CTD, the Sercel MATS 200 acoustic modem, and the DVL Doppler Logger (300 kHz). These items were also located in the forward dome. The AUV's flexibility, in terms of housing a variety of scientific instruments installed on its sensor platform, has made it suitable for constantly evolving scientific purposes.

The control system consists of two units, the Vehicle Control Computer (VCC), which was installed on the AUV, and the combination of the Surface Control Computer (SCC) and Mission Planning Workstation (MPW), which were installed in a control van on-board the ship. The VCC directly controls the whole system, e.g. dealing with error messages, controlling actuators such as thrusters, managing energy output, and controlling the emergency system. The operation software of the VCC is based on the real-time-capable UNIX derivative QNX and the software framework ACE. At the same time, this operation system also runs the SCC. The SCC is an Intel-based standard PC with a Graphic User Interface (GUI) for monitoring the AUV. Since both the OS and GUI of the AUV were run on QNX, they could be modified by users if necessary.

An Ethernet-LAN was established for directly communicating with the AUV. Firstly, the deck cable (100MBit/s LAN) was used for on-board accessing of the data recorded by the AUV. Secondly, when the AUV was in water, an Ethernet-RF-LAN modem was used for communication. The RF could communicate the AUV within distances of 1 - 2 km. The position of the AUV was calculated from the USBL system. Every 5 seconds, an acoustic transmit-pulse was sent to the diving AUV and a reply pulse was received on-board the vessel. After that, an exact position of the diving AUV could be calculated from two USBL systems (in the AUV's case): IXBLUE POSIDONIA for water as deep as 6,000 mbsl, and IXBLUE GAPS for water as deep as 3,000 mbsl.

The mission plan for the AUV was created on the MPW with the software MIMOSA© IFREMER. The operator could directly draw transects with a mouse to create a mission plan in the MIMOSA software and edit it with a set of tools. This graphic display of the mission was then converted into an I.S.E. vehicle-specific syntax, which consisted of waypoints (latitude and longitude), water depth, speed, and time span information. Finally, this mission was uploaded into the AUV VCC from the SCC control system. Mission mode was activated on the AUV, and then the AUV automatically performed the already-planned mission as written.

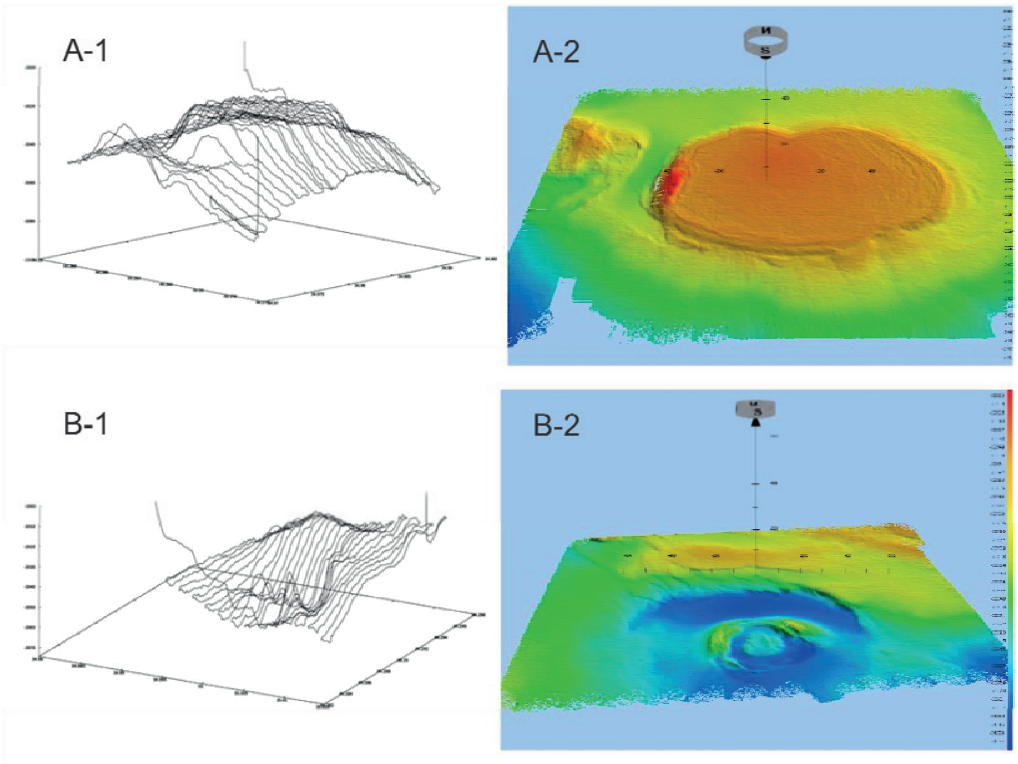

Figure 3-2: A-1: Underwater path of the AUV as a 3D plot of depth over time vs. position. A-2: Raw grid of Dvurechenskii MBES AUV mission. B-1: Underwater path of AUV as 3D plot of depth over time vs. position. B-2: Raw grid of Helgoland MBES AUV mission (Bohrmann, 2011a).

In the mission mode, the emergency system that was installed on the AUV was also very useful. During the whole dive time, the AUV would try to stay above the minimal navigation altitude (in this case, usually 40 m above the seafloor). The vehicle would stop its mission when it reached a critical altitude to avoid touching the seafloor. The vehicle would also turn on the backup battery if the main battery series power failed and for other emergencies such as the mission failure response, in which

case the damage and connection loss could be controlled by the emergency system.

3.2.2 Data Acquisition

The AUV's high-resolution bathymetric and side-scan data used in this study were acquired on the Dvurechenskii and Helgoland mud volcanoes in the Black Sea during the Cruise MSM15/2 of the *R/V* MARIA S. MERIAN. The RESON multibeam and BENTHOS dual-frequency (100/400 kHz) side-scan sonar were the main payload of the AUV to obtain this data. During the dive, the AUV was set to altitude mode, which meant that the AUV remained 40 m above the seafloor. To obtain full coverage, the spacing between two adjacent transect lines was set to 60 m, which has been proven to be very suitable for obtaining good data (Bohrmann, 2011a). After several tries, the Dvurechenskii and Helgoland areas were both successfully mapped (Fig. 3-2).

3.2.3 Data Processing

After simple preprocessing, the AUV bathymetric and side-scan sonar data used in this study, were extracted and then processed with the software MB-system (Caress and Chayes, 1996 and 2001). The processing diagram is shown in figure 3-3.

The data processing began with the pre-processing of the raw RESON 7k file. After the pre-processing step, the asynchronous navigation and altitude data were interpolated and embedded into the multibeam data to form a new 7k file. At this step, one could also suppress incorrect bathymetric data (too high or too low) with a depth-dependent filter. The roll bias from the vehicle could be also corrected. After setting basic attributes and completing the general correction of the whole area, it was necessary to manually clean data artifacts line by line in the single-file waterfall view (program MBedit), or piece by piece in the multi-file survey view (program MBeditviz). Next, a cross correlation between the apparent bottom slope in the swath bathymetric data and the roll time series was calculated before re-applying the pre-processing command. The cleaned data still needed some adjustment for seafloor features, so the navigation adjustment tool (MBnavadjust) was applied to match repeated seafloor features in overlapping swaths. Finally, a 1×1 m cell size bathymetric map was created using the command mbgrid. The main command for processing the side-scan sonar data was the mbbackangle command. Tables of the

average amplitude values in the swath sonar data, as a function of the grazing angle with the seafloor, were generated. Then the high-resolution (in our case, 1 m resolution) backscatter map was extracted using the mbgrid command.

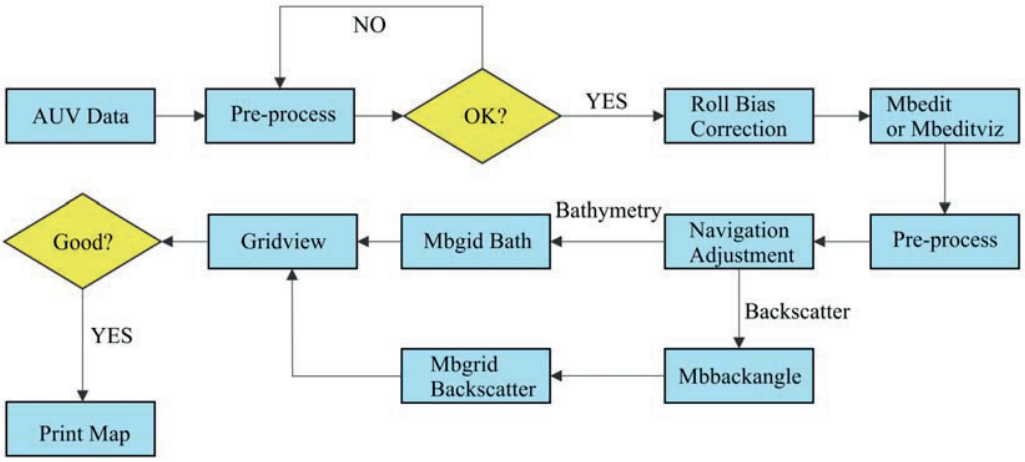

Figure 3-3: The process workflow of MB-system.

3.3 Multibeam Swath Bathymetric Data

The research ship-mounted multibeam data used in this study were obtained from the cruises of two scientific vessels, the *R/V* MARIA S. MERIAN and the *R/V* METEOR. Two types of seafloor topography instruments (one for the deep-sea and one for shallow to medium water depths) were mounted on the ships. The KONGSBERG EM120 was mounted on *R/V* MARIA S. MERIAN for measuring deep-sea bathymetry, and the EM1002 was mounted on the same ship for shallow areas. The instruments mounted on the *R/V* METEOR were different. The KONGSBERG EM122 was used for deep water while the EM710 was used in shallow areas.

3.3.1 Multibeam EM120 and EM122

Because the research area was located in a deep-sea area, the bathymetric data we used were from the EM120 and EM122 systems. The EM120 employs 191 beams for one ping, and swath widths of up to 150° can be obtained (recommended swath width is less than 130°). The main operating frequency used by this system is 12 kHz, and its depth-measuring capability ranges from 20 m to 11,000 m. The depth resolution

depends on environmental conditions and other limitations, but the main range is 10 - 40 cm, or about 0.2 - 0.3% of the water depth. In addition to the bathymetric data, the EM120 also provides a recording of backscatter amplitudes, which are similar to the backscatter strength of the side-scan sonar. The amplitudes reflect the seafloor roughness and sediment with higher resolution.

The KONGSBERG EM122 employs a frequency of 12 kHz and has the same depth range as the EM120 (20 - 11,000 m). It maps the seafloor topography with up to 288 simultaneous beams and swath widths of up to about 30 km are possible. The EM 122 can achieve a depth resolution of better than 0.2% in deep waters. The EM 122 provides the same seafloor topography and backscatter reflection as the EM 120, and can detect and record water column phenomena such as bubble flares.

3.3.2 Sound Velocity Profile (SVP)

To create more accurate bathymetric maps, another set of data, such as the sound velocity profile (SVP) of the water column, is necessary. A shipside SvPlus 3453 probe was applied to observe the SVP during the Cruise MSM15/2 of the *R/V*

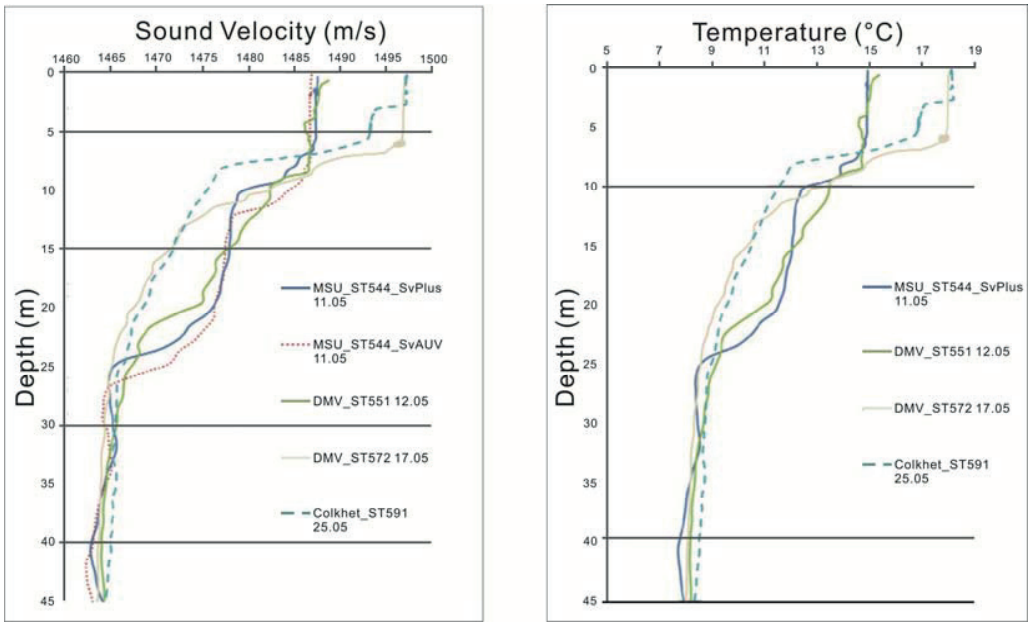

Figure 3-4: (left) SVP from AUV-CTD, (right) temperature profile from SvPlus (Bohrmann, 2011a)

MARIA S. MERIAN (Fig. 3-4). Because the SVP is highly dependent on water temperature, recordings observed at different times have significant differences.

During the cruise, the Dvurechenskii Mud Volcano (DMV) area was visited twice (on 12 and 17 of May, 2010). The temperature difference was about 3°C, which makes a sound velocity difference of about 10 m/s (Bohrmann, 2011a); such a difference in sound velocity could introduce a significant error in the water depth calculation.

3.3.3 Data Processing

A quick bathymetric and backscatter display was performed on-board with NEPTUNE, and the final bathymetric and backscatter maps were processed with the open-source software from MBARI, MB System or CARIS HIPS and SIPS. The raw data was corrected using the SVP. Data points that indicated erroneous depths were cleaned manually or automatically with the system's tools. Adjustments were made for navigation and to interpolate the values for obtaining an accurate data grid. All the swath bathymetry and backscatter maps were present in the ESRI software ArcGIS in the Mercator projection with datum WGS84. ArcGIS and the IVS Fledermaus displayed the data in 3D views (Fig. 2-4).

3.4 ATLAS PARASOUND

In order to measure the shallow sub-profile of seafloor sediment and gas-bubble flares in the water column, a single-beam echo sounder (ATLAS PARASOUND P70), was permanently installed on the *R/V* METEOR and *R/V* MARIA S. MERIAN. The ship-mounted ATLAS PARASOUND parametric echo sounder utilizes the parametric effect to generate a low-frequency secondary signal (0.5 - 6.0 kHz) by emitting two primary signals of higher frequencies (e.g., 18 and 22 kHz, individually and the High-frequency ranges from 18 to 33 kHz). The secondary low-frequency signal was confined within a cone with 4° as a very narrow opening transmission angle. This low-frequency signal can be used to measure the shallow seafloor sediment profile. Its maximum penetration is more than 200 mbsf. The sub-bottom profiles provided by the PARASOUND data provided information about the sedimentological and tectonic nature of the near-surface sediment. In this study, it was especially important to identify the faults around the study area, which could provide important evidence for formation processes. The primary high-frequency signals could be used to detect bubble flares, which often indicate seepage sites. Free gas causes the incident acoustic energy on the rising bubble stream to be presented as elongated, flare-shaped reflections in echograms (Nikolovska et al., 2008). In our research area, both mud

volcanoes showed active gas emissions during Cruises MSM15/2 and M84/2. In former investigations, they sometimes appeared as inactive mud volcanoes with no flares. The PARASOUND is effective in the depth range 10 - 11,000 mbsl, and the detected diameter of the signal was only about 7% of the water depth.

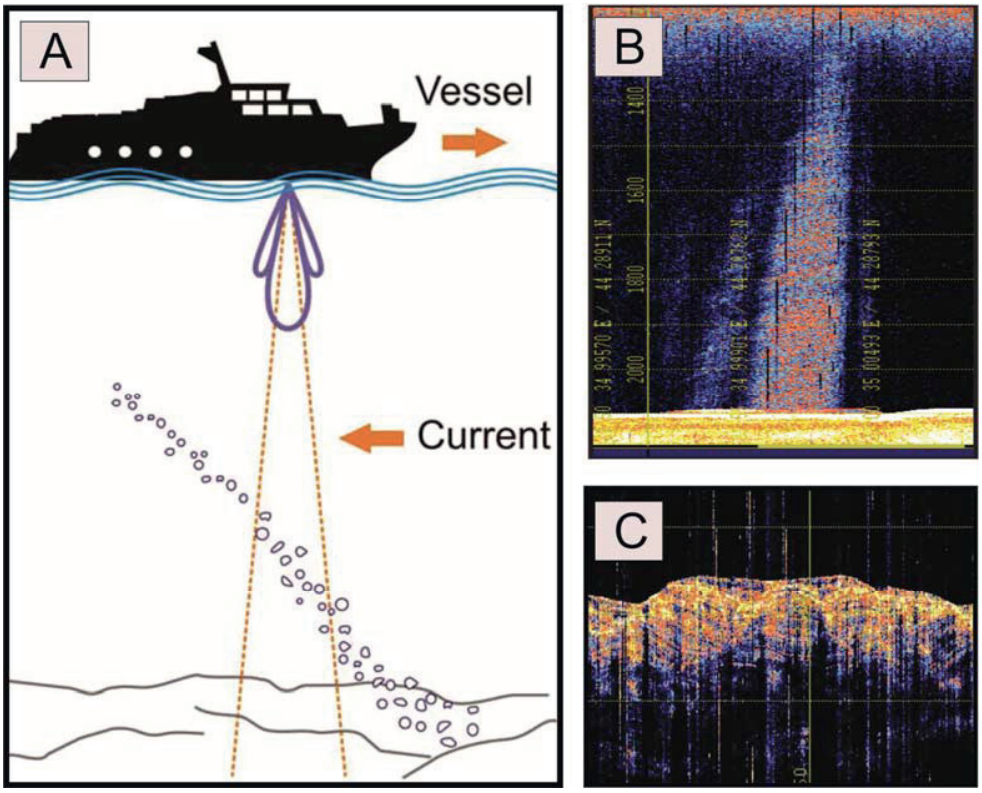

Figure 3-5: A: The data-measuring process of the PARASOUND echo sounder (Veloso et al., 2015). B: The observed gas flare on an echogram. C: The observed shallow subsurface on an echogram.

The measured PARASOUND data were stored as two files types (PHF-water column and SLF-sub-bottom profile) that were then replayed by the ATLAS PARASTORE software. The specific setting applied during the data recording was chosen in accordance with the water depth and required lateral resolution. In cases where extraneous acoustic and electronic noise had to be removed, a band-pass filter was used during recording or replaying.

3.5 Side-Scan Sonar

Side-scan sonar can record more detailed, varied, and higher-resolution imagery of the seafloor than ship-mounted multibeam or single-beam sonar. It provides information

concerning seafloor structure, the sediment materials (soft or hard), seafloor roughness, and biological colonization. Side-scan sonar transmits one beam on each side of the vessel. These beams are narrow along the track and wide across the track, and thus provide wide coverage. The area of seabed covered can range from a few tens of meters to 60 km or more. Side-scan sonar employs frequencies of 1 kHz - 1 MHz, The average speed of sound is about 1,500 m/s in the ocean, so the corresponding wavelength is 1.5 mm - 1.5 m. The wavelength determines the resolution of the image and therefore the minimum identifiable size of seabed structures, which is important for seafloor interpretation.

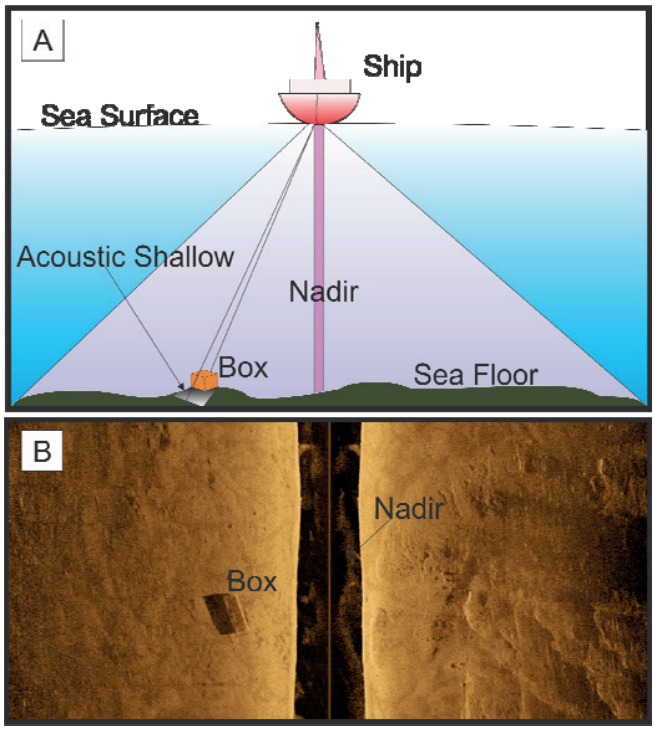

Figure 3-6: A: The side-scan data measuring process from the ship-mounted side-scan sonar and its results. B: is from a side-scan sonar example from the Deepvision sonar system (http://deepvision.se/).

The strength of the energy that is reflected back to the sonar is the backscatter, which is used for seafloor interpretation. The backscatter is a reflection of seabed geometry (slope, fault scarps, etc.), sediment attributes (composition, density, etc.), and surface character (micro-scale roughness, biological colonization, etc.). Fault scarps, gravel, or hard sediment and high-level roughness of the seafloor usually show as brighter or stronger backscatter, while a smooth seafloor and soft sediment always appear as low backscatter.

The processing of side-scan sonar data depends on the actual situation and the corrections that the data require. A slant range correction is always required in

creating a side-scan map. The distance between the target point and the sonar is called the slant range. It is not the same as the distance between the target point and the sonar's nadir, which is the point on the seafloor directly below the sonar. After eliminating the backscatter of the slant range, which is a representation of the water column, the seafloor imagery is left. Then, a correction for backscatter balance can be performed. Other corrections could include those for navigation, amplitude, histogram, mosaic, across-track data, and along-track data. These can be part of the processing as needed.

In our study, the side-scan sonar data was obtained from the BENTHOS dual-frequency (100/400 kHz) side-scan sonar, which was mounted on the AUV. Processing of the data was done with the open-source software MB-System. The replay of the raw side-scan data, especially the representation of the flares in the water column, was shown in the CARIS HIPS and SIPS software package.

3.6 Remotely Operated Vehicle (ROV)

In addition to indirect seabed observations by hydro-acoustic sonar, a visual observation of the seafloor is also very important. It is, however, very time consuming compared to other seafloor study methods. Yet its advantages are still significant. It provides high resolution, detailed, and visual information about seafloor geology and biology; it can take specimens of very specific seafloor materials (sediment, biological material, bubbles, etc.) while looking at the seafloor. It can also carry side-scan sonar as payload, which can record much higher resolution side-scan seafloor imagery than ship-mounted or towed sonar systems.

For this study, we used MARUM´s visual seafloor observation instrument, the remotely operated vehicle (ROV) QUEST 4000. QUEST 4000 was built to satisfy various offshore industrial needs by Schilling Robotics, Davis, USA. It weighs about 45 tons (Bohrmann, 2011a) and can dive to a maximum depth of ≃4,000 m. It has a high electrical energy capacity, which supports long working times and provides a large payload capacity. It accepts many types of instruments for imaging and sampling. The ROV connects to the research vessel via an armored steel umbilical cable, through which it can be remotely supervised by operators on the ship. One limitation of the ROV is that it requires a very long cable to sustain its necessary freedom of movement.

In this study, the ROV data was obtained during Cruise MSM15/2. During that cruise, QUEST performed two dives (numbers 263 and 267) at the Dvurechenskii mud volcano and two dives (numbers 268 and 272) at the Helgoland mud volcano. It obtained samples and recorded data that included gas and sediment samples, temperature measurements, seafloor videos and photos, and sonar data. During dive 263, only the T-stick was deployed. During dive 267, a long-term (more than 3 years) sediment temperature logger was found and recovered by the ROV. High-definition images taken by the Zeus video camera and the Scorpio still camera were used to document the sediment features related to mudflow and gas emission sites. During dives 268 and 272, seafloor features were recorded in the form of digital still photographs taken by the “Insite Scorpio,” high-definition camera "Insite Zeus Plus Colorzoom" and video DSPL. Gas-bubble samples and shallow sediment temperature measurements were also taken by the ROV robotic arm by means of deploying the relevant instruments (gas bubble sampler and T-stick).

3.7 Corers and Sediment Sampling

Seafloor sediment samples used in this study were taken during Cruises MSM15/2 and M84/2 at the Dvurechenskii and Helgoland mud volcanoes with three types of devices. The first device was the conventional gravity corer (GC). The MARUM GC is normally deployed with a 6 m steel barrel corer that drills by force of gravity (total weight is about 1,250 kg). On this device, two types of corers were used: I) the classic steel lamella and II) the other with robust steel lids. Temperature loggers could also be mounted as outriggers on the steel barrels to measure the temperature of deeper sediments. The maximum rope speed, when hoisting the corer, was usually less than 1.2 m/s because higher rope speeds caused intolerably loud noise from the winch. Thus, the rope speed was 0.5 - 1.2 m/s. The standard rope speed for lowering or hoisting a tool was 1 m/s.

The second device was the Dynamic Autoclave Piston Corer I (DAPC). It was developed for recovering and preserving pressurized sediment samples. It was designed to preserve shallow sediment layers to a maximum length of 2.65 m width *in-situ* pressure, which in the current study was the pressure at water depths of about 1,500 m. It was therefore especially suitable for recovering gas-hydrate-bearing sediment samples. The DAPC-I has a total length of 7.2 m, and its weight is ≃500 kg. The pressure chamber is about 2.6 m in length and 180 kg in weight. The underwater

USBL navigation system POSIDONIA was mounted on the cable (50 or 100 m above the DAPC) to provide highly accurate position information.

The third device was the Minicore (MIC). The MIC from MARUM can take 4 cores at once. Each of them has a length of 60 cm and a diameter of 62 mm. Typical rope speeds for lowering the MIC into the sediments were 0.4 - 0.6 m/s.

Chapter 4

Formation of the Helgoland Mud Volcano and its Activity in the Sorokin Trough, northern Black Sea

Tingting Wu[1], Heiko Sahling[1], Tomas Feseker[1], Rebecca Rendle-Bühring[1], Jiangong Wei[1, 2], Paul Wintersteller[1], Yann Marcon[3], Thomas Pape[1], Miriam Römer[1], Gerhard Bohrmann[1]

[1] *MARUM, University of Bremen, Klagenfurter Str., 28359 Bremen, Germany*

[2] *Guangzhou Marine Geological Survey (GMGS), Huanshidong Road, 510075 Guangzhou, China*

[3] *Alfred-Wegener-Institut Helmholtz-Zentrum für Polar- und Meeresforschung, 27570 Bremerhaven, Germany*

Submitted to *Marine and Petroleum Geology*

4.1 Abstract

The significance of submarine mud volcanoes as contributors to the global methane flux, global carbon cycle and thus to climate change, is still unclear. This is due to insufficient knowledge concerning their numbers, distribution, development and activity. Our research aims to help fill this gap through a detailed investigation of the recently classified Helgoland Mud Volcano (HMV), Sorokin Trough, northern Black Sea. We provide an account of its morphology, root and activity, evaluate its active formation mechanism and discuss methane emissions. In contrast to the traditional ship-mounted multibeam and single beam echo sounder PARASOUND system, the additional use of a near-to-seafloor, Autonomous Underwater Vehicle and Remotely Operated Vehicle provided high resolution micro-bathymetry and backscatter maps and, high definition (HD) seafloor imaging. Findings show that the HMV is a double-ringed seafloor structure consisting of two annular depressions (Inner Moat and Outer Moat), two annular positive reliefs (Inner Crest and Outer Crest) and one Active Center. Elevated water temperature anomalies indicate additional heat brought up to the surface through the upward migration of mud from a deep sub-surface source (diapir) via the central conduit. A NW-SE aligned fault across the HMV, which correlates with the high water temperature anomalies, suggest that the HMV's activity might also be fault controlled which could result in more violent eruptions. We suggest that the HMV has experience at least two mud eruptions, accompanied by gravity-driven sediment movement from the northwest. Gas emissions from the Active Center were seen to migrate ≥800 m in the water column. This methane, then dissolves and oxidizes very fast without its hydrate skin (outside the Gas Hydrate Stability Zone) therefore it is potentially impossible that it reaches the sea surface. We infer that the methane emitted from the HMV would thus not effect atmospheric methane concentrations and as a consequence, have very limited impact on climate change.

Keywords: mud volcano, Autonomous Underwater Vehicle, Black Sea, side-scan sonar, hydro-acoustic, gas hydrate, Remotely Operated Vehicle, micro-bathymetry

4.2 Introduction

Submarine mud volcanoes (MVs) are geological seafloor structures associated with gas emissions, pore water seepage, and mud expulsion (Milkov, 2000; Kopf, 2002). They usually consist of two types of periods defined by their activity, including an active period, which is usually characterized by catastrophic events with strong mud eruptions and gas emissions, and an inactive period (relative quiescent period), which is characterized by moderate activity (Deville and Guerlais, 2009). As the root of submarine MVs can be traced to depths of several kilometers below the seafloor (Kopf, 2008; Pape et al., 2014), the material extruded from MVs provides important information about the geological history of an area (Akhmanov, 1996) and the presence of potential hydrocarbon reservoirs (Ivanov et al., 1998; Blinova et al., 2003; Sahling et al., 2009; Pape et al., 2010b).

Although the global distribution of submarine MVs is extensive, they are mainly found in areas of rapid sedimentation or compressive tectonics (Milkov, 2000). Seismicity could contribute to the trigger process (Mellors et al., 2007; Davies et al., 2008; Tingay et al., 2008; Manga et al., 2009), but the activity of submarine MVs is mainly controlled by the local pressure regime within the sediment (Deville and Guerlais, 2009). Their formation mechanism has therefore been a topic of discussion since their discovery (Milkov, 2000), and two main mechanisms have been recognized: (1) fluid migration driven by shale diapirs and, (2) fluidized mud migration along faults and fractures (Kopf, 2002). Furthermore, gas emitted from submarine MVs is mainly composed of methane (Blinova et al., 2003) and varying amounts of CO_2, H_2S, and other hydrocarbon gases. Since methane is an important greenhouse gas (Lashof and Ahuja, 1990) and plays a key role in the global carbon budget (Dickens, 2004) and climate change (Judd et al., 2002), its emission from submarine MVs into the water column, and its influence on the atmosphere, has become a focal point of research in recent years (Dimitrov, 2002; Etiope et al., 2002; Wallmann et al., 2006; Foucher et al., 2010; Tsunogai et al., 2012). The significance of submarine MVs contribution to the global methane flux is still unclear, due to insufficient knowledge concerning the number and distribution of submarine MVs and their activity in terms of their formation and development (Milkov et al., 2003), which is usually accompany by varying amount of gas emission. This research, therefore aims to improve our understanding of submarine MVs formation and development through the analyses of

data collected from the recently classified Helgoland Mud Volcano (HMV) (Bohrmann, 2011a).

The HMV is located in the vicinity of the well-studied Dvurechenskii Mud Volcano (DMV) in the Sorokin Trough, which is one of the main areas with abundant MVs in the Black Sea (Blinova et al., 2003; Bohrmann et al., 2003; Sahling et al., 2009). However, because the HMV has only recently been classified, little is known about it. This study will therefore provide I) a detailed account of the HMV morphology, root, and activity; II) an evaluation of its active formation mechanism; and III) a discussion of gas emissions that have migrated from the deep subsurface.

In the past, submarine MVs have mainly been investigated by hydro-acoustic methods, such as seismic, ship-based multibeam, and side-scan sonar investigations (Kopf, 2003; Somoza et al., 2003; Zitter et al., 2005; Talukder et al., 2007). However, the resolution of the ship-based hydro-acoustic system limits the possibility of studying the morphological structure in detail. Consequently, this hinders a better understanding of the activity and formation mechanisms of MVs. Our investigation will therefore use a high-resolution data set collected with a near-to-seafloor autonomous underwater vehicle (AUV), which was applied to obtained high resolution bathymetry and backscatter data on the HMV. Sub-bottom profiling and water column profiling were conducted using a ship-based single beam echo sounder, ATLAS PARASOUND. The temperature loggers and cameras mounted on the frame of the Remotely Operated Vehicle (ROV) provided measurements of the ambient bottom water temperatures and visual observation of the seafloor, respectively.

4.3 Study Area

The central western basin (Ivanov et al., 1996) and the Sorokin Trough (Limonov et al., 1997; Bohrmann et al., 2003) are the two main areas where MVs have been discovered in the Black Sea (Fig. 4-1). Our study area is located in the Sorokin Trough, which is a 150 km-long and 50 km-wide depression along the Crimean Peninsula margin with water depths ranging between 800 and 2,200 meters below sea level (mbsl) (Tugolesov et al., 1985). The compressional tectonic regime, which has existed since the Eocene (Nikishin et al., 2003) and the weight of the overburden, led to the intrusion of water-saturated clay from the Maikopian Formation, which in turn, led to the formation of diapiric structures (Krastel et al., 2003). Most Black Sea MVs

are situated on the top or edge of these mud diapirs as an expression of mud extrusion from the seafloor (Ivanov et al., 1998).

In this study, we focused on a collapsed MV at a water depth of 2,060 mbsl, in the vicinity of the well-studied DMV within the Sorokin Trough (Fig. 4-1). Although this site was discovered during the 1996 TTR-6 Cruise (Woodside et al., 1997), no special attention had been paid to this mud volcano, which was first given its name, the HMV, during a research cruise (MSM15/2) in 2010 on-board the German R/V MARIA S. MERIAN (Bohrmann, 2011a).

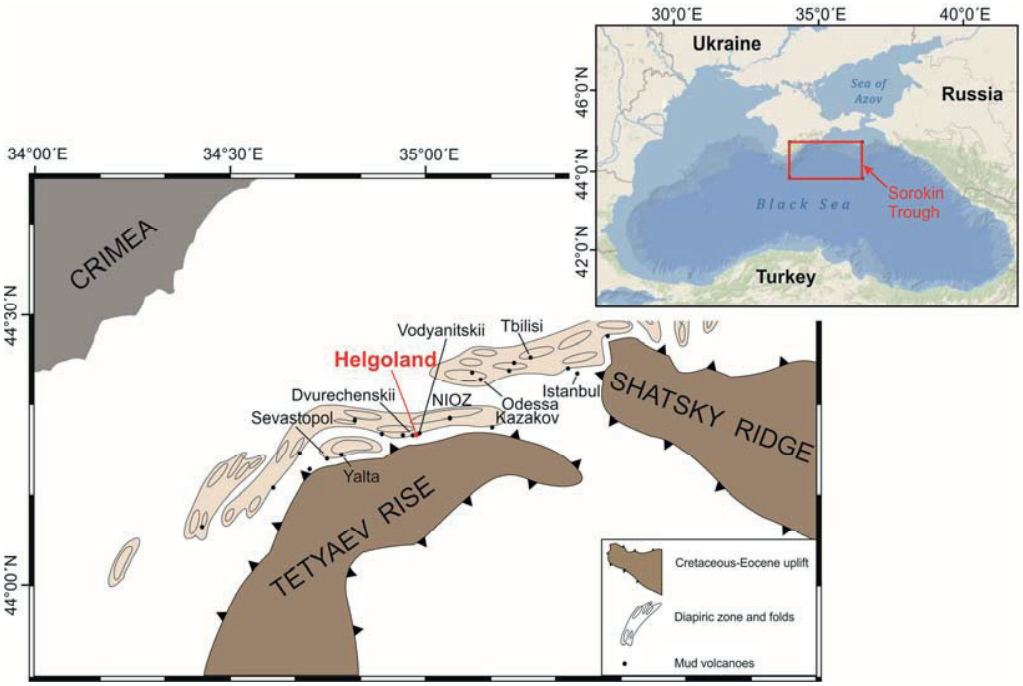

Figure 4-1: Mud volcano field at the Sorokin Trough between the Tetyaev Rise and Shatsky Ridge in the northern Black Sea (modified after Woodside et al., 1997). The Helgoland Mud Volcano (HMV) is a small mud volcano in the Sorokin Trough which is in close vicinity to the well-studied Dvurechenskii Mud Volcano (DMV). The inset map shows the location of the Sorokin Trough in the northern Black Sea.

4.4 Materials and Methods

In this study, diverse data collected with various methods during several research expeditions, including M72/3 in 2007 (Bohrmann and Pape, 2007), MSM15/2 in 2010 (Bohrmann, 2011a), and M84/2 in 2011 (Bohrmann, 2011b) were used.

The multi-beam bathymetric surveys were carried out using the ship-mounted Kongsberg Simrad EM120 (MSM15/2) and the EM122 multibeam echo sounders (M84/2). The EM120 and EM122 systems consist of 191 beams and 432 beams, respectively. The main frequency is 12 kHz, and the coverage angle is up to 150°. The bathymetry data collected from both systems was processed using the software MB-System (Caress and Chayes, 1996 and 2001).

During MSM15/2, a high-resolution bathymetric map and backscatter map of the HMV (Fig. 4-2A, Fig. 4-3 and Fig. 4-4A) were produced using MARUM's AUV Seal 5000. The AUV was steered 40 m above the seafloor at a speed of 3 knots, in order to obtain the best performance of the AUV-mounted RESON 7125b Multibeam echo sounder (400 kHz) to acquire micro-bathymetry and the BENTHOS dual frequency for side-scan sonar (100/400 kHz) acquisition. The interval of the track lines was designed to be 60 m. Both, the bathymetric and the backscatter map of 1 m resolution were produced using MB-System software (Caress and Chayes, 1996 and 2001).

A 6-m gravity corer was deployed to obtain gravity cores from the HMV to study the lithology and gas hydrate distribution in the shallow sediment during Cruises MSM15/2 (Bohrmann, 2011a) and M84/2 (Bohrmann, 2011b). The core site locations are shown in figure 4-5. During Cruise MSM15/2, GeoB14340 and GeoB14341 were taken in the Inner Region of the HMV from the Outer Crest and Inner Crest, respectively. During Cruise M84/2, GeoB15525-1 and GeoB15525-3 were recovered from the same location as GeoB14341, at Inner Crest. GeoB15530 was taken at the boundary between the Inner Moat and Active Center. In addition, the Dynamic Autoclave Piston Corer (DAPC; Abegg et al., 2008) was used to obtain pressure sediment cores containing sedimentary gas at two stations (GeoB14308; 15530).

During Cruise MSM15/2, two ROV dives were conducted for seafloor observations and bottom water temperature measurements. Seafloor observations were achieved using three camera systems mounted on the frame of the ROV QUEST 4000 (from MARUM, Bremen): two forward-looking video-cameras, i.e. a high-definition Insite ZEUS PLUS Colorzoom camera (HD camera) and a DSPL SSC 6500 Colorzoom camera (DSPL camera), as well as a downward-looking photo-camera (CANON Powershot G10, 15 MP). Images from the photo-camera were stitched together to form photomosaics of the seafloor (Fig. 4-9) with the LAPM Tool (Marcon et al., 2013; Marcon, 2014). Additionally, bottom water temperature measurements were

conducted using an autonomous miniature temperature logger (MTL; ANTARES Datensystem GmbH; Germany) installed on the frame of the ROV. The resolution of the MTL was 0.0006 °C and the interval of the recording time was set at 1 second to provide a continuous temperature record. All water column temperature data used in this study were measured below 2,040 m water depth.

Samples of gas venting from the seafloor at the Active Center of the HMV were collected at three sites (GeoB14339-1; 14339-3; 14356-1) with the Gas Bubble Sampler (GBS; Pape et al., 2010a) operated with the ROV. In addition to three ROV-mounted GBS stations, another DAPC (GeoB14308) station was also erected at the central area of the HMV (Fig. 4-5). The gases were retrieved via degassing from the DAPC and from the GBS on-board. Samples of sedimentary gas (DAPC), hydrate-bound gas (GC), and vent gas (GBS), were analyzed on-board, for their molecular compositions, with a gas chromatograph as described elsewhere (Bohrmann and Pape, 2007; Pape et al., 2010a). Stable carbon isotope ratios ($^{13}C/^{12}C$) of CH_4 in samples representative of all the gas types collected, were determined by GC-isotope ratio mass spectrometry (GC-IRMS) in Bremen. Carbon isotopic ratios are reported in δ-notation in parts per mil (‰) relative to the Vienna PeeDee Belemnite (V-PDB) standard.

Sub-bottom profiling and water column profiling were conducted by using the ship-mounted single beam echo sounder ATLAS PARASOUND during all cruises. The primary high frequency of 19 kHz was configured to look at the water column. This configuration was optimized to detect gas bubbles in the water column (Nikolovska et al., 2008). The opening angle of the transducer was 4°, leading to a footprint size of approximately 7 % of the water depth. The secondary low frequency of 4 kHz was configured for sub-bottom profiling. Data processing was conducted using the ATLAS PARASTORE software (El Naggar et al., 2007; Gerchow, 2009).

4.5 Results

4.5.1 Seafloor Mapping

In comparison to the DMV, which is a clearly positive seafloor feature, the HMV is a negative feature, forming a clear depression (Fig. 4-2A). The high-resolution bathymetric map obtained from the multibeam mounted on the near-to-seafloor AUV

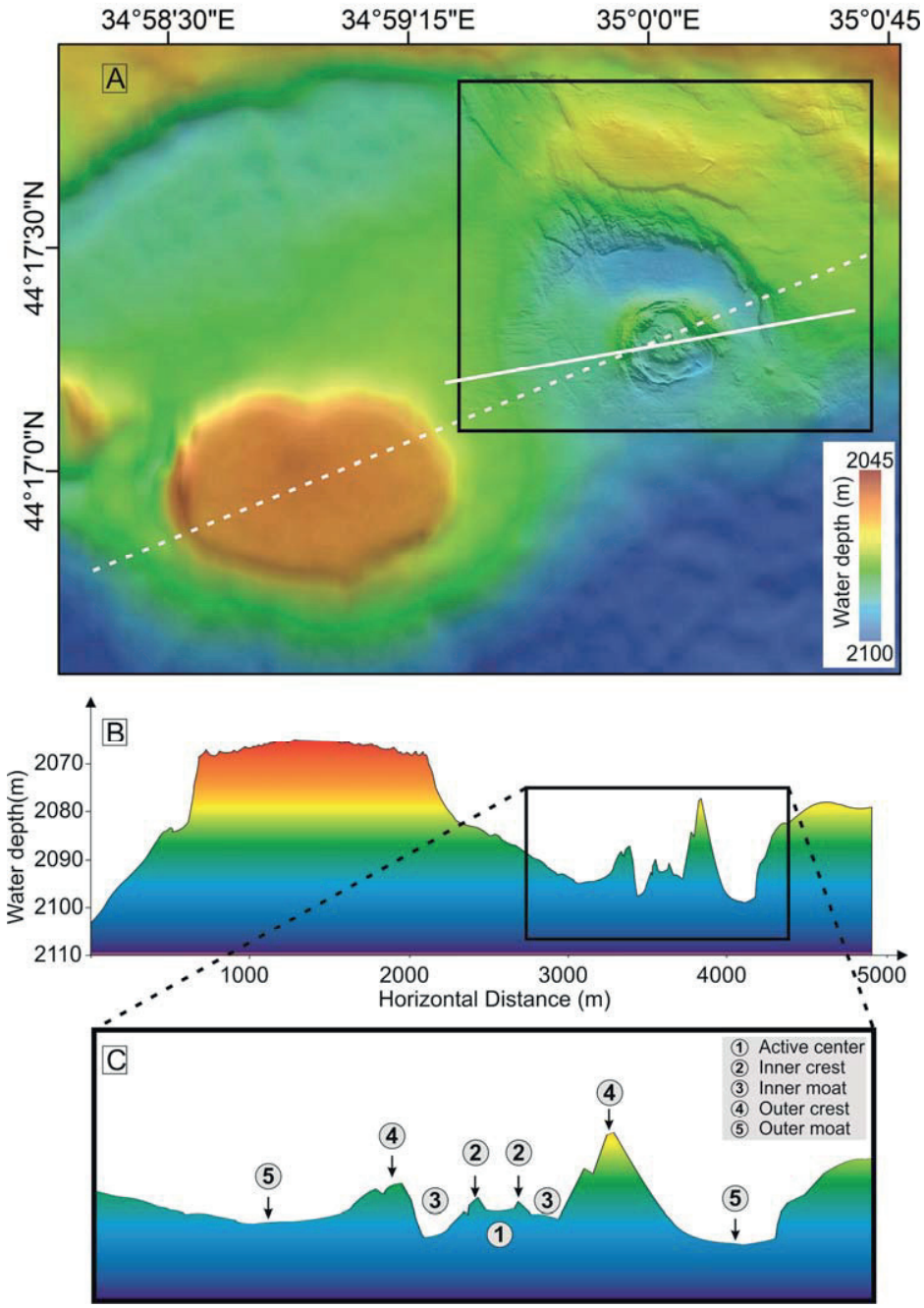

Figure 4-2: A: bathymetrical map of the DMV and the HMV. The black box indicates the area of the HMV where the AUV was applied to obtain a high resolution micro-bathymetric map as shown in figure 4-3. The solid white line which crosses the crests and moats around the Active Center shows the Parasound track line (see Fig. 4-8). B: Profile of the seafloor elevation along the dashed white line across the DMV and the HMV as shown in figure 4-2A. C: Enlarged view of the HMV with annotations of the double ring structure.

shows that the HMV is a 1,200 m-diameter, double concentric seafloor structure. Results of the HMV's morphological micro-features show that it can be divided into five ring-like areas arranged from the center to its rim according to its morphology (Fig. 4-2C). These fields can furthermore be allocated to an Inner Region (the Active Center (AC), the surrounding Inner Crest (IC), and the Inner Moat (IM)), and an Outer Region, composed of the Outer Crest (OC) and the Outer Moat (OM) shown in figures 4-2C and 4-4B.

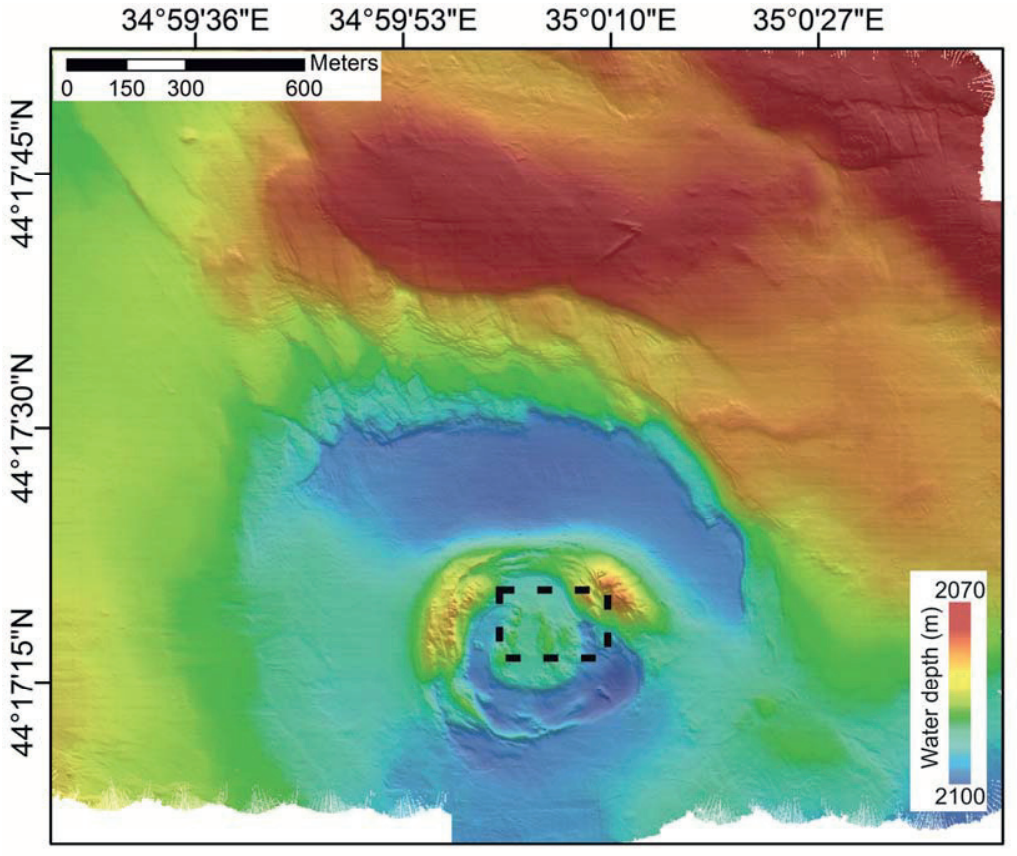

Figure 4-3: Micro-bathymetry obtained by AUV Seal 5000 which shows the microstructure of the HMV and the area in the vicinity. The dashed line box shows the area investigated by the ROV and gravity cores as shown in figures 4-5, 4-9 and 4-11.

The AC of the HMV, a N-S elongated depression, is located in the geometrical center and is bordered by the IC, which has a positive relief of ≃10 m above the surrounding seafloor. The AC is connected to the IM through gaps in the southern and northern parts of the IC (Fig. 4-3 and 4-4A). Because the AC is higher than the IM, mud is inferred to flow from the AC to the IM through the gaps. The IM and OM are two

annular depressions with smooth topographies. They are separated by the OC, which is a positive seafloor feature with a maximum relief of ≃25 m above the surrounding seafloor. The depth of the area around the HMV increases from north to south (Fig. 4-3). Seafloor erosion, which might be caused by the topography difference, could be observed at the northern border of the OM where the bathymetrical gradient is relatively high.

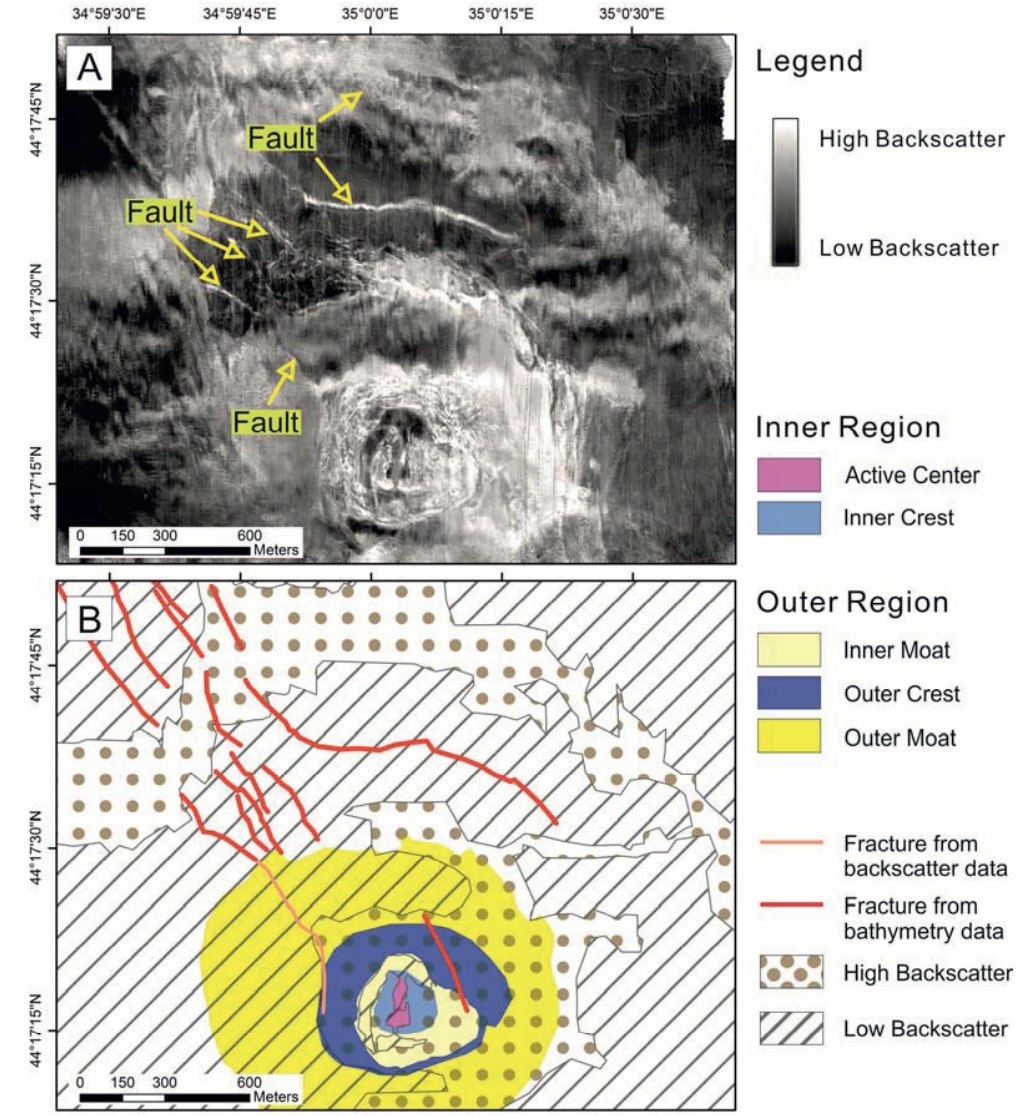

Figure 4-4: A: Backscatter map of the HMV. B: Interpretation of the HMV based on the high resolution bathymetry and backscatter maps obtained by AUV Seal 5000. The HMV and its surrounding field could be divided into five different areas based on the sediments and the seafloor morphology. Fractures were inferred from both backscatter and bathymetry data.

The high-resolution backscatter map obtained from the side-scan sonar mounted on the AUV provides information not only about the seafloor morphology, but also about the sediment reflection properties (Fig. 4-4). In general, backscatter within the HMV is higher than that in the surrounding area. Within the HMV, the intensity of the backscatter corresponds well with the five different areas defined by the micro-bathymetry. The AC, the IM, and the northern part of the OM show relatively low backscatter. In contrast, high backscatter is observed in most of the area within the IC and the OC. A large patch of high backscatter around the HMV could be seen in the northern part surrounding of the mud volcano. High amplitude reflections in the water column documenting gas emission sites at the seafloor were observed in the raw side-scan sonar map (Fig. 4-6).

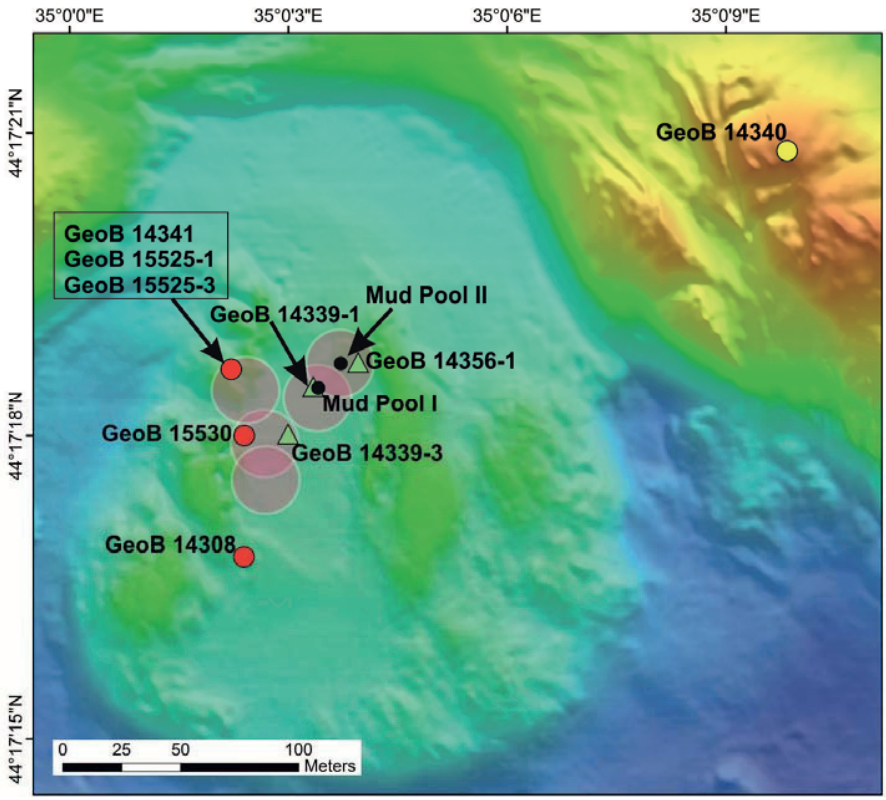

Figure 4-5: Location of the cores taken in the center of the HMV. The red dots and yellow dots indicate the location of the sediment cores with and without gas hydrate, respectively. The black dots show the location of the major seafloor features known from the seafloor observation. The green dots show the Gas Bubble Sampler sampling sites. The areas in pink indicate the location of the flares inferred from the side-scan sonar data.

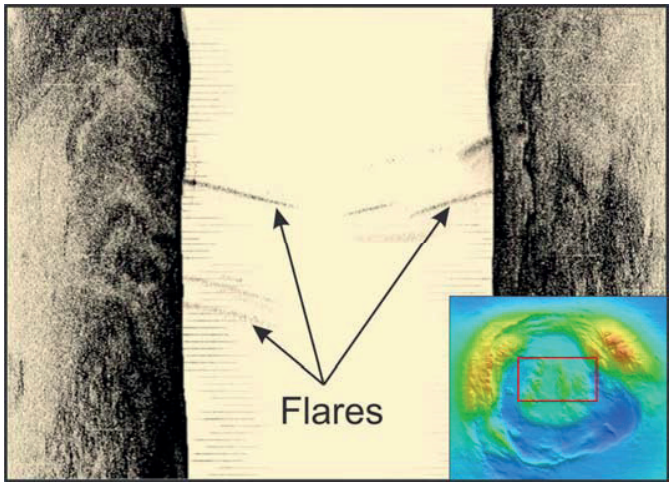

Figure 4-6: A side-scan sonar map obtained with the AUV shows the gas emission flares, represented by high amplitude reflectors, from the center of the HMV into the water column.

4.5.2 PARASOUND Investigations

Acoustic water column data and subsurface sediment profiles provided information on gas release and sub-surface sedimentary structures, respectively. Distinct sediment layers and tectonic induced normal faulting were evident in the sub-bottom profile of the Outer Region of the HMV (Fig. 4-7A). These findings correspond well to the circular fault interpreted from the backscatter data (Fig. 4-7B and for orientation see Fig. 4-7C). In the Inner Region of the HMV a typical blanking zone in the subsurface was observed. This could represent the accumulation of gas in the shallow sediment of the mud volcano (Fig. 4-8A). At the same location, the water column profile above the center of the HMV, showed strong backscatter that extended up to 1,200 m above the seafloor. This gas flare represents distinct methane seepage (Fig. 4-8B).

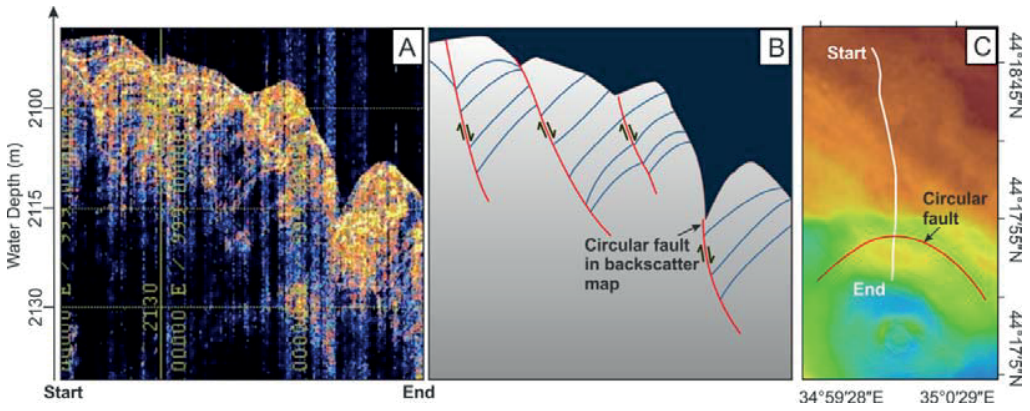

Figure 4-7: A sub-bottom profile (A) and a subsurface sedimentary interpretation (B) along a transect indicated by the white line in (C), from the area surrounding the HMV to the HMV's Outer Crest.

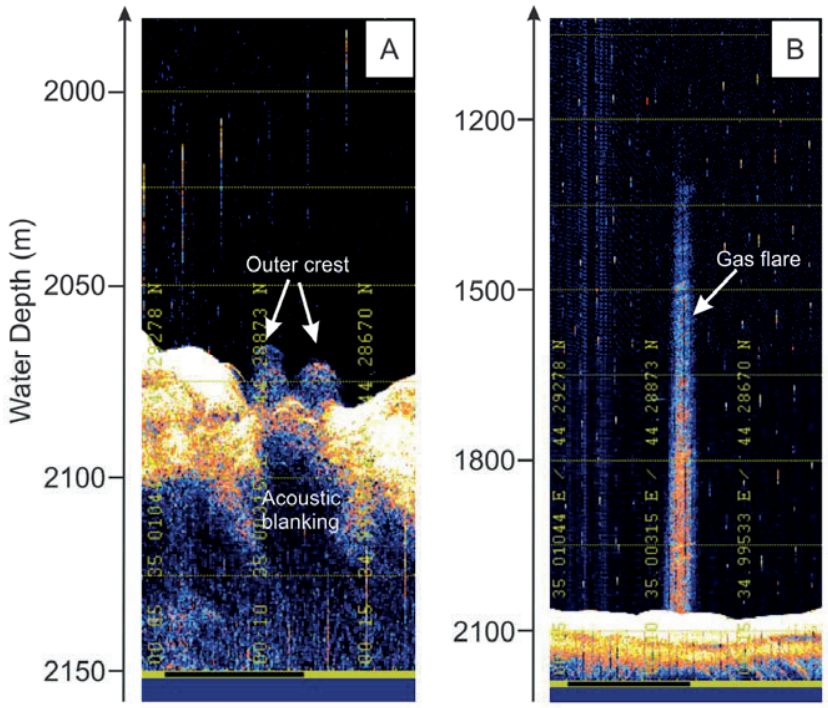

Figure 4-8: Sub-bottom profile (A) and water column profile (B) of the HMV recorded by PARASOUND. Gas was inferred to be accumulated within the shallow sediment of the HMV as indicated by acoustic blanking (Profile A). Gas emissions were clearly recorded as high backscatter in the water column in profile B (a so-called gas flare).

4.5.3 Seafloor Observations

Visual seafloor inspections of the HMV's Inner Region, obtained from the different cameras, show that the sediments and the seafloor features in this area are spatially heterogeneous. The track lines of the ROV dives to the Inner Region are shown in figure 4-9, and the corresponding images in figure 4-10.

Observations made for the HMV show that the center is where the seepage activity of the mud volcano is most intense. As documented by the presence of mud pools (Fig. 4-9 and 4-10A) and occurrence of gas bubble emissions (Fig. 4-10B), the center was the most active area of the HMV. Mud Pool I (Fig. 4-9) had an oval shape with clearly defined rims. A second mud pool (Mud Pool II) was observed ≃17 m to the northeast of Mud Pool I. For Mud Pool II (location Fig. 4-5) rims were not identified but light muddy sediment with bubble emissions were observed. Using the ROV, we also observed gas bubbles emitted more or less continuously from the mud pools. Mud

was entrained in the water column, but the ascending gas bubble emissions led to a certain amount of water column turbidity. A patch of mud flow was observed in the AC (Fig. 4-10C), which record its spreading process from its erupted center to surroundings. The light grey to dark grey color spectrum depicts different dewatering stages of mud flows that erupted at different times.

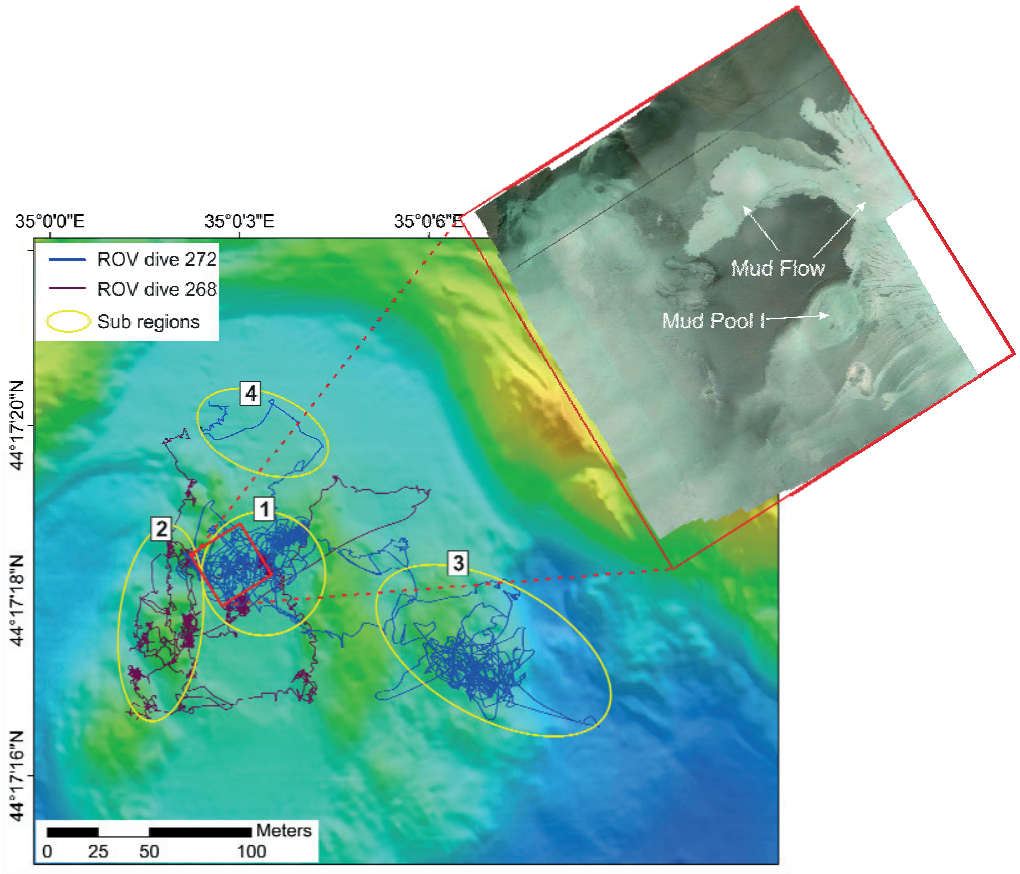

Figure 4-9: Track lines of the two ROV dives during Cruise MSM15/2. The ROV dives cover three areas including (1) the Active Center (2, 3) the Inner Crest and (4) the Inner Moat. The photo mosaic (the inset) is a combination of the photos taken by the HD camera mounted on the frame of the ROV.

In contrast to the AC (evidence of gas emission sits, mud pools and etc.), the IC is less active (collapsed structures, gas bubbles, bright bacterial mat or bright mud). The western part of the IC is characterized by several bright patches (Fig. 4-10D), which might be consolidated mud flows partly covered by bacterial mats. Gas bubble emissions were also observed from a recently formed collapsed structure (Fig. 4-10E). In the eastern part of the IC, the seafloor shows evidence of gravity-driven movements, by the gliding and sediment creeping features (Figs. 4-10F and G). In the

IM, grayish patches and mud flows were observed (Figs. 4-10H and I), they were located at the northern and eastern parts of the mosaic (Fig. 4-10C sub-map), which could have originated from Mud Pool II (Fig. 4-5) 17 m to the south. Those sediments were transported from the AC at different times.

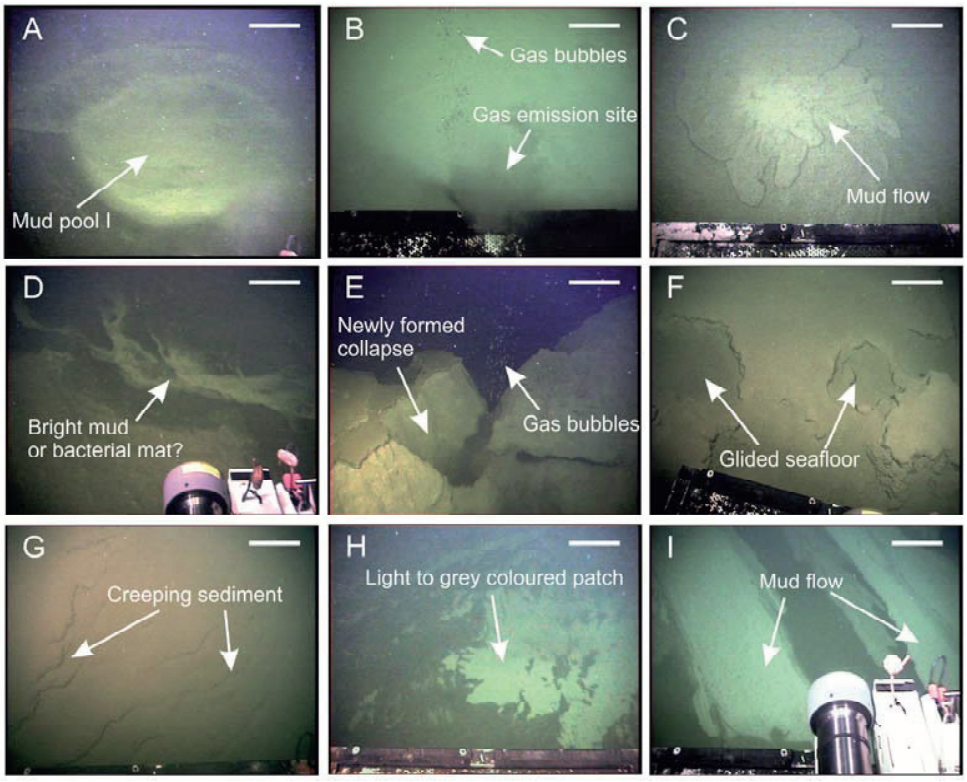

Figure 4-10: Photos taken during the ROV dives (Fig. 4-8). Photos A, B and C were taken from the Active Center of the HMV which shows the typical characters of a mud pool, gas bubble emissions and mud flow, respectively. Photos D-G were taken from the Inner Crest. Photos H and I were taken from the Inner Moat. The white scale bar shown in each figure represents a length of ≃30 cm.

4.5.4 Temperature of Bottom Waters

The water temperatures measured over the center of the HMV ranged from 9.107°C to 10.756°C. When we subtract the normal, ambient Black Sea water temperatures, which changes with depth, the abnormal water temperature values are extracted (Fig. 4-11A). These show temperature anomalies where the bottom water over the HMV increased from 0.027°C to1.652°C, with the highest value directly over the AC (Fig. 4-11A). This indicates that additional heat is being released from the HMV into the surrounding water. Moreover, the distribution of the high temperature values shows

the same orientation as the fault that crosses the HMV, which was interpreted from the micro-bathymetry and backscatter maps. In addition, elevated water temperature values, up to 1.652°C higher than the ambient bottom water, were observed sporadically (red spots in Fig. 4-11A).

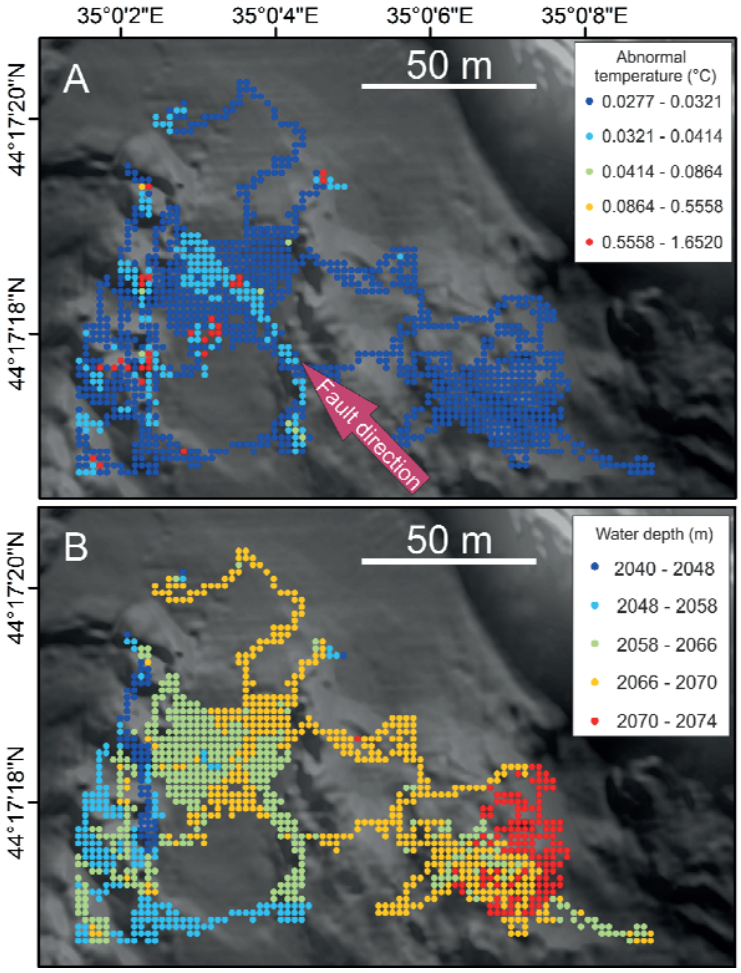

Figure 4-11: A: Temperature anomalies of the bottom water at the center of the HMV expressed by subtracting the normal ambient Black Sea water column temperatures from the temperature obtained from the T-loggers mounted on the frame of the ROV. Elevated temperatures are distributed linearly in the direction of the inferred fault. B: Water depth of the ROV measurement sites.

4.5.5 Composition of Sedimentary, Hydrate-bound Vent Gas

Methane was the dominant constituent of the gas venting from the HMV. From the analyses (in mean/average), it contributed ≥99.784 mol-% (Σ (C1–C4, CO_2)) of the

compounds, followed by carbon dioxide (>0.104 %), ethane (>0.035 %) and propane (>0.004%). Accordingly, the respective molecular hydrocarbon ratio (C_1/C_{2+}) was ≥1,689. In addition, venting gas collected at station GeoB14339-3, that was characterized by fresh mud and relatively intense gas emission, was enriched in C_{2+} hydrocarbons relative to the other two GBS stations (GeoB14339-1; 14356-1). Compared to all vent gas samples, sedimentary gas taken during degassing of DAPC core GeoB14308 revealed depletions in methane, propane, as well as *iso* and *n*-butane but, enrichments in carbon dioxide. $\delta^{13}C$ of methane in sedimentary, hydrate-bound and vent gas ranged between –58.1 and –63.6 ‰.

4.5.6 Lithology

The lithology of the HMV's Inner Region, as observed in the OC core GeoB14340, shows the typical sediment sequence for the Black Sea. It consists of a fine-laminated sequence of alternating white coccolith-rich laminae, sapropelic mud, a pale-grey mud unit and sapropels, and a sapropelic mud unit, which corresponds to Units I and II of the five main lithological units of the Black Sea (Bohrmann, 2011a). In contrast, the IC core GeoB14341 contained homogenous grayish clay with a strong odor of hydrogen sulfide. White gas hydrates with bubble fabric structure were recovered at sediment depths of less than two meters from cores, GeoB 15525-1 and GeoB 15525-3 located in the IC region and, GeoB 15530 on the boundary between the IC and AC. Gas hydrate was also recovered from GeoB 14308 which was recovered in the AC.

4.6 Discussion

4.6.1 Morphology, Root, and Activity of the HMV

4.6.1.1 Morphology

The Sorokin Trough is an area in the Black Sea where MVs have been extensively researched (Blinova et al., 2003; Bohrmann et al., 2003). Based on their morphological shapes, MVs in the Sorokin Trough can be divided into three categories, including I) cone-shaped, II) flat-topped, and III) collapsed structures (Krastel et al., 2003). The high resolution bathymetry map shows that the HMV is a double-ring seafloor structure consisting of two annular depressions (IM and OM),

two annular positive reliefs (IC and OC), and one AC (Fig. 4-4). Therefore, based on the classification by Krastel et al., (2003), the HMV, with a diameter of ≃ 1.6 km, falls into category III), a typical collapsed structure.

4.6.1.2 Root

The DMV, which is in the vicinity of the HMV, is located on top of a mud diapir caused by the compressional tectonic regime between the Tetyaev Rise and the Shatsky Ridge in the south and the Crimean Peninsula in the north (Krastel et al., 2003). Diapirs underneath MVs can sometimes served as a feeder channel or conduit and act as a path for mud transportation from the deep subsurface. The feeder channel, which facilitates mud transport at the DMV, was interpreted to have originated from 4 km below the seafloor, as seen in the seismic data (Krastel et al., 2003). From the seismic data and figure 4-1, we can see that the same diapiric zone occurs beneath both the DMV and the HMV. Therefore, mud breccia extruded from the HMV potentially originates from a depth of 4 - 5 km, stratigraphically the Oligocene to Lower Miocene Maikopian Formation, which is the same root for the DMV.

4.6.1.3 Activity

4.6.1.3.1 Fault Formation

There are two major types of mud volcano activity, including (1) explosive mud eruptions with huge amounts of fluid and gas, and (2) continuous or intermittent modest flow of mud and gas at gryphons (Deville and Guerlais, 2009). Normally, MVs with collapsed structures are inferred to experience violent mud eruptions (Kopf, 2002). Previous studies proved that the neighboring DMV, which is located on top of fault zones that reach the seafloor, experiences violent mud eruptions (Krastel et al., 2003). In our study, we also observed a NW-SE fracture/fault, which cuts through the HMV (Fig. 4-4). Therefore, we inferred that this fault/fracture might serve as the pathway for upward fluid migration, also resulting in violent mud eruptions.

4.6.1.3.2 Thermal Impact of the HMV's Fluid Discharge on Bottom Waters

Both bottom water and sediment temperature distribution could reflect the activity of MVs. Temperature elevations both in the shallow sediment and the bottom waters have been observed for many MVs, for instance, the DMV in the Black Sea (Feseker et al., 2009) and the Håkon Mosby Mud Volcano offshore northern Norway (Foucher et al., 2010; Pape et al., 2011).

In this study, the bottom water temperature at the HMV center ranged between 9.107°C and 10.756°C. In contrast to the normal Black Sea bottom water temperature the temperature at the center of the HMV was therefore elevated by between 0.027°C and 1.652°C (Fig. 4-11A). The normal Black Sea bottom water temperature was calculated from an equation that inferred from the measured temperature vs. depth profiles (http://sfp1.ims.metu.edu.tr/ODBMSDB/). The equation is: temperature = 0.0001506×depth+8.793 (°C) and it is only used for calculated temperatures below a water depth of 1800 m where there is no temperature measurement data. Kaul et al. (2006) pointed out that a 4 m thick mud flow needs only 3 - 4 months before it is cooled down after an eruption event. Therefore, we infer that the observed elevated water temperatures over the center of the HMV have been caused by heat convection brought by the upward mud advection through the central conduit, indicating that the HMV was recently active. This assumption is also supported by evidence that the thermal gradient of shallow sediment at the AC is ≃ 1.2°C/m (Bohrmann, 2011b), which is much higher than the ambient value of 0.037°C/m (Feseker et al., 2009). The sporadically high temperatures indicated in figure 4-11 by red dots shows temperature elevations up to 1.652°C (Fig. 4-11A). This is thought to be caused by highly active emission sites. We should be sure that the comparatively higher temperature values do not correspond to the points with high water depth. After careful observation of the water depth map of the ROV measurement sites (Fig. 4-11B), we can see that there is no apparent trend or correlation between the higher temperature values and water depth. As a result, it could be inferred that the higher temperature values along the line might be the result of high fluid flow controlled by the fault.

4.6.2 Active Formation Mechanism of the HMV

The material erupting from the MVs is normally composed of gas, fluidized mud, mud clasts, and rock fragments (Kopf, 2002). Among MVs, low backscatter usually represents normal hemipelagic sediment and fluidized mud, whereas high backscatter usually indicates the presence of carbonate crusts, gas hydrates, and mud clasts and/or

rock fragments (Volgin and Woodside, 1996; Limonov et al., 1997). The high-resolution backscatter map of the HMV therefore indicates the deposition of the various lithologies, which in turn, contribute to a better understanding of the HMV's activity and formation process.

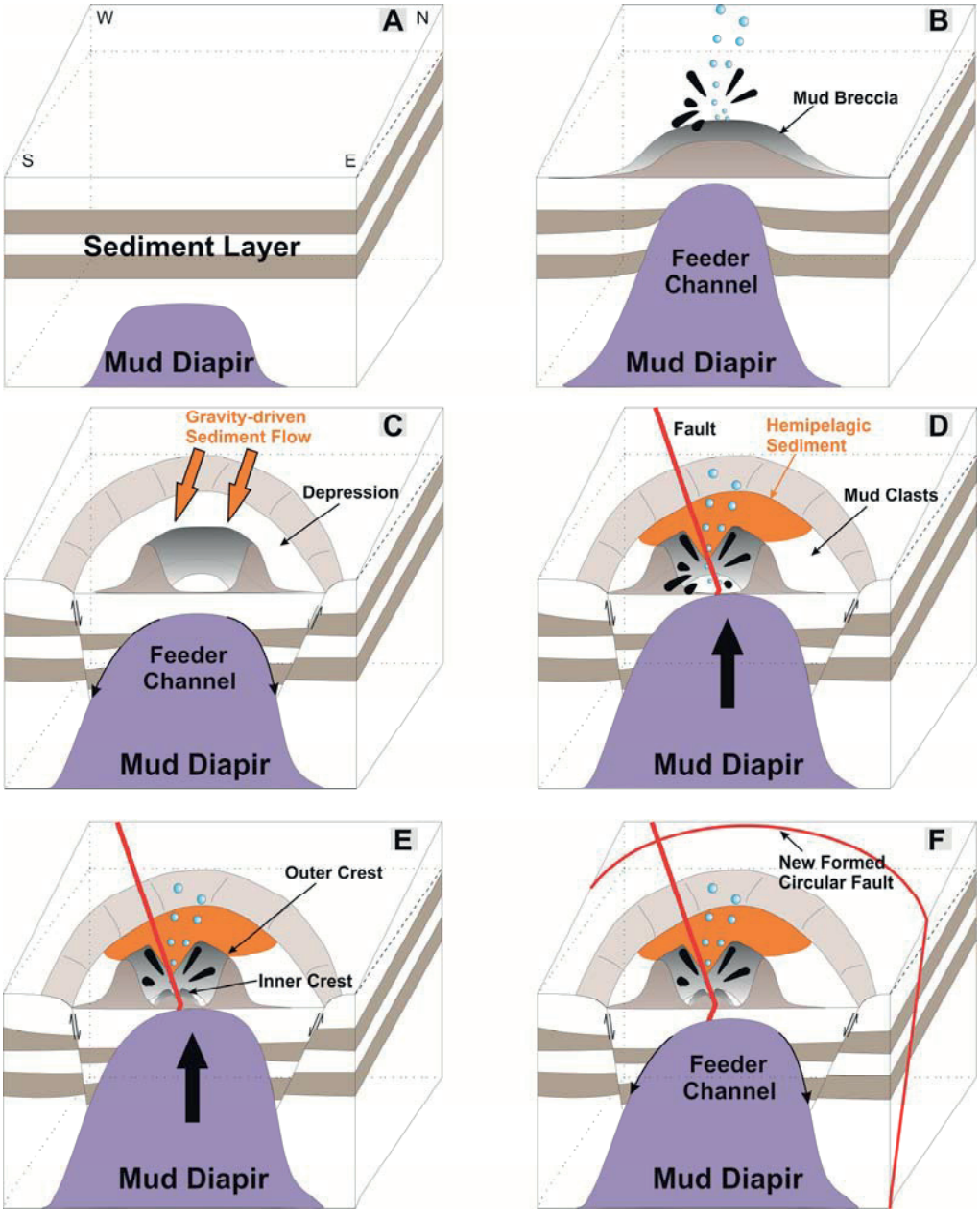

Figure 4-12: The model explains the potential formation mechanism of the HMV controlled by mud diapir and gravity-drive sediment flow.

Based on the double concentric ringed elevated structures (The IC and the OC) from

both the micro-bathymetric and high-resolution backscatter map (Fig. 4-4A), we inferred that the HMV has experienced at least two violent eruptions in the past, accompanied by gravity-driven sediment movements (Fig. 4-12A-F). During the period of the first eruption (Fig. 4-12B), the HMV formed a bulge on the seafloor due to a continuous supply of mud (with high enough pore-fluid overpressure) from the deep subsurface through the feeder channel. Mud breccia consisting of fluidized mud clay and mud clasts flowed out of the AC to the IM through northern and southern seafloor gaps (which have lower elevation than around area of the IC) in the IC. At that time, the OM was inferred to be covered by mud breccia. When the overpressure beneath the feeder channel was no longer able to support the supply of fresh mud (Fig. 4-12C), the OM depressed due to the shrinkage of the sediment volume in the subsurface (Neurauter and Roberts, 1994) and a crater also formed in the center of the HMV (Fig. 4-12C). The fresh mud lost water and became consolidated. The high backscatter patches of the OM and the high backscatter of the OC and IC, therefore, are all believed to represent mud clasts (Fig. 4-12D). The gravity-driven sediment flow would have been generated due to the elevation difference caused by the depression of the OM (Fig. 4-12C). The western part of the OM, which shows relatively low backscatter, is therefore inferred to be covered by typical hemipelagic sediment transported from the northwest of the HMV (Fig. 4-12D).

During the second period of mud eruption, the seafloor within the HMV crater bulged (Fig. 4-12D). The process of the second eruption is very similar to that of the first eruption. However, the magnitude on violence of the second eruption is likely to have been much smaller. The influence of the second eruption was therefore constrained to the crater, the IM and IC. During the second active period, mud extruded from the AC and flowed out to the IM through gaps in the IC. The southern part of the IM shows high backscatter due to consolidation and the mud clasts. In contrast, the northern part of the IM and the AC are covered by fresh and fluidized mud, indicated by low backscatter.

4.6.3 Fate of the Gas

Gas emission is a major feature of active MVs. It was also discovered in the active HMV. In this study, gas emissions from the seafloor were observed both indirectly from the hydro-acoustic data (Fig. 4-6 and 4-8), as well as directly, from the seafloor observations (Fig. 4-10B and E). Gas samples were taken using GBS and DAPC and

retrieved and analyzed on-board. The molecular hydrocarbon ratio (C_1/C_{2+} ≥1,689) indicates that sedimentary gas (DAPC), hydrate-bound gas (GC), and vent gas (GBS) at the HMV predominantly originate from microbial production. The molecular composition and $\delta^{13}C\text{-}CH_4$ ratios of these gas samples resemble those reported for sedimentary gas from the DMV (Blinova et al., 2003; Feseker et al., 2009) and vent gas from the Vodyanitskii MV (Sahling et al., 2009). As shown in figure 4-1 and Krastel's (2003) research, we believe the DMV and HMV belong to the same diapir zone. Therefore, it might be speculated that at least the HMV and the DMV share their gas source(s).

Since methane is the dominant gas emitted at the HMV and is also a greenhouse gas (Lashof and Ahuja, 1990), it is important to discuss its fate. There are at least four fates for the methane, including: (1) formation of gas hydrate, (2) accumulation within the sediment as a gas reservoir, (3) consumption by bacteria in sediments, and (4) emission from the seafloor into the water column.

Gas hydrate is a crystalline compound composed of water and gas molecules (Bohrmann and Torres, 2006). The formation of gas hydrates requires low temperatures and high pressure (Sloan, 2003). When gas migrates from the deep subsurface, it will form gas hydrate at a depth where the pressure and temperature conditions are suitable (Bohrmann and Torres, 2006). Gas hydrates have been discovered in gravity cores GeoB15525-1 and GeoB15525-3, indicating that the shallow sediment of the IC is well in the gas hydrate stability zone (GHSZ; Bohrmann and Torres, 2006). Along with the observed gas bubble emission into the water column it also shows that methane concentrations exceed solubility in shallow sediments of the HMV AC and IC. Because the HMV is only about 1.5 km away from the center of the DMV, and shares the same sea water environment, the GHSZ of the HMV could also be referred to as the GHSZ of the DMV (Bohrmann et al., 2003; Feseker et al., 2009).

Notably, the bottom water or sediment temperature of a MV normally increases due to large amounts of heat brought up by fluidized mud from the deep subsurface (Feseker et al., 2008). This has been verified by relative warming of the bottom waters above the HMV (Fig. 4-11). The elevated temperatures, especially within the central conduit, prevents methane from forming hydrate, but facilitates gas accumulation in the shallow sediments due to the low permeability of the mud (Feseker et al., 2009). This

is evidenced by the gas accumulation represented by a blanking zone in the sub-bottom profile within the shallow sediments of the HMV's center (Fig. 4-8A). High pressure is likely to build up due to the continuous gas accumulation, which could potentially become one of the factors for periodically violent mud eruptions.

The remaining gas, which does not form hydrate, migrates to a shallow depth in the sediments where it is partly or totally consumed by anaerobic methane oxidation (AOM) (Suess and Whiticar, 1989; Borowski et al., 1999). When the methane flux is high enough, the surviving methane, which is neither enclosed in the hydrate nor consumed by the AOM, will be emitted from the seafloor into the water column. Within the GHSZ, gas bubbles migrate through the water column with a hydrate coat on the surface of the bubble (McGinnis et al., 2006; Sauter et al., 2006), efficiently preventing the methane from dissolving or being oxidized (Rehder et al., 2002). This could explain why the gas bubbles observed in this study travelled more than 800 m in the water column up to a depth of ≃1,300 m (Fig. 4-8B). However, because methane bubbles without the protection of hydrate or oil coatings are dissolved and oxidized very fast (outside the GHSZ), it is potentially impossible for methane bubbles to reach the sea surface and be emitted into the atmosphere. We inferred, therefore, that methane emitted from the HMV might have a very limited impact on the global carbon budget.

4.7 Conclusions

The newly classified Helgoland Mud Volcano was investigated, using a variety of instruments (e.g. AUV, gravity corer, ATLAS PARASOUND, temperature loggers, and an ROV). The major conclusions drawn are as follows:

1. Morphology: The HMV is a negative seafloor structure with a collapsed structured morphology consisting of a double ring seafloor structure composed of two annular depressions (IM and OM), two annular positive reliefs (IC and OC) and one AC.

   Root: A mud diapir below the HMV, inferred from the seismic data (Krastel et al., 2003) is the likely source of the mud breccia extruded from the HMV via a central conduit. Elevated water temperature anomalies over the HMV are caused by the upward mud migration through the central conduit.

Activity: The presence of a NW-SE fault across the HMV and a correlating distribution of higher water temperature anomalies over the HMV suggest that the activity of the mud volcano might be controlled by the fault. This could result in more violent mud eruptions.

2. The active formation mechanism of the HMV is a combination of diapirism and fault formation. Furthermore, micro-bathymetry and backscatter map data indicated that the HMV has experienced at least two mud eruptions accompanied by gravity-driven sediment movement from northwest of the HMV.

3. Gas emissions from the AC of the HMV were confirmed both indirectly via ATLAS PARASOUND and directly, by seafloor observations. Based on the water column profiling, methane emitted from the HMV cannot reach the sea surface and therefore has no effect on atmospheric methane concentrations.

4.8 Acknowledgments

We thank the captains and crews of *R/V* METEOR and *R/V* MARIA S. MERIAN for support during the research cruises M72/3 and M84/2 and MSM15/2. We also thank the ROV QUEST team from MARUM for handling the Remotely Operated Vehicle (ROV). The work was partly funded through the DFG - Research Center and the Cluster of Excellence "The Ocean in the Earth System" MARUM - Center for Environmental Sciences. Tingting Wu was sponsored by the China Scholarship Council (CSC).

Chapter 5

Mud Transportation Characteristics of the Sorokin Trough Dvurechenskii Mud Volcano, northern Black Sea

T. Wu[1], T. Feseker[1], H. Sahling[1], R. Rendle-Bühring[1], J. Wei[1,2], G. Bohrmann[1]

1 MARUM, University of Bremen, Klagenfurter Str., 28359 Bremen, Germany

2 Guangzhou Marine Geological Survey (GMGS), Huanshidong Road, 510075 Guangzhou, China

5.1 Abstract

Knowledge on the internal and surficial mud movements of mud volcanoes is essential to understand their activity and evolution. In this study, we use data collected for the Dvurechenskii Mud Volcano (DMV) in the Sorokin Trough, northern Black Sea to I) determine morphological signatures and processes for mud movement II) evaluate the vertical and horizontal mudflow, temperatures and velocities and III) discuss the formation time of the DMV.

Detailed bathymetric and backscatter maps cannot, however, be achieved using standard ship-based multibeam systems. Therefore, we used state-of-the-art, data acquisition methods mounted on an Autonomous Underwater Vehicle (AUV) and a Remotely Operated Vehicle (ROV) during cruise MSM15/2 (2010). These methods include AUV-mounted multibeam and side-scan sonars, and ROV mounted HD-cameras. In addition, a long term T-mooring (>3 yrs) and *in-situ* gravity core mounted temperature loggers were used during cruise M72/3 (2007) and MSM15/2 (2010) and M84/2 (2011), respectively. They were deployed to obtain a high resolution bathymetric seafloor map, visual seafloor imaging, and internal and external mud temperatures for the first time at the DMV.

The data shows distributional variations in the DMV's mud temperature gradients which range from 0.336 - 0.468°C/m on the margins and 5.884°C/m in the center. High temperature anomalies of up to 23°C at 75 mbsf, in the center of the DMV plateau, were also observed. Together with ubiquitous concentric ridges, that radiate out from the summit, these findings might be the internal and surfical manifestation for cyclic mud eruption processes. This also suggests that the DMV is experiencing a relatively active period. Vertical mud flow velocities of 0.22 m/day and horizontal mud flow velocities around the conduit of 0.19 - 0.22 m/day, could be inferred from either real *in-situ* data and/or theoretical models. Based on a simplified model that utilizes the estimated vertical and horizontal velocities it was feasible to approximate the time of the DMV's formation. Estimates suggest that the DMV is ≃22 - 26 yrs old. However, these age estimates may be erroneous due to some factors not integrated into the model e.g. mud consolidation, cyclic mud eruptions and seafloor erosion via deep water currents. These state-of-the-art data acquisition methods have therefore provided information on the DMV's mud migration characteristics and allowed for an

evaluation of vertical and horizontal mud flow patterns and velocities and thus helped improve our understanding of MV activity and evolution.

Keywords: Black Sea; Dvurechenskii Mud Volcano; mud movement; AUV; sediment temperature

5.2 Introduction

Mud volcanoes (MVs) are terrestrial and marine morphological structures created by a pressurized mud diapir which breaches the earth's surface (Higgins and Saunders, 1974; Kopf, 2002). They occur almost everywhere on the Earth and are commonly associated with compressional tectonics at convergent margins (Higgins and Saunders, 1974; Barber et al., 1986; Kopf et al., 1998). Mud volcanoes have been studied intensively for many years due to their association with the occurrence of hydrocarbons and fluid discharge, which are important components of the global carbon cycle (Milkov, 2000; Dimitrov, 2002). Earlier research suggests that MVs are an important source of methane (CH_4) in the atmosphere and oceans (Dimitrov, 2003; Milkov and Etiope, 2005). The total amount of CH_4 emitted from MVs is estimated to be ≃33 Tg/year (Milkov et al., 2003). However, the activity of mud volcanoes is not constant and comprises both Activity Phases of mud eruption and, Dormant Phases of inert mud (Deville and Guerlais, 2009; Foucher et al., 2010). It is therefore, important to have comprehensive knowledge on the characteristics of mud volcano activity to better estimate methane emissions.

Historical data provides useful information to decipher the temporal variability of onshore MV activity over a timescale of years to tens of years (Planke et al., 2003). Such information is however, generally missing for deep offshore mud volcanoes. Studies on submarine MV activity can only be achieved by either I) seafloor observations using cameras or other proxies, such as temperature (Feseker et al., 2008; Feseker et al., 2009) and pressure (Feseker et al., 2014) or, II) through detailed high resolution bathymetric mapping of the seafloor morphology (Foucher et al., 2010). In recent case studies on the active Håkon Mosby Mud Volcano on the southwest Barents Sea Shelf, Foucher et al. (2010) used a comparative analysis of the high-definition bathymetric and backscatter maps obtained in 2003 and 2006, to observe subtle morphological changes over the entire crater and interpreted them to be the consequence of mud eruption events (Foucher et al., 2010). Feseker et al. (2014)

extended the Håkon Mosby Mud Volcano research through a time series data analysis for pressure, temperature, pH and seafloor photography using a benthic observatory, collected over a period of 431 days. 25 pulses of hot subsurface fluids were documented, accompanied by eruptions that changed the landscape of the mud volcano. They also observed substantial lateral flow of mud at average velocities of 0.4 m/day, and significant emissions of CH_4 and CO_2.

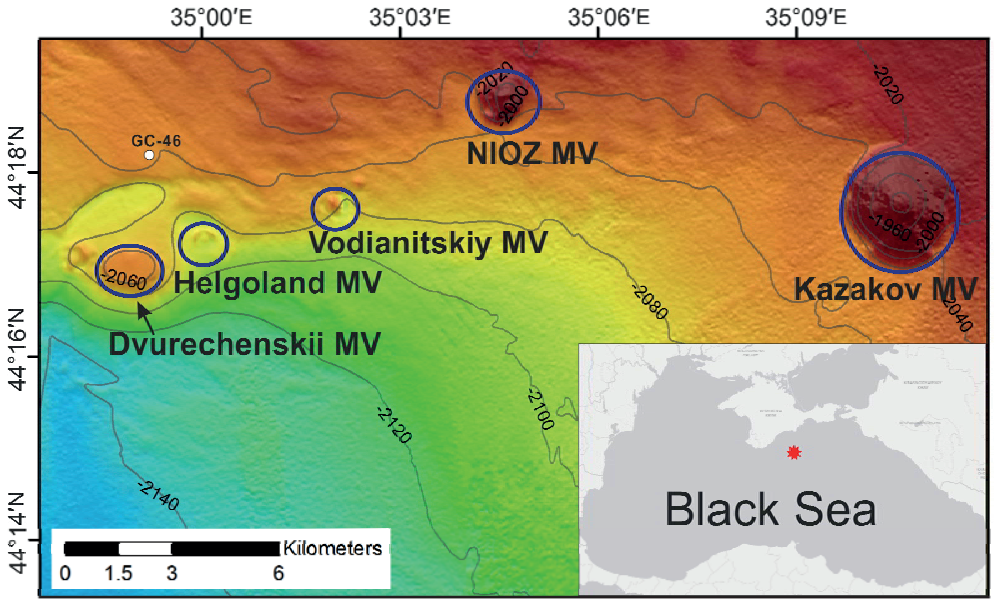

Figure 5-1: The Dvurechenskii Mud Volcano (DMV) forms one of the deepest and most easterly positioned mud volcanoes in the Sorokin Trough chain of mud volcanoes located between ≃1,950 and ≃2,100 mbsl, on the northern margin of the Black Sea. The location of gravity core mounted temperature logger GC-46 that was taken ≃3 km north of the DMV center (Longitude 34°59.162′, Latitude 41°18.166′) to obtain the ambient hemipelagic sediment temperatures.

Other studies on mud volcanoes in the Black Sea during +/- the last decade focused on the Sorokin Trough MVs (Fig. 5-1) in the northern part of the Black Sea (Blinova et al., 2003; Bohrmann et al., 2003; Krastel et al., 2003; Greinert et al., 2006). The Sorokin Trough is a 150 km long and 50 km wide depression along the Crimean Peninsula margin with water depths ranging between 800 and 2,200 m (Tugolesov et al., 1985). The compressional tectonic regime and the weight of the overburden have lead to the intrusion of water-saturated clay of the Maikopian Formation that has formed diapiric structures on the seafloor (Krastel et al., 2003). Most mud volcanoes

are situated on the top or edge of the mud diapirs as an expression of mud extrusion from the seafloor (Ivanov et al., 1998).

In this study, we focus on the Dvurechenskii Mud Volcano (DMV) of the Sorokin Trough, which is a flat-topped structure with a diameter of ≃1,000 m, and located at a water depth of 2,100 m. We will use detailed high resolution bathymetric and backscatter maps, visual seafloor imaging and internal and external *in-situ* mud temperature observations obtained for the first time at the DMV. As this form of data cannot be obtained using standard ship-based multibeam systems, we used state-of-the-art, data acquisition methods mounted on an Autonomous Underwater Vehicle (AUV) and Remotely Operated Vehicle (ROV), as well as a gravity core mounted temperature logger during two scientific cruises (MSM15/2 [2010] and M84/2 [2011]) and a gravity core mounted long term sediment temperature mooring (T-mooring) which was deployed during cruise M72/3 (2007) and retrieved during cruise MSM15/2. The procured data was compiled to I) determine morphological signatures and processes for mud movement, II) evaluate the vertical and horizontal mud flow temperatures and velocities of the DMV conduit and plateau and III) discuss the formation time of the DMV.

5.3 Materials and Methods

The DMV was investigated during three research cruises with *R/V* METEOR (M72/3 in 2007 and M84/2 in 2011) and the *R/V* MARIA S. MERIAN (MSM15/2 in 2010). Equipments such as an AUV, ROV, temperature loggers, and T-mooring were deployed.

5.3.1 Autonomous Underwater Vehicle (AUV)

The AUV Seal 5000 from MARUM is an autonomous underwater vehicle fabricated by the company I.S.E with a maximum diving depth of 5,000 m. During cruise MSM15/2 (Bohrmann, 2011a), an AUV dive was conducted at the DMV at water depth of ≃2,000 m. The AUV was set to navigate 40 m above the seafloor at speed of 3 knots, in order to obtain the best performance. The distance between the two track lines was designed at 60 m to ensure complete mapping coverage of the DMV.

A RESON MBES 7125-B Multibeam echo sounder (400 kHz) was utilized to obtain a high resolution bathymetric map of the DMV. A high resolution backscatter map was acquired by deploying the BENTHOS dual frequency (100/400 kHz) Side-Scan Sonar. The Motion Reference Unit (MRU) and Inertial Navigation System (INS) or Photonic Inertial Navigation System Inertial Unit (from the IXSEA Company) provided information on the heading, pitch and roll of the AUV.

Onshore processing of the multibeam sonar and dual frequency side-scan sonar data was carried out post-cruise using an open-source software package (MB-system software, Caress and Chayes, 1996 and 2001) to obtain high resolution bathymetric and backscatter maps of the DMV, respectively. The slope angle map, which was calculated from the high resolution bathymetric map, was produced using the ArcGIS software.

5.3.2 Remotely Operated Vehicle (ROV)

Seafloor observations were achieved using seafloor visual cameras mounted on the ROV QUEST 4000 from MARUM, Bremen. During Cruise MSM15/2, two ROV dives were conducted in the southern area of the DMV summit (Fig. 5-2 pink area) to obtain detail on the seafloor morphology (Fig. 5-2).

The seafloor observations were achieved using three camera systems mounted on the ROV: two forward-facing video cameras i.e. a high-definition Insite ZEUS PLUS Colorzoom camera (HD camera) and a DSPL SSC 6500 Colorzoom camera (DSPL camera), as well as a downward-facing photo-camera (CANON Powershot G10, 15 MP). The HD-images were analyzed post-cruise to define and classify variations in the DMVs seafloor sedimentological and morphological features.

In addition, *in-situ* sediment temperature measurements were made using T-stick probes on the ROV (Fig. 5-2). Eight probes were embedded in a T-stick with an equal spacing of 0.066 m to obtain 8 simultaneous temperature readings. The recording here was set at ≃10 min to allow the thermometers to acclimatize to the ambient temperatures. The measurements were operated by the ROV QUEST 4000. For detailed information on the operating procedure referred to Bohrmann et al. (2011a).

5.3.3 Temperature Loggers and T-mooring

In-situ sediment temperature data was collected during cruises MSM15/2 and M84/2, using both gravity core mounted temperature loggers and T-mooring. The T-mooring was deployed during the research Cruise M72/3 in 2007 (Bohrmann and Pape, 2007) and retrieved during Cruise MSM15/2 in 2010 (Bohrmann, 2011a). The position of the *in-situ* measurements is shown in figure 5-2.

For GC-2, 3, 5, 6 and 42 and 46, temperature measurements were achieved using temperature loggers mounted on a 6-m gravity corer. All the deployments showed shallow penetration into the sediment, except GC-5, 6 and 42. These three deployments (in the conduit?) penetrated up to 76 mbsf. For GC-5, 6 and 42, a gravity corer was deployed to a pre-defined depth and was retrieved at 5 - 10 m intervals with a recovery rate of 0.2 m/sec until the corer had totally left the seafloor. For each depth interval measurement, the corer was suspended in the mud for 10 min to obtain equilibrium with the surrounding sediment temperatures. The GC-46 temperature logger was taken due north of the DMV to obtain the ambient sediment temperatures (see Fig. 5-1). Detail on the measurement parameters and information on the operating procedure are referred in Wei et al. (2015). Onshore additional corrections or calibrations of the temperature data were not required and plots were compiled.

T-mooring was designed to measure long-term variations in the sediment temperatures however in this paper we are singularly interested in the migration of the T-mooring. A 6-m gravity corer, with 8 temperature loggers attached, was deployed 156 m south of the summit during the 2007 *R/V* METEOR Cruise M72/3 (Fig. 5-2). After 1,166 days, it was recovered in 2010 during Cruise MSM15/2 (Bohrmann, 2011a). The deployment (start) and retrieval (end) positions of the T-mooring determined from the GPS positions of the *R/V* METEOR and *R/V* MARIA S. MERIAN were compared.

5.4 Results

5.4.1 High Resolution Bathymetry and Backscatter Maps

The high resolution bathymetric map shows that the DMV is a positive topographic

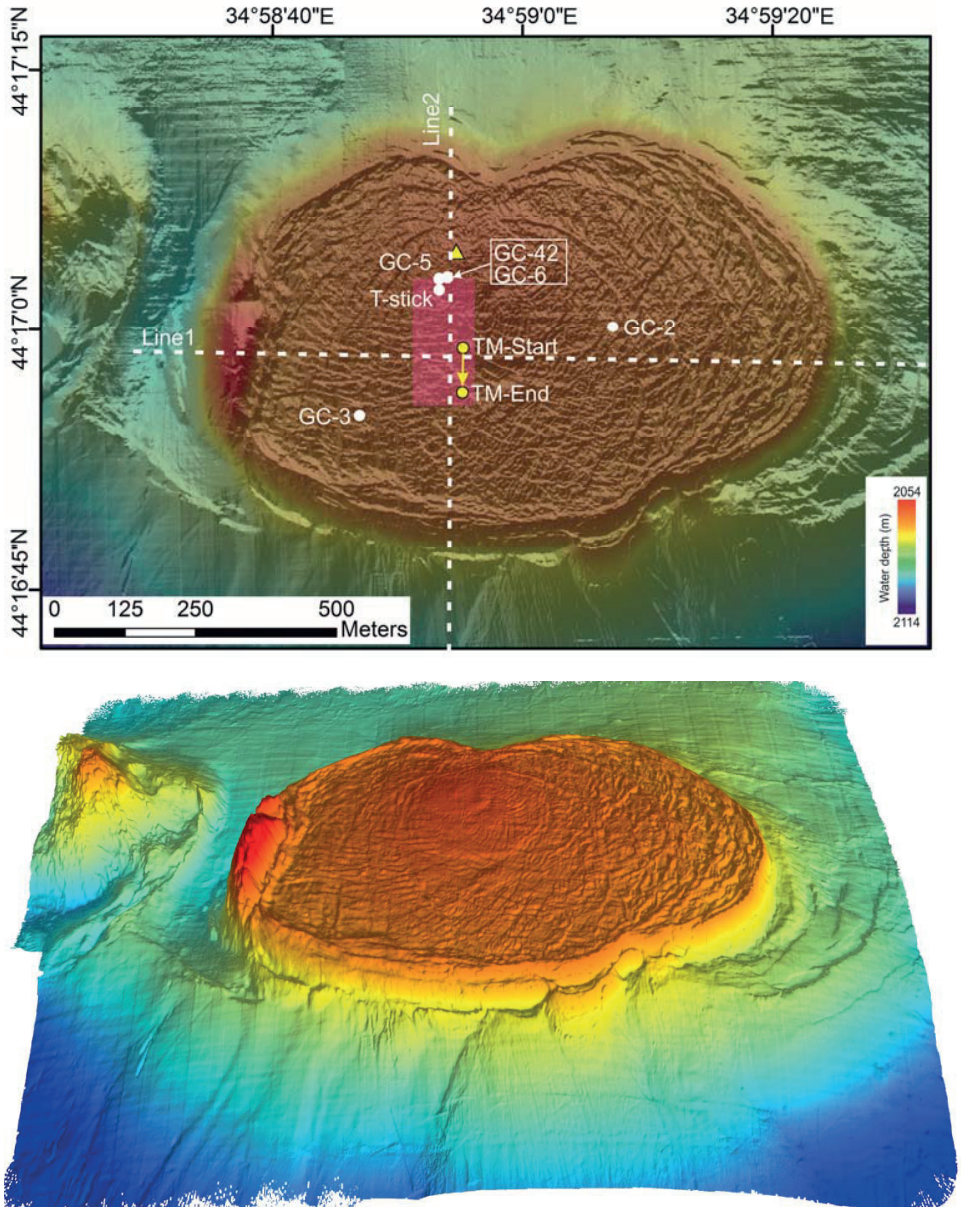

Figure 5-2: The (upper) high resolution bathymetric map of the DMV obtained using the AUV. The yellow triangle indicates the position of the DMVs summit which is also inferred to be the surface expression of the mud conduit. Locations of the gravity corer with T-mooring are represented by yellow dots which migrated 78 m during their deployment between 2007 and 2010. The yellow arrow shows the migration direction. The locations of *in-situ* sediment temperature measurements are shown as white dots. Two transect lines are indicated by white dashed lines. Line 1 runs E-W and Line 2 N-S. The area defined in pink, shows the surface coverage of the ROV HD-photographic imaging (Fig. 5-6). The lower map represents a 3-D visualization of the DMV and clearly shows the location of the summit. The location of GC-46 is not marked on the map because it is located further North (see Fig. 5-1).

feature with a pie-like shape (Fig. 5-2). Topographically the DMV can be divided into 3 main areas; I) a central flat area or plateau (Fig. 5-2), where the slope from the central summit to the margin has an angle of between 0.5° and 1.0° (Fig. 5-3) and the flanks of the DMV, which can be divided into II) steep cliffs on the upper margin with slope angles of between 9.6° and 28.0° (Fig. 5-3) and III) gentle slopes on the lower margin. The length of the N-S axis is ≃1 km while the length of the E-W axis is ≃1.6 km. The summit of the DMV is about 3 - 4 m higher than the break to the peripheral flank region, and is located at approximately 300 m northwest of the geometric center.

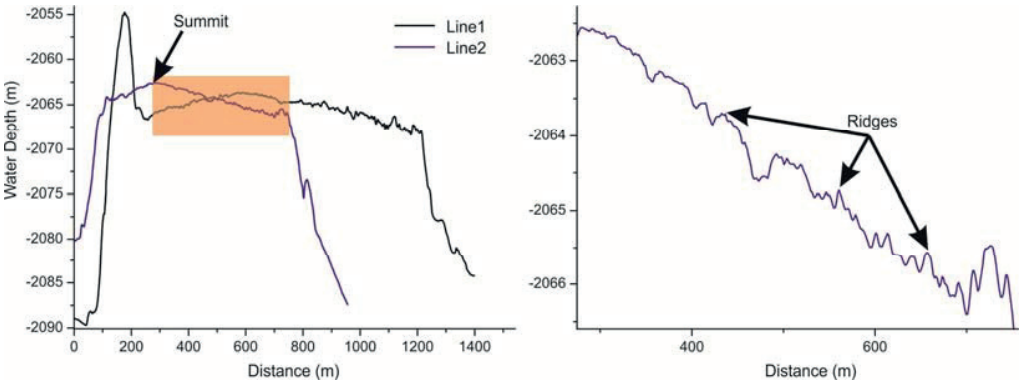

Figure 5-3: Two elevation transect profiles across the DMV. Line1 runs E-W and Line 2, N-S. The position of the transects across the DMV is shown in figure 5-2.

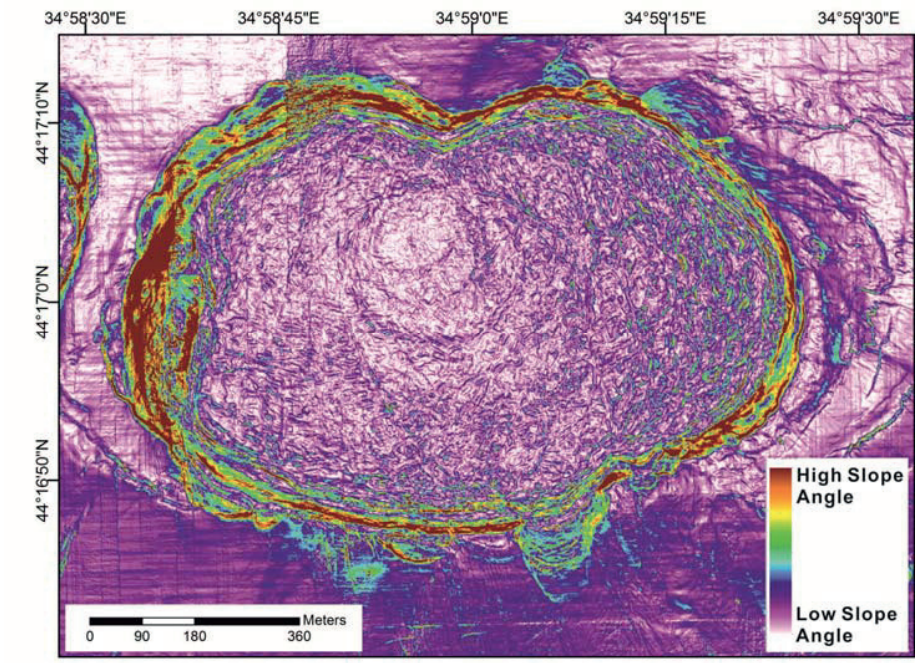

Figure 5-4: A Slope Angle Map-based on the bathymetric data, showing the steepness of the DMV.

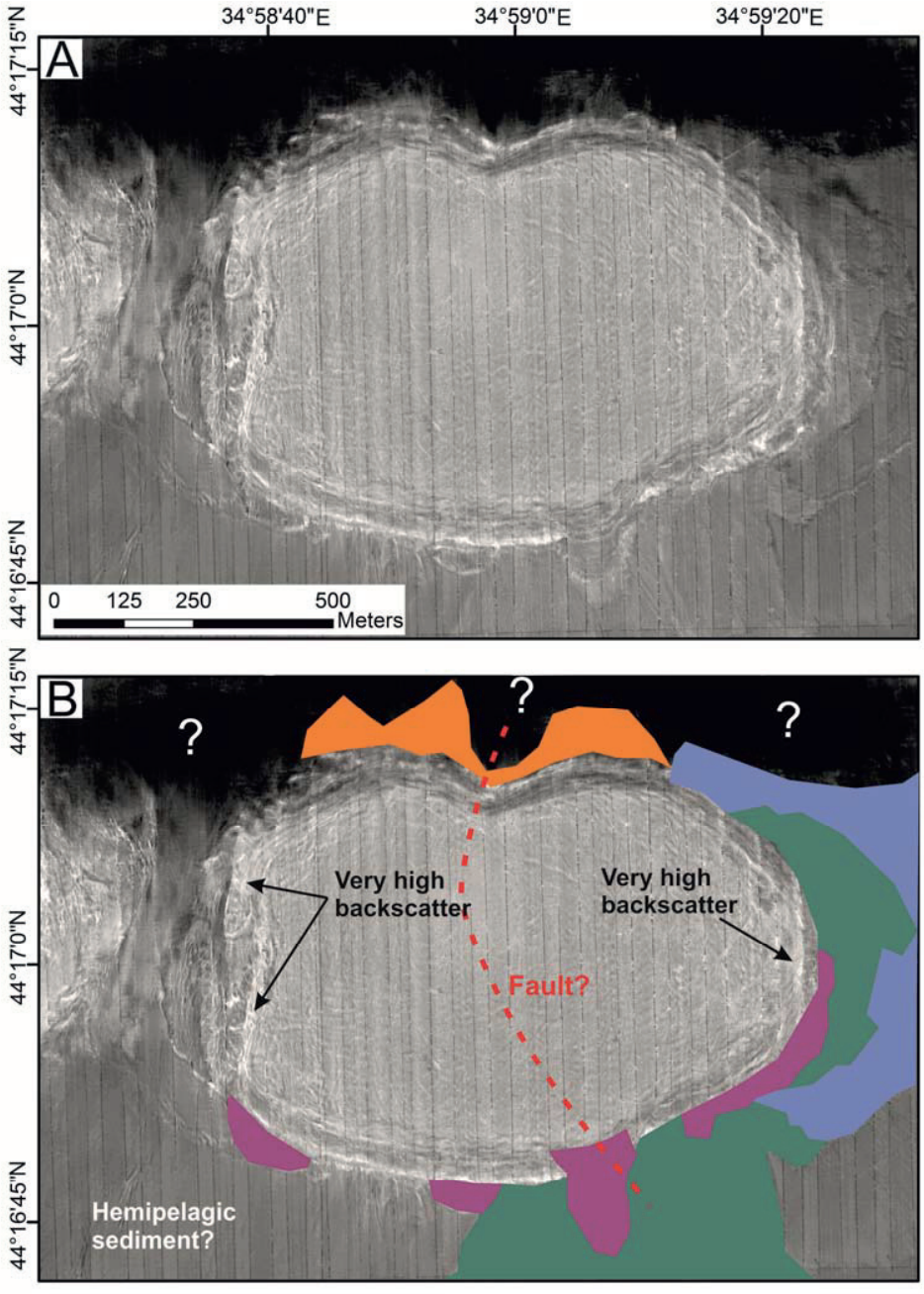

Figure 5-5: A: Backscatter map of the DMV obtained using the AUV. Light color represents high backscatter and dark color low backscatter. B: Interpretation of the backscatter map: areas marked by the 4 color infill represent different time periods of inferred mud flow. A construe fault line (red dashed line) cuts though the DMV in a N-S direction. The high backscatter (light grey) of the DMV indicates the presence of mud clasts, whereas the low (dark grey) backscatter of the surrounding seafloor sediments is inferred to represent hemiplegic material. The question mark, represent areas where, after data processing, the backscatter signals was too low for an interpretation.

Detailed morphological features that cannot be seen using traditional multibeam mapping techniques are clearly depicted with the AUV-mounted high resolution bathymetric map system. This data clearly shows concentric ring structures and ridges on top of the DMV. The concentric ring structures, composed of several concentric cycles radiate out from the summit which forms the central point. These concentric rings could also be observed in the Slope Angle Map derived from the bathymetry data (Fig. 5-4). The concentric ring structures, which are inferred to represent mud eruptions at periodic time intervals, mainly develop in a southeasterly direction due to a decrease in the topographic elevation. Although the elevation of the DMV surface decreases gently from the central summit to the marginal slopes, small topographical variations can be observed and are interpreted as decimeter (dm) high ridges. The steepness and height of the small ridges increase from the summit to the margin.

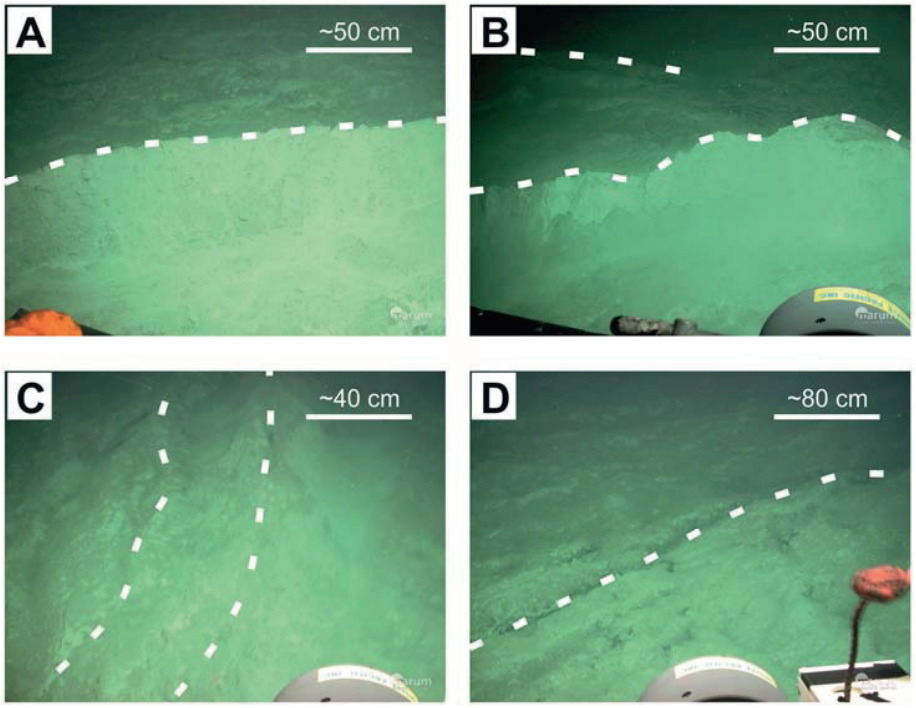

Figure 5-6: HD-photos of the seafloor SW of the DMV's summit. Dashed lines indicate the position of ridges interpreted from the seafloor observation.

In the high resolution backscatter map, the DMV mainly shows high backscatter (light color, see Fig. 5-5A), while the surrounding seafloor area mainly shows low backscatter (dark color, see Fig. 5-5A). High backscatter is inferred to be caused primarily by mud clasts from mud eruptions, whereas low backscatter is inferred to

represent the hemipelagic sediment (Van Rensbergen et al., 2005). Patches of high backscatter eliminating from the margin of the DMV, and penetrating the area of low backscatter surrounding the DMV, might represent individual gravity driven mud flows that occurred at different intervals in time (Fig. 5-5B).

5.4.2 Seafloor Observations

Seafloor observations from the HD photographic imaging show that the DMV is covered by dark greyish material (Fig. 5-6). Another seafloor feature of the DMV is the ubiquitous ridges which are tens to hundreds of centimeters high. These observed ridges in the HD-images correspond with the concentric ridges detected in the high resolution bathymetric map.

5.4.3 Migration of the T-mooring

Time series temperature measurements of the DMV's sediment were conducted with a gravity corer which during its 1,166 days of deployment (156 m south of the summit) migrated to 234 m south of the summit (Fig. 5-2). These results show that the gravity corer drifted 78 m during its deployment period (Table 5-1).

Table 5-1: Deployment data for the T-mooring taken from Cruise Report Bohrmann and Pape (2007) and Bohrmann et al. (2011a)

T-mooring	Time (days)	Ship	Cruise	Distance to summit (m)	Top Sensor (°C)	Bottom Sensor (°C)
Deployment	7 March 2007	*R/V* METEOR	M72/3	156	10.2	15.8
Retrieved	18 May 2010	*R/V* MARIA S. MERIAN	MSM15/2	234	10.1	13.9
Disparity in Deployment Data	1,166	-	-	78	0.1	1.9

This information has been used to deduce the horizontal mud velocity of the DMV. During this time period, the temperature recorded by the top sensor decreased from

≃10.2°C to ≃10.1°C, while the temperature recorded by the bottom sensor decreased from ≃15.8°C to ≃13.9°C (Bohrmann et al. 2011a).

5.4.4 *In-situ* Sediment Temperatures

In-situ sediment temperatures were measured at different sites on the DMV (Fig. 5-2 and Fig. 5-7). The ambient bottom water temperatures at this location are ≃9.1°C. Temperature gradients were calculated using a linear regression for Sites GC-46, GC-2, GC-3 and the T-stick. GC-46, which was measured in the hemiplegic sediment of the seafloor surrounding the DMV shows a temperature gradient of 0.032°C/m and is taken as a representation of the ambient background sediment temperatures in this area (Tab. 5-2). GC-2 and GC-3 were deployed furthest away from the summit, in the outer sector of the central flat area and show a temperature gradient of 0.336°C/m and 0.468°C/m, respectively. The T-stick measured sediment temperatures in the very shallow sediments in the middle of the central flat area and shows a temperature gradient of 5.884°C/m which is much higher than those in the outer sector and from the sediments of the surrounding seafloor.

Table 5-2: Information on the *in-situ* sediment temperature measurements.

GC	Cruise	Date	GeoB	Latitude (N)	Longitude (E)	Water (mbsl)	max depth (mbsf)	Gradient (°C /m)
GC-42	**M84/2**	**27.03.2011**	**15527**	**44°17.041**	**34°58.891**	**2051**	**76**	
GC-46	**M84/2**	**29.03.2011**	**15533-1**	**44°18.166**	**34°59.162**	**2054**	**8.55**	**0.032**
GC-2	**MSM15/2**	**12.05.2010**	**14310**	**44°16.990**	**34°59.110**	**2059**	**15**	**0.336**
GC-3	**MSM15/2**	**12.05.2010**	**14311**	**44°16.910**	**34°58.770**	**2059**	**13**	**0.468**
T-Stick	**MSM15/2**	**13.05.2010**	**14314-1**	**44°17.030**	**34°58.880**	**2040**	**0.57**	**5.884**
GC-5	**MSM15/2**	**18.05.2010**	**14335**	**44°17.040**	**34°58.880**	**2057**	**55**	
GC-T-6	**MSM15/2**	**18.05.2010**	**14336**	**44°17.041**	**34°58.891**	**2057**	**69**	

GC-5, GC-6 and GC-42, which were deployed closest to the summit, in the center of the DMV, penetrated into the sediment to a depth of 76 mbsf. These measurements

provide valuable information on the temperature of the deep subsurface in the conduit. In general, all three profiles follow a similar trend with sediment temperatures ranging between 16°C and 17°C, indicated by the black dashed line in figure 5-7. However, in addition, each profile shows same anomalies with abnormally high temperatures of up to 22°C at variable depths.

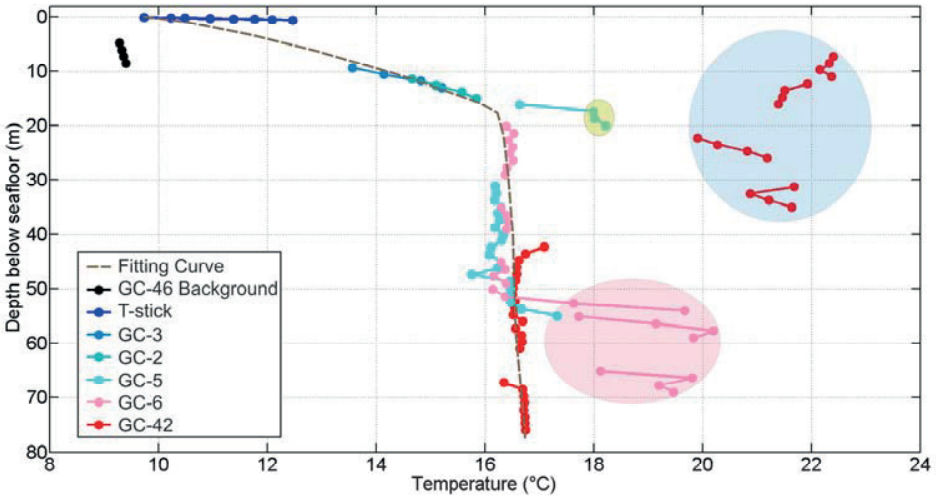

Figure 5-7: *In-situ* sediment temperature profiles. The GC logger data show a typical depth related temperature profile whereby temperature increases with depth within the mud volcano (the blue to red colors indicate a temperature increase, from cold to hot, respectively). The ambient temperature around the DMV is measured with GC-46 at ≃9 ºC (black points). The recording of the GC-6 loggers (2010) show a constant temperature of ≃16 ºC from 20 to 50 mbsf. Compare to the normal temperature gradient profile (fitted curve), two significant anomalies were observed at the GC-42 and GC-6 sites. A minor area with a small high anomaly is indicated in light green. The temperatures defined by the pink area (measured in 2010) between 50 and 70 mbsf are much higher. Similarly, abnormally high temperatures (measured in 2011) are also observed at the shallower location (defined by the blue area). Results show that the deeper area (pink) temperatures are lower than at the shallower location (blue). This suggests that the fluid mud at the shallower location derives from a much deeper source area within the mud volcano.

5.5 Discussion

5.5.1 Mud Eruption Characteristics of the DMV

Thermal structure of the mud volcanoes provides information on fluid and mud transportation (Feseker et al., 2008; Feseker et al., 2009). *In-situ* sediment temperature profiles at non-seep sites are normally linear, indicating that the thermal regime is controlled by heat conduction. At mud volcanoes however, the thermal regimes are normally dominated by heat convection caused by mud and fluid advections (Feseker et al., 2008). Our temperature profiles within the conduit and mud pools of the DMV are composed of two distinct features which might indicate that the mud and fluid transportation is controlled by two regimes. First, all the profiles, including GC-5, GC-6 and GC-42, follow a general smooth curve (dashed black line) as shown in figure 5-7. The shape of the curve indicates that the temperature regime is mainly controlled by heat convection caused by a continuous upward fluid flow from the deep subsurface. The second feature of the temperature profile is characterized by areas at different depths, representing high temperature anomalies (up to ≃22°C) that are seen as distinct positive offsets from the main temperature-depth profile curve (Fig. 5-7). Fluid and mud migration in mud volcanoes show different cyclic phases of activity, including catastrophic events and periods of relative quiescence characterized by moderate activity (Deville and Guerlais, 2009). We infer that the smooth temperature mainly represent the period of moderate activity while the abrupt temperature elevation anomalies represent catastrophic mud eruptions.

Although the T-mooring gravity corer migrated 78 m south of the summit deployment position, it stayed at a constant depth in the sediment. This indicated that the sediment moved laterally at constant depths over the migration period. Furthermore, this implies that a 6-m thick sediment unit was moved as a singular block with the same internal speed. Seafloor morphology provides additional evidence of mud movement on the concentric rings seafloor. A rough seafloor surface, composed of ≃dm scale ridges is expressed radially from the center of the plateau to the margin (Fig. 5-2 and Fig. 5-3). These ridges might be formed by forces generated by newly erupted mud from the central conduit (Dupré et al., 2008).

The surface of the DMV shows high backscatter, while the surrounding seafloor shows low backscatter (Fig. 5-5). The high backscatter is mainly caused by mud breccia which contains mud clasts (Krastel et al., 2003). The intensity of the backscatter at the edge of the DMV is higher than that in the center. We infer the mud breccia at the edge is older than that in the center and experienced a long period of dewatering and consolidation. High backscatter patches around the DMV show

different intensities which might indicate that several gravity driven flows occur at different periods in time.

5.5.2 A Mud-Transportation Model for DMV

5.5.2.1 Vertical Mud Velocity

Mud brings heat from the deep subsurface and shows abnormally high temperatures within the mud conduit (Feseker et al., 2008). In this study, we observed two distinct temperature anomalies (in GC-6 and GC-42) with elevated mud temperatures, in the conduit. GC-6 and GC-42 are both deep penetration temperature cores, measured at same location, at different times (GC-42 measurements were carried out 313 days after GC-6). A temperature constant area, with temperatures of ≃16°C was observed in both profiles. This temperature constant area, observed between 20 and 50 mbsf

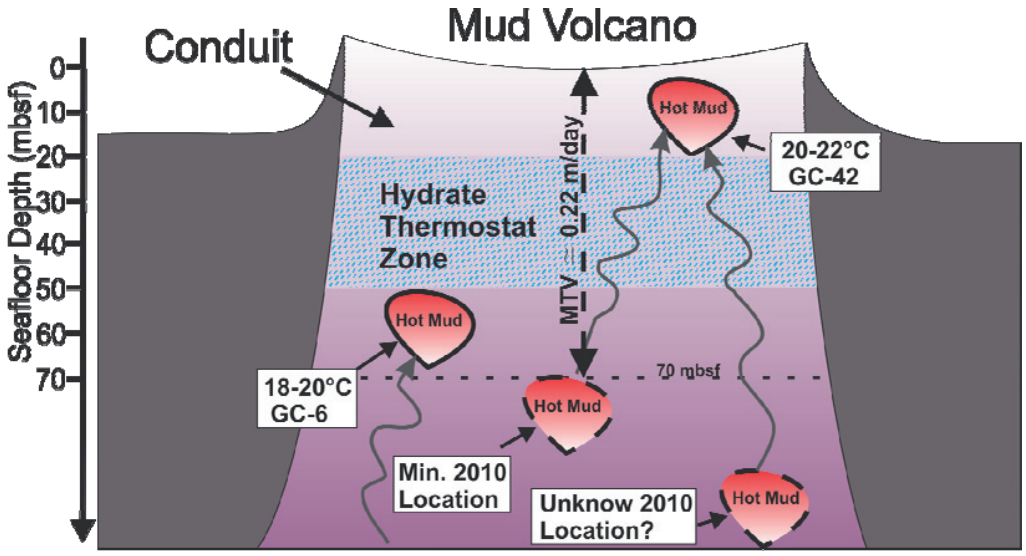

Figure 5-8: A model to show the minimum calculated mud migration velocity in the DMV's central conduit. The ≃16°C hydrate thermostat zone by Feseker et al. (2009b) is marked from 20 to 50 mbsf (blue dashed zone). The minimum depth of the GC-42 mud anomaly at 70 mbsf, and a possible unknown greater depth of its position in 2010, is labelled. The vertical migration of the high temperature mud anomaly (GC-42) can be used to calculate the mud transport velocity (MTV), whereby MTV = Depth (70 m)/Time (313 days).

within the DMV, was first discovered by Feseker et al, in 2009 and explains a gas hydrate thermostat zone (Feseker et al., 2009) (Fig. 5-8). The two additional high

temperature anomaly regions were observed at different depths: 1) an anomaly of 20 - 22°C near the seafloor surface at 10 - 35 mbsf, just above the ≃16°C thermostat zone (in GC-42) and 2) an anomaly of 18 - 20°C at 50 to 70 mbsf just below the ≃16°C thermostat zone (in GC-6). The high temperature anomaly above the gas hydrate thermostat zone provides new evidence for the migration of muds (that original below the hydrate thermostat zone), in the central summit due to a sizable eruption. These results support the findings of Sevensen et al. (2009) who suggest that the formation of the submarine mud volcano is controlled by the eruption of large volumes of mud. The deep-lying highest temperature value of the GC-6 profile observed in 2010 is lower than the highest temperature value of the GC-42 profile, recorded in 2011, that was observed near the seafloor surface. Since they are located at the same position, we can infer that the high temperature surface anomaly obtained in 2011 originated from even deeper than the high temperature deep-lying anomaly obtained in 2010, i.e. from a hotter source >70 m (Fig. 5-7). Because this high temperature surface anomaly (GC-42) was only record in 2011, we must assume it was located deeper than the high temperature deep-lying anomaly (GC-6) at 70 mbsf recorded in 2010. Thus the GC-42 anomaly has taken 313 days for an upward migration of at least 70 m. The lowest average velocity of upward migrating mud is therefore calculated to be ≃0.22 m/day (Fig. 5-8).

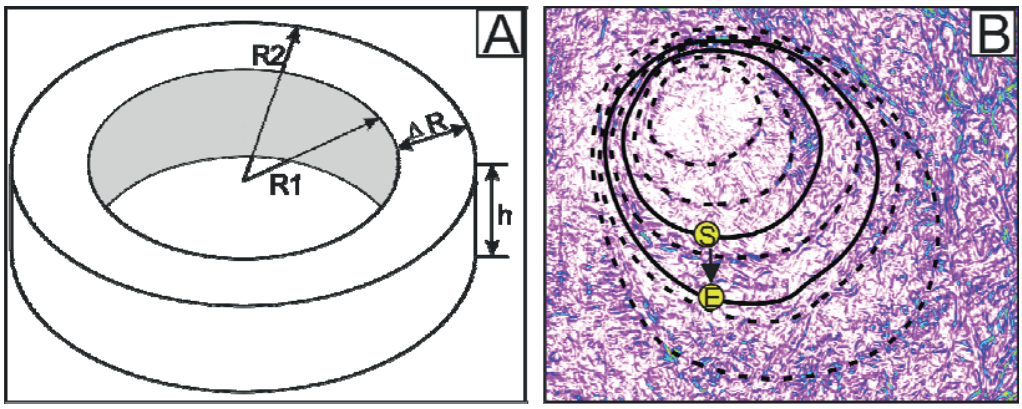

Figure 5-9: Schematic diagram of two models used to calculate the horizontal mud velocity. A: abstract circular model. B: realistic model based on the observed topography Ridges. Dashed lines show the distinct seafloor ridges from figure 5-4. The yellow dots and black arrow show the start (2007) and end points (2010) of the T-mooring, respectively. Solid lines are the interpolated cycles across the T-mooring.

5.5.2.2 Horizontal Mud Velocity

Research of horizontal mud velocity is important to understand the behavior and evolution of mud volcanoes (Feseker et al., 2014). In contrast to mud volcanoes on land, quantifying mud movement on the seafloor is still problematic due to the lack of information. In this study, the migration of the T-mooring gravity corer provides important information to allow for a preliminary estimation of the horizontal mud flow velocity for the DMV.

Assuming that the mud flow out of the central conduit is constant, we can use two models, including an abstract (hypothesised) circular model and a realistic (true data) contour model, to calculate the horizontal mud velocity.

Abstract (Hypothesised) Circular Model:

The abstract circular model is based on two concentric cylinders with a radius of R1 and R2 which represent the distances from the start and end point of the gravity corer migration to the central summit, respectively (Fig. 5-9A). The volumes of these two cylinders (V_1 and V_2) can be expressed as Eq. 1 and Eq. 2.

Eq. 1 $$V_1 = \pi R_1^2 h$$

Eq. 2 $$V_2 = \pi R_2^2 h$$

In these two equations, h represents the height of the cylinder. The increasing rate of the cylinder volume, which is also the mud flux from the conduit (Q), could be expressed as Eq. 3. Δt is the time period of 1,166 days between 2007 and 2010.

Eq. 3 $$Q = \frac{V_2 - V_1}{\Delta t} = \frac{\pi R_2^2 h - \pi R_1^2 h}{\Delta t}$$

Another expression to calculate the mud flux is by multiplying the area of the cylinder wall ($2\pi Rh$) and the horizontal mud flow velocity (v_H). R could be any radius between the R1 and R2 (Eq. 4).

Eq. 4 $$Q = 2\pi Rh \times v_H$$

By combining Equations 3 and 4, horizontal mud flow velocity could be expressed as shown in Eq. 5.

Eq. 5 $$v_H = \frac{R_2^2 - R_1^2}{2R\Delta t}$$

The horizontal mud flow velocity is a function of only R because R2, R1 and Δt are 234 m, 156 m and 1,166 days, respectively. Figure 5-10 show an increase in the perimeter size of the cylinder cycles and, a decrease in the horizontal mud flow velocity as the radius of the cylinder increases.

Realistic (True Data) Contour Model:

The topography of the DMV is not consistent in all directions radiating out from the summit. It is irregular, being higher in the north and lower in the south. Mud erupted from the central summit therefore accumulates and develops more in a southeast direction and not in all directions equally. Consequently, it is more accurate to use a Realistic Contour Model than the Abstract Circular Model.

In the Realistic Contour Model, the contours were obtained by selecting the most perspicuous concentric rings (Fig. 5-9B). Contours across the start and end points of the T-mooring gravity corer were estimated by interpolation based on the concentric rings selected from the DMV map of the AUV.

Mud flux, as expressed in Eq. 6, is a function of S_1, S_2, h and Δt. S_2 and S_1 represent the areas of the contours which are 99,431 m^2 and 48,590 m^2, respectively.

Eq. 6 $$Q = \frac{V_2 - V_1}{\Delta t} = \frac{S_2 h - S_1 h}{\Delta t}$$

Another expression to calculate mud flux is by multiplying the area of the cylinder wall (Ph) and the horizontal mud flow velocity (v_H) as defined in Eq. 7. P represents the length of any contour line between the two endmember contour lines (the start and end points), respectively.

Eq. 7 $$Q = Ph \times v_H$$

By combing Equations 6 and 7, the horizontal mud flow velocity, based on the Realistic Contour Model, can be expressed as:

Eq. 8 $$v_H = \frac{S_2 - S_1}{P\Delta t}$$

The length of the contour line is theoretically linearly correlated with the distance between the summit and a point on the contour. Therefore, the constant could be expressed as:

Eq. 9 $$P = \frac{P_2 - P_1}{R_2 - R_1} \times R$$

By substituting the P_2, P_1, R_2 and R_1 with 1,134 m, 793 m, 234 m and 156 m, respectively, the correlation between P and R is obtained with:

Eq. 10 $$P = 4.96R$$

Based on Equations 9 and 10, the horizontal mud flow velocity can be expressed as a function of R:

Eq. 11 $$v_H = \frac{S_2 - S_1}{4.96R\Delta t}$$

Figure 5-10 shows the increase in length of the cylinder cycles and the decrease in horizontal mud flow velocity as the radius increases.

5.5.3 Formation Time of the DMV

In principle vertical mud flow velocity at the boundary of the conduit should be very similar to the horizontal velocity at this location since this defines the start of the horizontal mud migration. In this study, the vertical mud flow velocity is estimated to be 0.22 m/day and the horizontal mud flow velocity is estimated to lie between 0.19 (from the Realistic Contour Model) and 0.22 m/day (from the Circular Model) at a distance of 60 m from the summit in the direction of the migration T-mooring gravity corer.

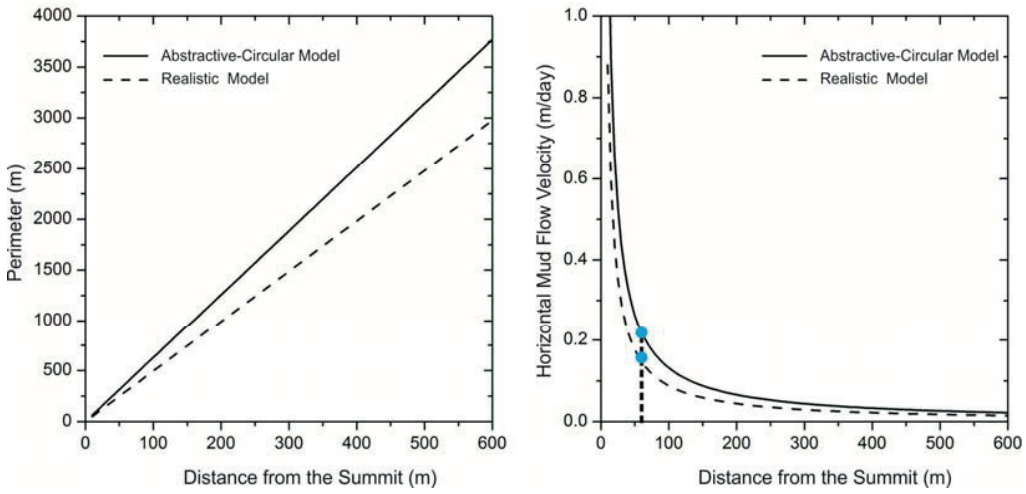

Figure 5-10: Plots depicting changes in the mud velocities from the perimeter from I) the DMV (left) and II) the horizontal mud flow velocity with distance from the summit (right). The blue dots show the location of GC-6 and GC-42 which are ≃60 m from the summit of the DMV.

Due to knowledge about the estimated vertical and horizontal mud flow velocities, the time of the DMV formation could in theory, also be estimated. An approximation of the DMV's formation time could be estimated as a division of the total volume of the DMV and the vertical mud volumetric flow rate. V and F represent the volume of the DMV and the volumetric flow rate, respectively:

Eq. 12
$$t_1 = \frac{V}{F}$$

The total volume of the DMV (V) could roughly be estimated by multiplying the DMV's surface area with the average height. The surface area is 778,196 m^2 and the average height is 26 m as determined using the ArcGIS software. The mud flow volumetric flow rate is expressed by the multiplication of the vertical mud flow velocity (v_v) and the area of the mud conduit cross section (πR^2):

Eq. 13
$$F = \pi R^2 \cdot v_v$$

Considering a radius of 60 m for the mud conduit, and a vertical mud flow velocity of 0.22 m/day, the formation time of the DMV is estimated to be approximately 22 years.

The assumption that it is possible to estimate the formation time of the DMV by using the horizontal mud flow velocity is, that mud at different depths moves, as a whole, with the same horizontal velocity. The formation time (t_2) is expressed as the time needed for the mud to be transferred from the center of the DMV to its margin in the direction of the migrating T-mooring gravity corer. This is expressed by the integration of all the times needed at various distances from the center. v_R represents the mud flow velocity at locations with a distance of R from the center:

Eq. 14 $$t_2 = sum(\frac{\Delta R}{v_R})$$

If the distance from the summit of the DMV to the start of the peripheral flank region is 500 m in the direction of the migrating T-mooring gravity corer, the formation time of the DMV would be estimated at approximately 26 years.

Although the estimated formation time of the DMV using both methods is quite comparable, the age of the DMV might be considerably older due to factors that were not considered in the estimate including I) mud consolidation, II) cyclic mud eruption and III) seafloor erosion. Fresh mud erupted from the central conduit is normally rich in water. The water content of this mud then decrease as the sediment consolidates.

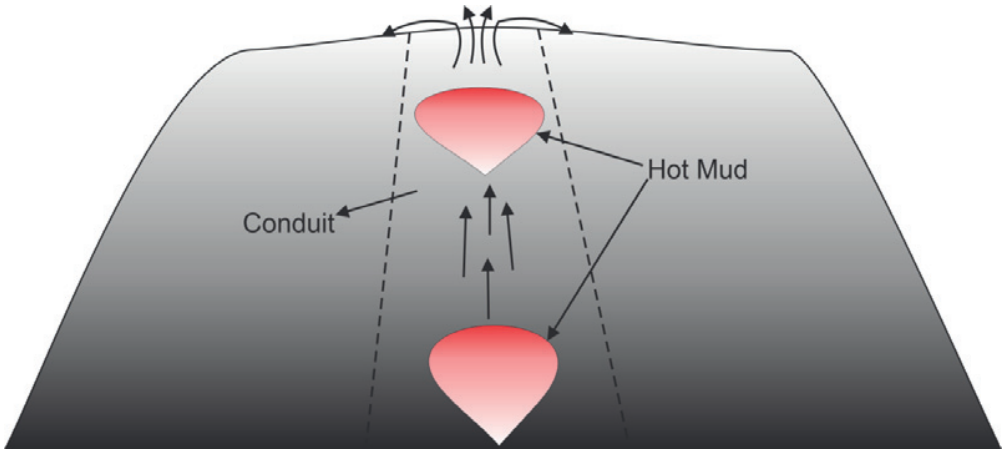

Figure 5-11: A mud eruption model of the DMV, which shows the cyclic eruption of mud plumes transported from a deep source to the DMV's surface through a central conduit, separated by periods of inactivity.

This has also been observed in the central craters of active terrestrial mud volcanoes, which are also filled with high water containing mud (Planke et al., 2003; Yang et al., 2004). Therefore, the original volume of the DMV was much larger than it is at the present day. The estimation of the mud volcano formation time is based on the assumption that continuous mud flow occurs, however activity of mud volcanoes is normally composed of catastrophic events and periods of inactivity (Fig. 5-11) (Deville and Guerlais, 2009). Since the DMV was experiencing a relative active phase, the estimated velocity might be much higher than the average mud flow velocity over the DMV's lifespan to date, which would lead to discrepancies in the formation time. A further factor that could lead to an erroneous age is erosion by deep water currents that might decrease the total volume of the DMV (Özsoy and Ünlüata, 1997).

5.6 Conclusions

Using state-of-the-art AUV and ROV measured data acquisition methods, a high resolution bathymetric seafloor map was constructed, and HD-quality seafloor observations and *in-situ* sediment temperature measurements, could be made for the DMV. This data provided information on the mud transport characteristics of the DMV and allowed for an evaluation of vertical and horizontal mud flow patterns and velocities. Major conclusions of this study are drawn as follows:

1. The pie-shaped DMV is characterized by ubiquitous ≃dm high sediment ridges which form concentric ring structures radiating out from the summit (the central point). This evidence might be the surficial manifestation for cyclic mud eruption processes.

2. Numerous sediment lobes and patches emanating from the margin of the DMV, observed as variations in the backscatter intensity, are interpreted to represent individual gravity driven mud flows that occurred at different intervals in time.

3. Shallow sediment temperature gradients increase from ≃0.032°C/m in the hemipelagic seafloor sediment surrounding the DMV, to 0.336 – 0.468°C/m in the outer reaches of the central plateau and 5.884°C/m in the center of the DMV plateau. Anomalies with abnormally high temperatures might be caused by the cyclic eruption of hot mud plumes from deep subsurface and suggest that the DMV is experiencing of relatively active phase.

4. Both vertical and horizontal mud flow velocities for the DMV could be inferred from either real *in-situ* data and/or theoretical conjecture. The vertical velocity of the mud flow in the conduit is inferred to be a minimum of 0.22 m/day. The horizontal mud flow velocity on the central plateau estimated using two models based on the 78 m-migration of the T-mooring gravity corer over a time period of 1,166 days, and at 60 m from the summit, is estimated to be between 0.19 - 0.22 m/day.

5. Based on simplified models that utilize the estimated vertical and horizontal mud flow velocities, it was feasible to approximate the time of formation for the DMV. Estimations suggest that the DMV is ≃22 to 26 yrs old. However, due to some addition factors, such as mud consolidation, cyclic mud eruption and seafloor erosion, not integrated in the model, the age of the DMV might be erroneous.

5.7 Acknowledgments

We thank the captains and crews of *R/V* METEOR and *R/V* MARIA S. MERIAN for support during the research cruises M72/3 and M84/2 and MSM15/2. We also thank the ROV QUEST team from MARUM for handling the Remotely Operated Vehicle (ROV). The work was partly funded through the DGF - Research Center and the Cluster of Excellence “The Ocean in the Earth System” MARUM - Center for Environmental Sciences. Tingting Wu was sponsored by the China Scholarship Council (CSC).

Chapter 6

An Inter-relationship Model for Two Neighboring Mud Volcanoes

Tingting Wu[1], Rebecca Rendle-Bühring[1], Jiangong Wei[1,2], Gerhard Bohrmann[1]

1 MARUM, University of Bremen, Klagenfurter Str., 28359 Bremen, Germany

2 Guangzhou Marine Geological Survey (GMGS), Huanshidong Road, 510075 Guangzhou, China

6.1 Abstract

Research on marine mud volcanoes in the past has focused on individual mud volcano settings. The basic concept of mud volcano chain formation due to seafloor seepage of fluidized subsurface sediments and gases, as a result of the interaction between diapir and fault development is well documented. Here we aim to go one step further and evaluate the fault-induced inter-relationship of neighboring diapir-formed mud volcanoes. This will be achieved through the development of a model based on evidence obtained from high resolution surficial and sub-surface geological data and hydro acoustic data. These were retrieved from the Dvurechenskii Mud Volcano (DMV) and the Helgoland Mud Volcano (HMV) of the Sorokin Trough, Black Sea during three research cruises (M72/3 in 2007, MSM15/2 in 2010 and M84/2 in 2011). In adding to the ship-mounted PARASOUND data, micro-bathymetric and backscatter maps were obtained using an Autonomous Underwater Vehicle (AUV). Through the analyses of the data it was possible to build I) a geological evolution model for the DMV and II) a fault-induced inter-relationship model for the DMV and HMV. The main findings verify the presence of down-sag faults for both mud volcanoes. The fault-induced inter-relationship was confirmed by surficial evidence for the presence of ≃north-south orientated normal faults across both the DMV and HMV. These faults are the surficial corroboration of down-sag faults emanating from the neighboring mud volcano i.e. from the HMV and DMV, respectively. The affirmation that gas flare release sites occur in the vicinity of faults, through the margin-active gas flares, could support the theory that the activity of gas and mud expulsion migrates to be released from the margin of mud volcanoes when overburden pressure in the central areas stops gas and fluid discharge.

Keywords: mud volcano; Autonomous Underwater Vehicle; Black Sea; side-scan sonar; hydro-acoustic; down-sag

6.2 Introduction

Marine mud volcanoes, as with terrestrial mud volcanoes, are associated with regional tectonics and hydrocarbon deposits (Kopf, 2002). Due to their activity, geo-harzard risk and emission products (Robertson, 1996; Kopf, 1999), such as methane (CH_4), a global carbon cycle gas (Kvenvolden, 2002), comprehensive evaluation of their evolution and development has long been a focus of scientific interest (Barber et al., 1986; Brown, 1990). Studies have involved research into their formation mechanisms (Milkov, 2000), and their internal and surficial sediment mechanisms (Somoza et al., 2003) to improve our understanding of mud volcanoes (MVs).

Submarine mud volcanoes associated with tectonic compression zones, where deep over-pressured gas containing fluidized sediment ascend through highly permeable conduits, such as faults, fractures and diapirs (Hovland et al., 1997; Graue, 2000; Milkov, 2000; Dimitrov, 2002) form positive and/or negative seafloor structures (Foucher et al., 2010). Such diapir-formed submarine mud volcanoes are found on diapirs which are built by plate extension and subduction in the Sorokin Trough of the Black Sea (Krastel et al., 2003) where multiple mud volcanoes are aligned in a chain on the seafloor. Here the large diapirs are fed by the 4 – 5 km deep Oligocene to Lower Miocene Maikopian Formation (Krastel et al., 2003). The mud volcanoes also serve as conduits for gas seepage. The dominant gas methane forms greyish-white gas hydrate (or gas clathrate; Max, 2003) in the Sorokin Trough (Ginsburg et al., 1990; Limonov et al., 1994; Woodside et al., 1997; Bohrmann et al., 2003; Feseker et al., 2009) which lies within the gas hydrate stability zone (GHSZ: Bohrmann and Torres, 2006).

Two of these morphologically connected diapir-formed mud volcanoes, located at a water depth of <2,000 m, and separated (center to center) by ≃1,600 m, are the Dvurechenskii Mud Volcano (DMV; Bohrmann et al., 2003) and its more recently classified neighbor the Helgoland Mud Volcano (HMV, Bohrmann, 2011a) (see in Fig. 6-1). Since gas flares were first discovered above the DMV in 2002 (Shuyuhov et al., 2003), many research cruises have taken place (e.g. *R/V* METEOR M52/1, M72/2 and M73/3a, M84/2, and *R/V* MARIA S. MERIAN MSM15/2), making the DMV the most studied MV in the Sorokin Trough. Greinert et al. (2006) found that the DMV and the surrounding mud volcanoes had experience periods of activity and dormancy, which could be inferred from hydro-acoustic evidence of gas bubbles released from

the sediment into water column. Additional studies using ship-mounted instruments were the main methods for mapping the mud volcanoes. Ship-mounted multibeam bathymetry side-scan sonar data provided low resolution maps on the material and texture of the submarine mud volcano's surface sediments. Evidence of the thermal structure of the DMV shows high thermal gradients in the central summit area and relatively low thermal gradients at the margins (Feseker et al., 2009). The mud breccias recovered from both the DMV and HMV have high water content and high viscosity (Bohrmann et al., 2003; Feseker et al., 2009). Mud flows found at the DMV area, which show different backscatter strength on the backscatter map, are inferred to have been formed at different periods in time (Krastel et al., 2003). This low-resolution bathymetry constrained detailed investigations of, for example, surficial and shallow sub-surface tectonic signatures as seen in the sediments. As a result, during a more recent Cruise MSM15/2 (2010), high-resolution Autonomous Underwater Vehicle (AUV) micro-bathymetric maps and side-scan maps were produced for the HMV and DMV. The ship-mounted PARASOUND sub-bottom profiling of the DMV and HMV (in 2007, M72/3) was applied to allow for the interpretation of the faults and/or fractures in the sub-surface sediments of the seafloor surrounding the DMV.

The data showed that the DMV is a flat-topped pie-shaped, positive topographic seafloor structure. It is ≃1,000 m in diameter, ≃35 m height and can be divided into 3 topographic regions: I) the inner plateau and active center, II) the steep walled upper margin and the III) shallow sloped lower margin (Wu et al., [Chap. 5, this thesis]). In contrast the smaller HMV (≃1,200 m diameter, ≃20 m height) to the SE, is a negative, double-ringed, collapsed seafloor structure consisting of two annular depression (Inner Moat and Outer Moat), two annular positive reliefs (Inner Crest and Outer Crest) and one Active Center (Wu et al., [Chap. 4, this thesis]).

The down-sag formation process is widely accepted in the interpretation of development of circular geological depression structures (Branney, 1995; Acocella et al., 2000; Acocella, 2006). The formation of a moat around a submarine mud volcano can also be interpreted by this down-sag process (Wu et al., [Chap. 4, this thesis]). In addition, the presence of the frequent gas bubble release sites shows that faults and feeder channels facilitate mud eruptions (Capozzi and Picotti, 2002). When we combine these down-sag formation theories, a model for the development of the DMV

and HMV can be built and a correlation can be made to determine any formation relationships between the two neighboring mud volcanoes.

In this paper, three questions are raised and answered: I) What is the evidence for the down-sag faults of both the DMV and the HMV? II) Do the down-sag faults of the DMV and HMV influence each other's formation? and III) Where are the flare-releasing sites, and are they related to the presence and location of faults?

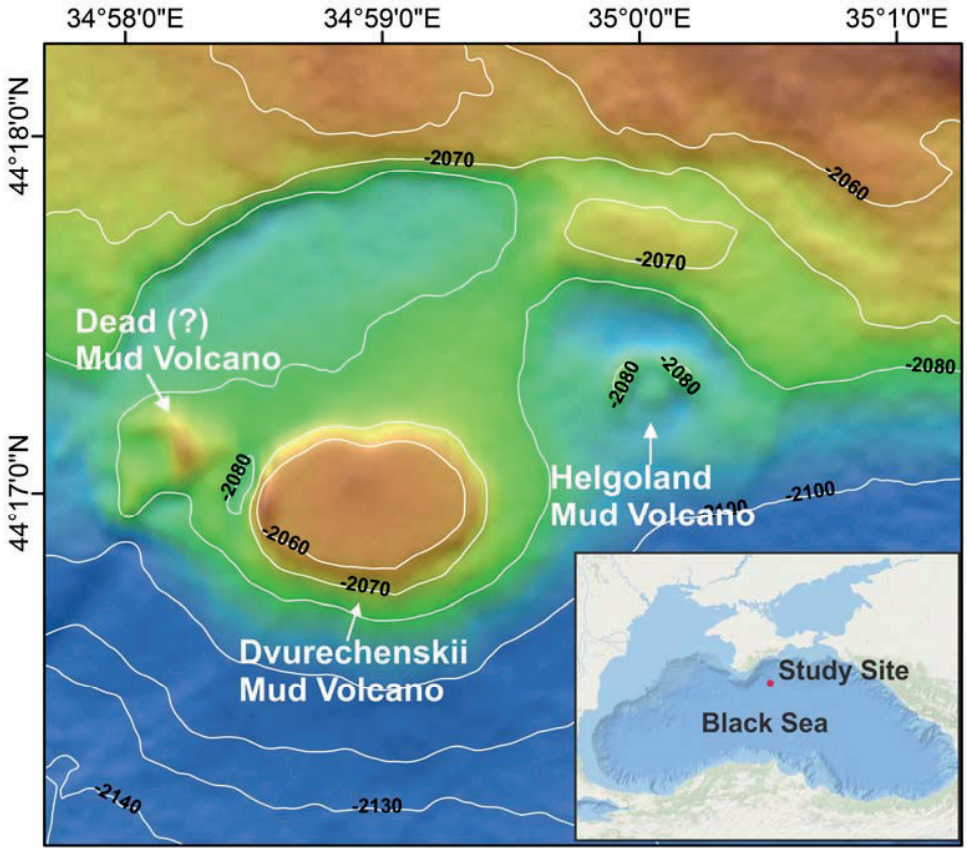

Figure 6-1: The Dvurechenskii Mud Volcano (DMV) and Helgoland Mud Volcano (HMV) are two neighboring marine mud volcanoes located in the Sorokin Trough at the northern margin of the Black Sea.

6.3 Methods

6.3.1 Ship-mounted Survey Techniques

The multibeam bathymetric data were obtained from the ship-mounted Konsberg Simrad EM122 multibeam echo sounder during the cruise M84/2. It consists of 432 beams. The main frequency is 12 kHz, and the coverage angle is up to 150°. The bathymetric data was then processed using the MB-system software (Caress and Chayes, 1996 and 2001) to produce a low resolution bathymetric map of the DMV, HMV and the dead (?) mud volcano (Fig. 6-1).

The sub-bottom profiling data was collected using the ship-mounted single beam echo sounder ATLAS PARASOUND P70 during the cruise M72/3 in 2007. The secondary low frequency of 4 kHz (Römer et al., 2014) was configured for sub-bottom profiling. Data processing was conducted using ATLAS PARASTORE software (El Naggar et al., 2007; Gerchow, 2009). The sub-bottom profiles for the DMV (Fig. 6-2, A, B and C) where produced to make a comparison with the sub-bottom profiles of the HMV (Fig. 6-2, D, E, and F, modified from Wu et al. [Chap. 4, this thesis]).

6.3.2 AUV-mounted Survey Techniques

The high-resolution multibeam survey was carried out at the DMV, during cruise MSM15/2 in 2010, using the MARUM AUV Seal 5000. The AUV was steered 40 m above the seafloor at a speed of 3 knots. This was required, in order to obtain the best performance of the AUV-mounted RESON MBES 7125B multibeam echo sounder (400 kHz). It was installed with an operating frequency of 400 kHz. The data was processed using the MB-system software (Caress and Chayes, 1996 and 2001) to acquire a high-resolution, micro-bathymetric map (Fig. 6-3-D, adapted from Wu et al. [Chp. 4, this thesis]). A high definition ridge map of the DMV's plateau was produced using the ArcGIS software package (Fig. 6-3-B) and is presented with the mudflows interpretation from the backscatter map of Wu et al. [Chp. 5, this thesis]).

The BENTHOS dual frequency (100/400 kHz) AUV-mounted side-scan sonar was able to record both the seafloor backscatter and the hydro-acoustic gas flares in the water column. The survey covered the DMV's plateau, margin and the surrounding seafloor area with the interval of 60 m for each track line.

High resolution backscatter maps with a definition of 1 m were produced using the MB-System software (Caress and Chayes, 1996 and 2001). These maps provided more detailed information on the structure and attributes of the mud volcanoes and on the surface sediments of surrounding seafloor, as shown in figure 6-3C and E. Figure

6-3-C was adapted from Wu et al. (Chp. 5, this thesis) and Figure 6-3-E was changed from Wu et al. (Chp. 4, this thesis) and were presented for a comparison with the DMV plateau's high definition ridge map.

The hydro-acoustic gas flares were distinguished based on the bubbles' resonance frequency (Greinert and Nützel, 2004). This was seen as high amplitude signals in the hydro-acoustic data of the unprocessed side-scan record (Fig. 6-4). The gas flares observed in the raw data were mainly concentrated in two areas: 1) at the central summit of the DMV's plateau and 2) on the western lower flanks of the DMV. The hydro-acoustic gas flare data was acquired using the CARIS HIPS and SIPS software package.

6.4 Results

6.4.1 Sub-Surface Interpreted faults from PARASOUND Sub-bottom Profiles

Two track lines across the DMV and HMV run in a north-south direction (Fig. 6-2C and Fig. 6-2F). The observed stratigraphic units found in the DMV are shown on the sub-bottom profiles and compared with the HMV units described in Wu et al. (Chap. 4, this thesis; Fig. 6-2A and D). The stratigraphic units mostly run parallel to the seafloor. The faults and fractures were identified from the short blocks in the horizontal units (see interpretation in Fig. 6-2B, and Fig. 6-2E). They are characterized by high-amplitude reflections (faults or fractures), which incline from the seafloor down into the deeper lying sedimentary units.

Four nearly equally spaced (≃600 - 800 m) normal faults were observed and interpreted from the sub-bottom profile across the HMV (Fig. 6-2E, Wu et al. [Chap. 4, this thesis]). One of these faults (labeled here as DSF4) occurs at the same location as an interpreted down-sag fault (DSF4) of the HMV, with distinct high backscatter that differs from the surrounding area (see Fig. 6-3F). Three similar normal faults/fractures were also seen in the sub-bottom profile across the DMV, and could also be located in an area of possible down-sag faults of the DMV. However, due to a lack of backscatter map profile coverage for the DMV, we are unable to confirm the observation in the sub-bottom profile.

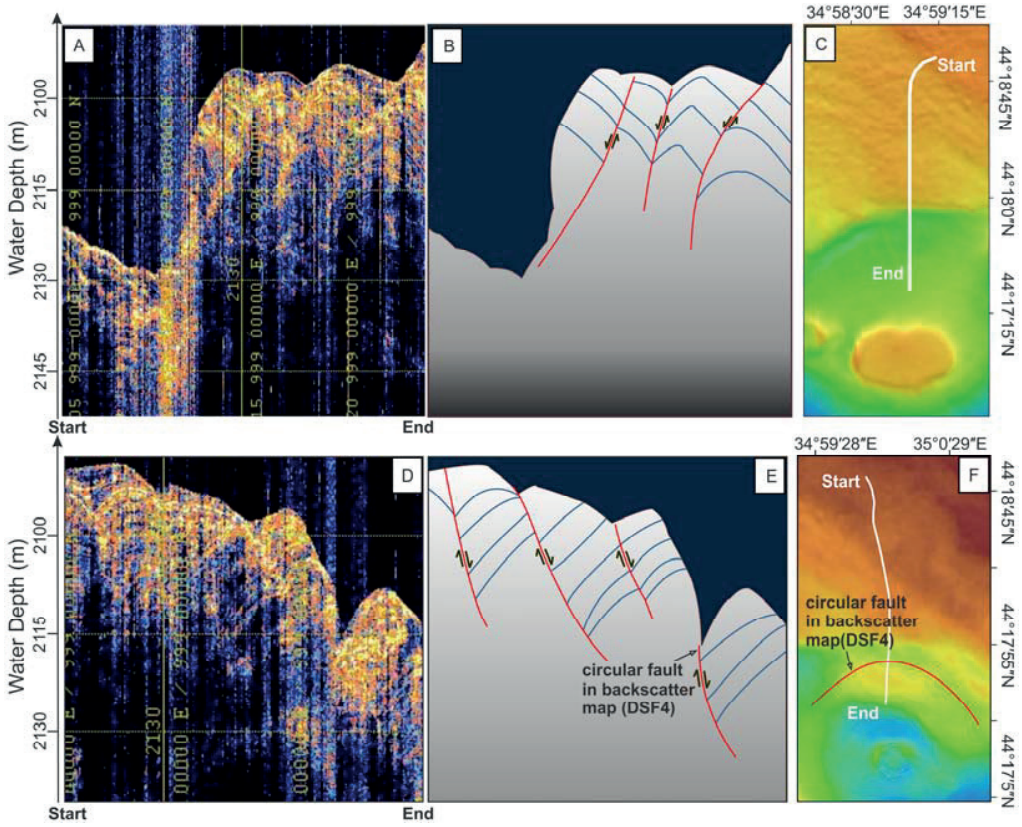

Figure 6-2: Ship-mounted Parasound sub-bottom profiles of the DMV and HMV and their interpretation profiles. The HMV profiles were taken from Wu et al. (Chap. 4, this thesis). A and D are sections of HMV and DMV sub-bottom profiles and B and C represent the interpreted fracture or faults of these profiles respectively. The white lines in C and E are the ship track during the recordings.

6.4.2 Micro-Bathymetry and Side-Scan Sonar Mosaic Map-Interpreted Faults

The morphological differences between the DMV and HMV are distinct (Fig. 6-1 and Fig. 6-3A) and include differences in their depth, shape, and size. Both of the mud volcanoes are located at >2,000 m water depth. However, the HMV is deepest, ≃15 m deeper than the DMV, and shows a lower elevation seafloor rise (Fig. 6-3A). The DMV and HMV vary in their topographic form. Whereas the DMV is a flat-topped pie-shaped, positive topographic seafloor structure, the HMV is both a negative and positive double concentric-ringed, collapsed seafloor structures consisting two moats and two crests, respectively.

Although there are many differences in the topographic structures of the DMV and the HMV, there are common aspects, too, such as faults cutting through and the circular moat structure around their main rises. On the bathymetric and backscatter maps of the HMV, some faults or fractures could be identified in the northeast corner (Fig. 6-3D and Fig. 6-3E). A circular moat structure was observed clearly around the

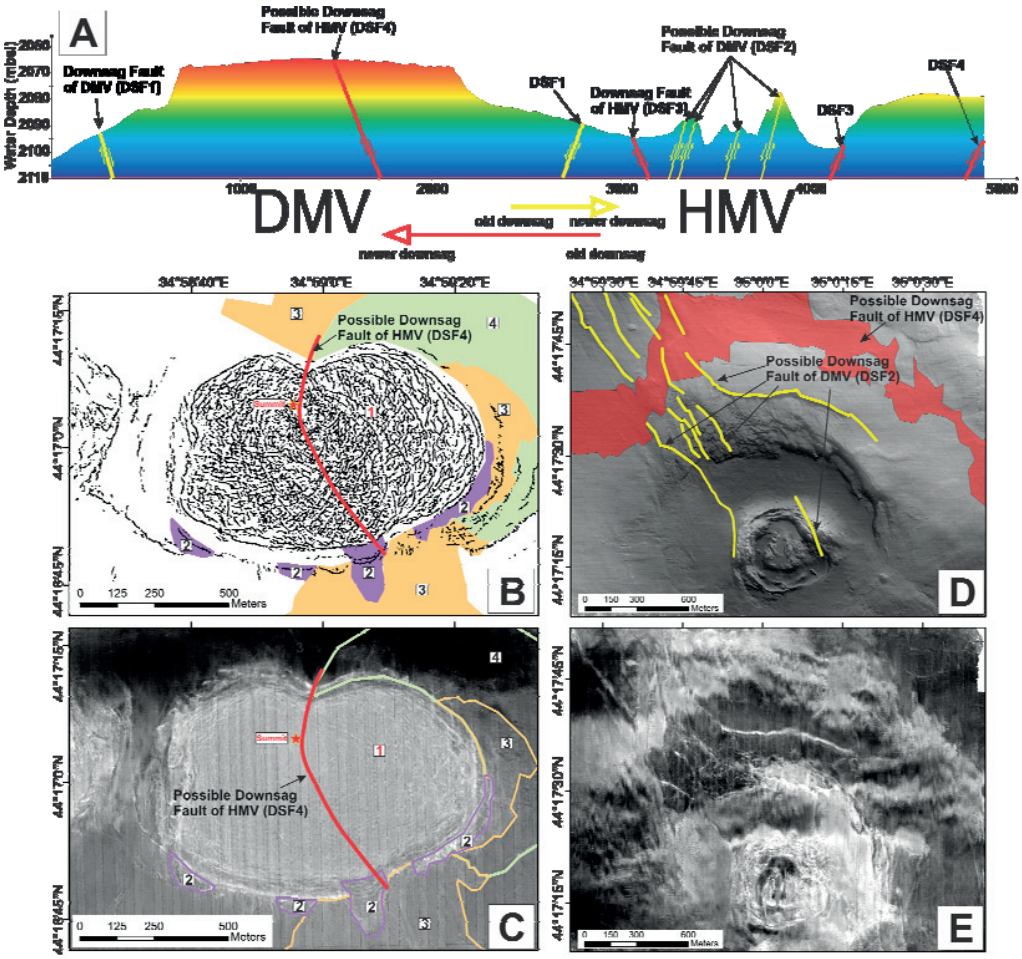

Figure 6-3: Interpreted faults of the DMV and HMV from bathymetry and backscatter maps and their possible inter-relationship through the presence and location of faults. In A, the red solid lines represent the downsag faults of the HMV; the yellow solid line shows the down-sag faults of the DMV. B shows the bathymetry calculated seafloor ridge map on the plateau of the DMV with the backscatter and bathymetry interpreted fault marked (red solid line) and backscatter based interpreted mud flows around it (colored blocks taken from Wu et al. [Chap. 5, this thesis]). C is the backscatter map of the DMV (modified from Wu et al. [Chap. 5, this thesis]). D shows the bathymetry map of the HMV with interpreted faults from both the bathymetry and backscatter map and E is the backscatter map of the HMV. Both are modified from Wu et al. (Chap. 4, this thesis).

HMV's central rise. This circular moat structure is also apparent on the bathymetry and backscatter maps of the DMV. However, the fault that is interpreted as crossing the DMV is calculated based on small surficial ridges on the plateau of the DMV. Most of the ridges on its surface are arc-shaped and radiate out from the central summit to the margins. The length of the ridges range from meters to hundreds meters, and they are symmetrically distributed along a line that is interpreted as a possible down-sag fault (DSF4: Fig. 6-3B). This fault was inferred from the mudflows on the backscatter map (Wu et al. [Chap. 5, this thesis]). The forming times of the numerous mudflows were conjectured to have occurred at different periods in time as indicated by the backscatter strength: High backscatter indicates an old mudflow, while low backscatter suggests new mudflow. The existence of the down-sag fault (DSF4) could further be proven based on the distribution and time of the mudflows, which occur at the DMV margin, where the fault extends to the surrounding seafloor.

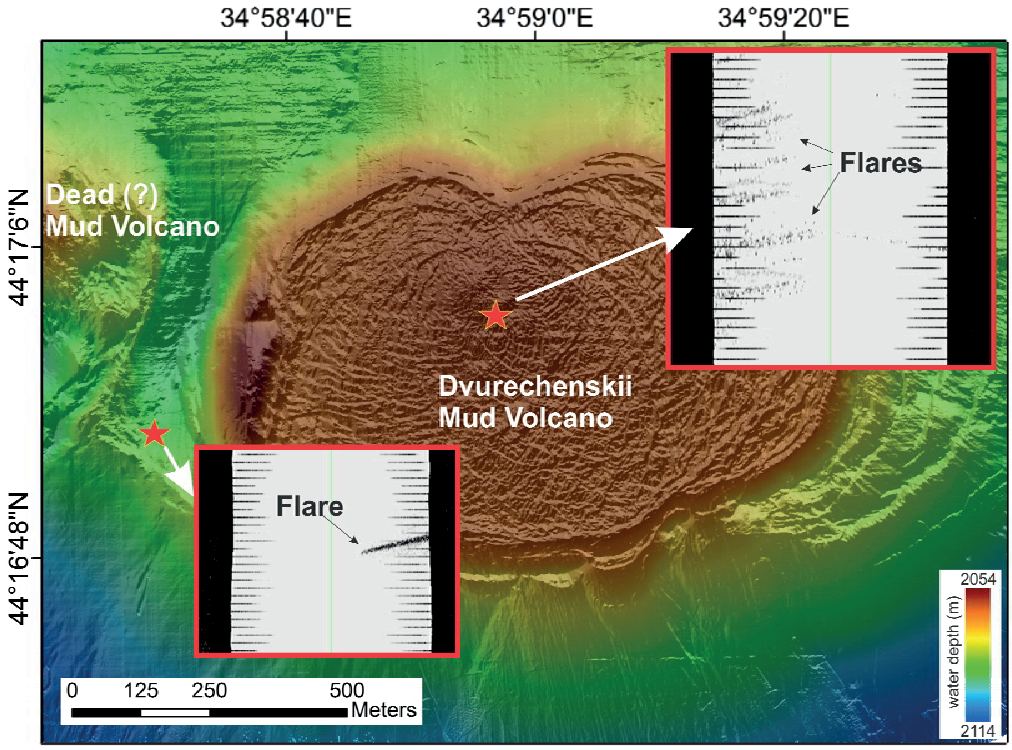

Figure 6-4: A 1 m resolution micro-bathymetry of the DMV with the location of side-scan sonar observed gas flares marked with red stars. The two inlay maps are raw side-scan sonar records depicting the gas flares in the water column above and close to the DMV.

6.4.3 Hydro-Acoustic Side-Scan Sonar Gas Flares and Their Locations

The gas bubble flares observed hydro-acoustically in the raw side-scan data were located at two sites in the DMV area: One site is located at the central summit, the most active area of the DMV. At this location, more than a dozen flares were identified (Fig. 6-4, right sub-figure). In addition, the backscatter signals of the gas flares were relatively weak, only appearing when adjusting the seafloor backscatter strength to be totally dark, which indicates that the DMV is in a moderately active period. The second gas flare site is located outside of the DMV. One single flare was shown in the side-scan sonar data; this single flare is located on the shallow sloped lower margin of the DMV between the plateau and its steep walled upper margin and, another topographic seafloor rise on the surrounding seafloor to the west. It is located ≃150 m away from the DMV's west edge. The DMV's marginal gas flare could be evidence for the possible inactivity of a small unidentified mud volcano located NW of the DMV (Fig. 6-4).

6.5 Discussion

6.5.1 Down-sag Faults of the Neighboring DMV and HMV

Previous research results have shown that the formation of a caldera is controlled by progressive subsidence (Evans et al., 2008). The caldera formation process can be divided into several specific stages. These stages from the down-sag model (Acocella, 2006) can be marked by distinctive structural features found in many calderas. This down-sag model can be applied to explain I) the architecture and development of calderas of magmatic volcanism (Park, 1990; Branney, 1995) or II) summit caldera depressions in mud volcanoes (Kopf, 2008). Evans et al. (2008) applied such a theory to the calderas at the summits of mud volcanoes, which are characterized by broad depressions with circular or elliptical outlines. He also suggests that the subsidence is caused by the loss of gas, fluids, and sediments during eruptions, followed by a phase of continued extrusive activity (Evans et al., 2008). In some mud volcanoes, a central raised area surrounded by a relatively deep moat, which in turn is enclosed by a circular rim, is also found. A series of normal faults, which dip towards the center of

the mud volcano, usually develop, underlying the rims of mud volcanoes (Kopf, 2008). This also corresponds to the subsidence caused by the release of mud and fluid. Sometimes, these rims are characterized by a gas emission sites (Planke et al., 2003) or biological markers (Marcon et al., 2014). As observed for HMV (Wu et al. [Chp.4, this thesis]), gas emission sites and bio-markers were not found at the margins of the DMV, however, the presence of down-sag faults has still been proven (see Fig. 5-4D and Fig. 5-1). The evidence for these down-sag faults is I) the circular-shaped high gradient seafloor collapse in the micro-bathymetric map as seen for example in the HMV in the Outer Moat and Outer Crest region (Wu et al. [Chap. 4, this thesis]), II) the high reflection signals in the sub-bottom profile data for the DMV and HMV represent fractures or faults as shown in figure 6-2, and III) the circular-shaped high backscatter area that forms the seafloor to the north of the HMV, which is a newly developed down-sag fault (defined here as DSF4) seen in the side-scan sonar map (Wu et al. [Chap. 4, this thesis]). Both the DMV and HMV are on top of a diapir (Krastel et al., 2003). The mud or gas fluid reservoir underneath them provides the mud volcano formation material through central conduits. After the material reaches the seafloor surface, mud volcano mounds form. With the continuing expulsion of mud breccia, the reservoir at depth depletes, and the central area of the mud volcano sinks and, eventually, collapses. A series of normal faults will then form around this central area of the mud volcanoes in response to the subsidence (Fig. 6-1 and Fig. 6-3A). The down-sag faults of the neighboring DMV and HMV, as evidence for subsidence, are shown to intersect (Fig. 6-3A).

6.5.2 The Activity and Morphology Linked to the Normal Faults and Possible Down-sag Faults

Mud volcanoes in some areas are aligned along active normal faults, because they allow surface leakage of fluids derived from deep sources e.g. >3 - 6 km (Capozzi and Picotti, 2002). As a result, methane seepages are often linked to faults, but the mud expulsion largely occurred during paroxysmal events, such as those triggering by earthquakes (Capozzi and Picotti, 2002). A mud volcano can only form with enough mud expulsion. As the main formation mechanism for both the DMV and HMV is diapiric (Krastel et al., 2003) this would produce enough mud expulsion. However, the DMV is probably located on a fault zone (Krastel et al., 2003), indicated by a characteristic reflection pattern shift in the seismic profile across the DMV, that

represents movement in the sub-surface sediment unit blocks. This suggests that the DMV activity is, at least partially affected by fault activity such as down-sag faulting.

One of the questions raised was: what is the relationship between the down-sag faults across the DMV and the HMV (Fig. 6-3) and the formation development of the mud volcanoes? In fact, a fault that runs across the DMV (DSF4) was inferred, based on the mud flows observed on the side-scan sonar map (Wu et al. [Chap. 5, this thesis]) and, the mud ridge patterns on the DMV's plateau surface from the processed micro-bathymetry map. Along the interpreted fault, ridges are symmetrically distributed and the observed new mudflows were found at the intersection of the fault and the edge of the DMV (Fig. 6-3 B and C; Wu et al. [Chap. 5, this thesis]). This suggests that the interpreted fault could affect the general morphology of the DMV. The HMV has more or less the same situation; a down-sag fault that we define as DSF2, is interpreted to +/- centrally cut across the HMV in a ≃NW-SE directions (Fig. 6-3 D and E), as observed in both the micro-bathymetric and side-scan sonar maps. Seafloor depressions were also found along this fault Wu et al. (Chap. 4, this thesis). Moreover, gas emissions and high abnormal water column temperatures were also observed along the fault (Wu et al. [Chap. 5, this thesis]). These findings suggest that the down-sag fault crossing the HMV has not only affected the morphology, but also affected the activity of the mud volcano. The evidence however, was not sufficient to prove that the faults across either the HMV or the DMV are deep rooted. Thus, we could not confirm that the fault (DSF4) crossing the DMV, is directly connected to the source reservoir in the Oligocene to Lower Miocene Maikopian Formation, 4 - 5 km deep. We conjecture therefore, that the mud volcanoes are affected by two formation mechanisms and are both diapiric and fault induced. Nonetheless, indubitably the faults impact the morphology and activity of the mud volcanoes and provide an escape pathway for over pressurized deep-source material and fluids (Medialdea et al., 2009).

6.5.3 A Fault-induced Inter-relationship Model for the DMV and HMV

Here, we suggest a hypothesis to explain the formation process of the two mud volcanoes based on compiled evidence in the micro-bathymetric, side-scan sonar and sub-bottom profile data and, most importantly, their mutual influence on one another.

A fault-induced inter-relationship model for the mud volcanoes, determined through the development of the down-sag faults, is shown in figure 6-5. The initial surfical activity of the DMV is shown in Step 1. The DSF1 is the down-sag fault (marked by light grey circles) of the DMV (Fig. 6-5, Step 2). The second developed down-sag fault (DSF2) of the DMV also crosses the HMV and controls and/or affects its activity (Fig. 6-5, Step 3). The DSF3 is the down-sag fault of the HMV (Fig. 6-5, Step 4), and the DSF4 of the HMV is thought to cross the DMV (Fig. 6-5, Step 5). Step 5 represents the present day situation as seen in figure 6-5-A.

Morphologically, the HMV is relatively concentric whereas, the DMV is oval-shaped with two kinks in the central region of the northern and southern margins, which are at the same location as the interpreted HMV-derived down-sag fault (DSF4). This suggests that the DSF4 affected the morphology of the DMV after its formation, yet affected the HMV during its formation. Furthermore, the double-ringed collapsed HMV is structurally more complex and smaller in size than the DMV. This could be caused by the mud volcanoes instablility, because it is still in the process of being formed. Both these new findings imply that the HMV could be a younger mud volcano than the DMV. This evidence supports the fault-induced inter-relationship model for the DMV and HMV described in figure 6-5. Formation of the older DMV (Fig. 6-5, Step 1) could have been initiated when a narrow-channeled conduit formed in response to northwest-southeast directional compression of the sub-surface diapir. After its initial erupted, the DMV was formed by the erupted mud breccias (Wu et al., Chap. 5, this thesis). The gas flares in the water column would have remained active during the mud eruption event.

The HMV experienced a similar formation process, after the initial formation of the DMV. In contrast however, the double-ringed structure of the HMV suggests that it underwent two periods of eruption and development (Wu et al. [Chap. 4, this thesis]). As the HMV is located at the down-sag fault region of the DMV (Greinert et al., 2006), one down-sag fault (DSF2) crosses the HMV (the red solid line shown in Step 3 of Fig. 6-5.). This fault and the compression from the thrusting belt may have initiated the active of the HMV and controlled its structural and morphological development. This down-sag fault (DSF2) became another channel for gas release in addition to the HMV's central conduit. After this gas release, as with the DMV, circular shaped down-sag faults (DSF3 and DSF4) formed around the HMV (Fig. 6-5,

Step 4 and 5). The down-sag fault DSF4 of the HMV then affected the continued development of the DMV.

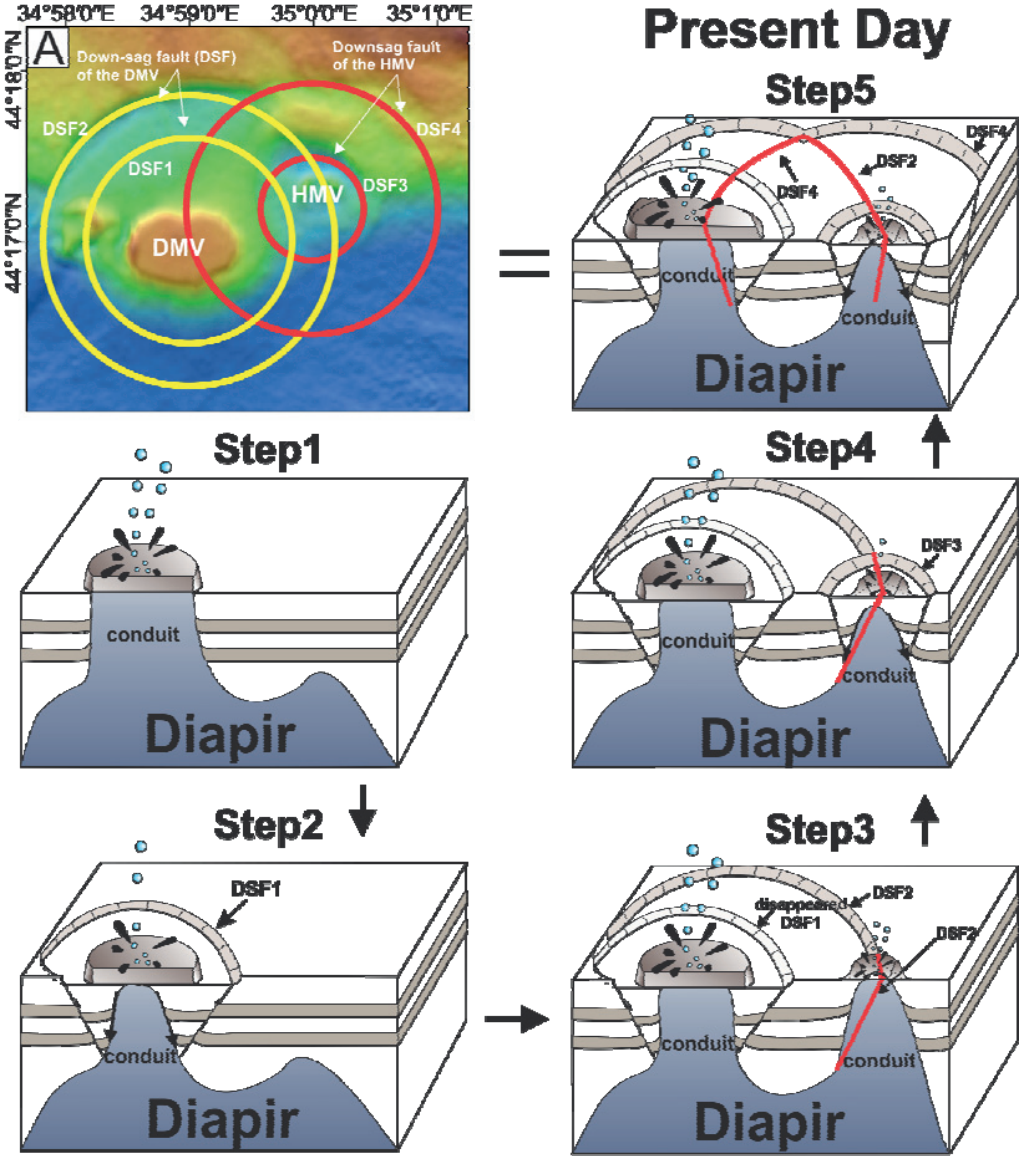

Figure 6-5: A shows a model of overlapping concentrical rings that represent down-sag faults of the DMV (yellow rings) and HMV (red rings). The fault-induced inter-relationship is clearly demonstrated for the neighboring mud volcanoes. The schematic diagrams indicated by Steps 1 to 5 represent the development of the DMV and HMV during the past. Step 5 shows the present day scenario as seen in figure 6-5A. Blue circular bubbles and mud splashes (black conical cones) represent the MV activity. The progressive growth and the rising of the uplift conduit with time, represents a mud eruption process that leads to the surficial manifestation of the HMV.

After this period of strong activity, the DMV entered a relatively stable dormant stage. The conduit activity declined, and a serious of circular shaped down-sag faults formed around the DMV, e.g. DSF1 and 2, figure 6-5, Step 2 and 3.

6.5.4 A Small Inactive (Possible Dead) Mud Volcano to the North-West of the DMV

Previous scientific research has shown that, when the overburden pressure of the top sediments is great enough, through gas hydrate formation and sediment loading, gas and mud are ardent to be released from the mud volcanoes margins. Once this process has been activated, the mud volcano will collapse (Stewart and Davies, 2006). Sometimes this is also marked by a biological marker such as the extinction of a biological micro-habitat on a mud volcano (Marcon et al., 2014). In the case of the DMV's development, this process seems to have occurred and is marked by a marginal rise- positive seafloor structure and gas flares in the water column. Two flares were observed on the DMV in June, 2002 (Greinert et al., 2006). One is at its center, and the other at its margin on a rise on the DMV's southwest edge (Fig. 6-4). Evidence for the morphological growth of this rise on the DMV's SW flank, is provided by markers in the sub-surface sediments: Layered bedding structures, as seen in the micro-bathymetry, are thought to represent sediment deposition events through mud eruptions at various times. The marginal location of the gas flare and sediment layers in the morphological rise, support the theory that suggests the migration of activity on mud volcanoes to their margins which occurs when certain environmental conditions prevail such as, the collapse of the mud volcanoes active center.

In close proximity to the rise and gas flare on the DMV's western margin, a positive seafloor structure located to the north-west could be observed on the micro-bathymetric map. Due to the AUV's seafloor coverage, this seafloor feature is only partially visible. However, from the ship-mounted multibeam echo sounder and PARASOUND data, which provide full coverage, no evidence for activity e.g. gas flares was observed. Together with evidence on its positive morphology and its geological location, we suggest that it is inactive (possibly dead). From our fault-induced inter-relationship model we developed for DMV and HMV, here we could interpret this inactive (dead?) mud volcano to have developed as a result of an old

down-sag fault of the DMV (DSF2). This also fits into the theory that the activity of gas and mud expulsion migrates to be release from the edge of a MV when the overburden pressure in the central area of a mud volcano stops its pathway, as seen for the DMV. This process would then allow for the formation of new mud volcanoes.

6.6 Conclusions

Through the analyses of high resolution surficial and sub-bottom profile data and, hydro-acoustic data it was possible to build I) a geological evolution model for the DMV and, II) a fault-induced inter-relationship model for the DMV and HMV.

1. Verification for the presence of down-sag faults is provided by evidence for I) micro-bathymetric scale circular-shaped high gradient seafloor collapse structure, II) high reflection signals of fault/fractures and, III) circular-shaped high backscatter structures manifested in the side-scan sonar map.

2. Documentation of a fault-induced inter-relationship between the DMV and HMV is corroborated by the presence of ≃NW-SE orientated normal faults across the DMV and HMV which form the surficial manifestation of down-sag faults that eminate from the neighboring mud volcano i.e. from the HMV and DMV, respectively.

3. Gas flare released sites were observed at the active centers of the mud volcanoes and/or on their respective margins. Their presence coincides with the geographical location of the mud volcanoes normal and down-sag faults. The margin-active gas flares could support the theory that the activity of gas and mud expulsion migrates to be released from the margins of mud volcanoes during their later developmental phase, when the overburden pressure in the central area stops gas and fluid discharge.

The evolutionary development stages of the neighboring mud volcanoes could therefore, explain their individual architecture and activity as well as their inter-dependence relationship.

6.7 Acknowledgements

We thank the captains and crews of *R/V* METEOR and *R/V* MARIA S. MERIAN for support during the Research Cruises M72/3 and M84/2 and MSM15/2. We also thank the ROV QUEST team from MARUM for handling the Remotely Operated Vehicle (ROV). The work was partly funded through the DGF - Research Center and the Cluster of Excellence "The Ocean in the Earth System" MARUM - Center for Environmental Sciences. Tingting Wu was sponsored by the China Scholarship Council (CSC).

Chapter 7 Conclusions and Outlook

7.1 Conclusions

In this thesis, I compiled data sets that included near-to-seafloor high resolution Autonomous Underwater Vehicle (AUV) micro-bathymetric and backscatter maps, Remotely Operated Vehicle (ROV) high definition (HD) seafloor imaging, *in-situ* sediment temperature data, and ship-mounted PARASOUND data for the DMV and HMV in the Sorokin Trough, the northern Black Sea. Based on these data sets, the activity and formation mechanisms of these two mud volcanoes and the interaction between them were discussed in Chapters 4 - 6. This chapter aims to summaries the main conclusions of the thesis set out in the three main questions proposed in the 'Main Objectives of This Study' in Chapter 1 (1.7).

What is the formation process of the HMV, and which factors control its activity?

The high-resolution micro-bathymetric map provides the opportunity to show the detailed structure of the seafloor morphology of the HMV; this cannot be achieved using ship-based multibeam. The HMV is a double-ring seafloor structure composed of two annular depressions, two annular positive reliefs, and one Active Center. Gas flares in the water column, imaged by the hydro-acoustic data of both the AUV and PARASOUND, indicate that the HMV was moderately active during the investigation. The high-resolution backscatter map shows different intensities, which are related to changes in the geology sedimentology. High backscatter represents the mud clasts, whereas low backscatter represents hemipelagic sediment. Based on the distribution of the high backscatter patches, the HMV was inferred to have experienced at least two eruption events, followed by seafloor subsidence and gravity-driven sediment movement from the northwest. The high water temperature values over the HMV indicate additional heat brought up to the surface through the upward migration of mud from a deep sub-surface source (diapir). In addition, the spatial trend for these high water temperature values which are aligned along a NW-SE running fault suggest that the fault is one of the control factors for the activity of the HMV. The disappearance of the (methane) gas emission flares ≃800 m above the HMV in the hydro-acoustic data infer that the HMV does not effect atmospheric methane concentrations and as a consequence, has very limited impact in global climate change.

What is the mud movement process of the DMV and its movement velocities, both vertically and horizontally?

A high-resolution micro-bathymetric map shows concentric ring structures developing out from the summit of the DMV. The ROV seafloor observations distinguished them as ≃dm-high ridges. These concentric ring structures and ridges are inferred to be the result of cyclic mud eruption events. The DMV is dominated by high backscatter, which has been classified to represent mud clasts that have migrated from the deep subsurface. At the DMV's margins, high backscatter patches of different intensities show gravity-driven flows at different times. The shallow sediment temperature gradient increases from the surrounding seafloor (0.032°C/m) to the DMV's plateau margin (0.336 - 0.468°C/m) and to the center (5.884°C/m) of the DMV. These high temperatures might represent cyclic eruptions of subsurface sediments and suggest that the DMV is experiencing a relatively active period. Based on *in-situ* high temperature anomaly data from the central conduit, vertical mud velocity in the feeder channel was inferred to be a maximum of 0.22 m/day. By using two simplified models, a horizontal mud velocity on the plateau of 0.19 - 0.22 m/day was estimated based on the 78 m-migration of a gravity corer over a time period of 1,166 days. By using the deduced mud velocities, the age of the DMV was estimated to be 22 - 26 years, based on a simplified model. However, these age estimates may be erroneous due to some factors were not integrated into the model. These include, mud consolidation, cyclic mud eruptions, and seafloor erosion via deep water currents.

How does the activity of the DMV and HMV affect each other's formation?

The high resolution micro-bathymetric and backscatter data show that both the DMV and HMV are surrounded by a circular subsidence. This seafloor subsidence is conjectured to result from internal mud volcano sediment loss after violent mud eruptions and is inferred to be down-sag faults. Our model shows that a fault-induced interrelationship exists between the DMV and HMV. This was confirmed by the presence of ≃north-south orientated normal faults across the surface of both the DMV and HMV. These faults are the surficial corroboration of down-sag faults eminating from the neighboring mud volcano i.e. from the HMV and DMV respectively. Furthermore, the affirmation from the hydro-acoustic data, that the gas flare release sites occur in the vicinity of faults, e.g. through the margin active gas flares, could support the theory that the activity of gas and mud eruption migrates to be released

from the margin of mud volcanoes when overburden pressure in the central areas stops gas and fluid discharge.

7.2 Outlook

The three case studies have shown on that the increasingly sophisticated remotely-operated deep-water instruments (such as AUVs and ROVs) improve the investigation possibilities of submarine mud volcanoes. The combination of high resolution micro-bathymetry, side-scan sonar mapping, high definition seafloor ground truth observations, and the *in-situ* analysis of water and sediment temperature data allows us to over carried out detailed research of mud volcanoes even in deep marine environments of over 2,000 m water depth. These studies provided new insights in analyzing I) the horizontal and vertical mud migration processes, II) mud volcano activity, III) the control factors and processes for mud volcano formation related to their activity, IV) and evaluating the inter-relationship of neighboring diapir- and fault-formed mud volcanoes and finally, V) and determining the affect of gas emissions such as methane, on the atmospheric methane concentrations and as a result climatic change.

The first manuscript (Chap. 4) geological evolution model for the HMV shows that its activity is fault controlled as well as a diapir-controlled. In previous research on mud volcanoes, scientists typically used ship-mounted, low-resolution seismic and bathymetric data and sonar observed gas flares, to investigate the relationship between the activity of mud volcanoes and the activity of faults. Our AUV and ROV water temperature and micro-bathymetric results show a more convenient way to analyze how faults can control the activity of the MVs. Because overall direct visual observations of the submarine mud volcanoes are difficult to obtain, the observation of overall seepages and their locations are also hard to come by. Water temperature values are therefore important markers for the activity of mud volcanoes and are good indicators for fault-induced MV actively. However, future of ROV data collection of the crossing normal faults needs to be carried out for the HMV and other MVs for comparison and validation of the method. The formation mechanism and formation process are inferred from hydro-acoustic data, temperature data, seafloor observation data, and previously established theories (e.g., the down-sag theory). Down-sag mostly explains the depressions of the crater, but the outside moat around the main elevation of the mud volcano still needs more concrete explanations in the future.

The second manuscript (Chap. 5) provides new mathematic methods to calculate the mud movement velocity, both vertically, inside the conduit and horizontally, on the surface of the DMV. These were based on deep sediment temperature data and long-term gravity-core mounted temperature logger observations, respectively. Although the mud movement process was already under investigation for both inland and offshore mud volcanoes, the methods in this thesis are new: and velocity can be calculated based on indirect observations. As a result, it is expected that, in the future, the calculated results could be proven from other methods; moreover, these mathematic methods could be improved and applied to other areas.

In the third manuscript (Chap. 6), a down-sag fault-induced inter-relationship model was built and applied to explain the formation process of the two mud volcanoes and how they affect each other. Although the circular-shaped high backscatter found around the HMV has been identified as a newly developed down-sag fault, and one of the normal faults was found on the sub-bottom profile at the same position. New evidence of this recently developed down-sag fault for the DMV is still required to substantiate our initial findings, because the area covered by the AUV was not big enough to date. In addition, more sub-surface data sets, such as sub-bottom profiles and seismic profiles are needed, so that the dip and strike of the fault can be clearly identified. The model outlined in the third manuscript (Chap. 6) is a developing one, so it is hoped that, in the future, new observations will provide more evidence to prove the current model.

Acknowledgements

First of all, I would like to express my sincere thanks to my supervisor, Prof. Dr. Gerhard Bohrmann, who gave me the opportunity to do my PhD research in his group at the Geoscience Department of the University of Bremen. He guided me to better understand the complex scientific issues and improved the quality of the manuscripts. He also gave me the opportunity to join a number of expeditions where I was able to improving my skill as a hydro-acoustic specialist and in other submarine exploration methods.

I greatly thank Dr. Heiko Sahling who helped me a lot with this work. The fruitful discussions and helpful suggestions from him was a great help. He critically reviewed the texts and figures in my manuscripts and gave me comments which greatly improved this work. I also would like to thank Dr. Tomas Feseker for his constructive comments and ideas that contributed to the manuscripts. He patiently explained to me how to process temperature data. I also greatly thank Dr. Rebecca Rendle-Bühring who guided me a lot in the structure and science of the manuscripts. Her critical reviews of the scientific text and figures, as well as her ideas, greatly improved the quality of the papers. Thanks also for the added support during the end phase of writing my PhD.

I special thank Paul Wintersteller and Christian dos Santos Ferreira who provided me enthusiastic technical help on processing hydro-acoustic data.

I thank Thomas Pape for his valuable suggestions and Yann Marcon for kindly providing his seafloor pictures of my research area. Miriam Römer I thank for introducing me to how to structure a manuscript when I started to write my first manuscript. I thank Jan-Hendrik Körber who patiently and kindly answered my ArcGIS questions. David Fischer and Patrizia Geprägs are thanked for always answering my questions with patience and kindness. I also thank Tobias Himmler, Michal Tomczyk, and Susan Mau who were always available to help and teach me lots about carbonates and geochemistry through presentations of their results. I would also like to thank Angelika Rinkel and Greta Ohling who always helped me with the official paper work and gave me good tips and suggestions to get through everyday life in Germany. I also thank the cruise crews of the *R/V* METEOR and *R/V* MARIA S. MERIAN for providing high quality data.

Acknowledgements

I thank all my friends for all the good time we spent together.

China Scholarship Council (CSC) and Ocean University of China I greatly thank for providing me with the scholarship to study in Germany. I thank my pre-supervisors Weigang Zhang and Sanzhong Li for their support and encouragement and my pre-teachers Jianxin Pei and Bing Xu for their unreserved trust and support.

I am grateful to my parents who support me in many aspects of my life and always encourage me with their infinite patience.

Finally, my very special thanks go to my husband Jiangong Wei for his company during my whole PhD work.

感谢中国国家留学基金管理委员会给我提供四年的奖学金让我能有机会在德国完成博士学业。感谢母校中国海洋大学，感谢张维冈、李三忠教授、裴建新老师和徐冰老师在我留学期间给我的支持和鼓励。

深深的感谢我的父母和亲人在我低谷的时候给我的鼓励支撑我继续向前，感谢他们无私的包容，谅解和支持。

最后，衷心感谢四年来一直陪伴和支持我的爱人尉建功。

References

Abegg, F., Hohnberg, H.-J., Pape, T., Bohrmann, G., and Freitag, J., 2008, Development and application of pressure-core-sampling systems for the investigation of gas-and gas-hydrate-bearing sediments: Deep Sea Research Part I: Oceanographic Research Papers, v. 55, p. 1590-1599.

Acocella, V., 2006, Caldera types: How end-members relate to evolutionary stages of collapse: Geophysical research letters, v. 33.

Acocella, V., Cifelli, F., and Funiciello, R., 2000, Analogue models of collapse calderas and resurgent domes: Journal of Volcanology and Geothermal Research, v. 104, p. 81-96.

Akhmanov, G.G., 1996, Lithology of mud breccia clasts from the Mediterranean Ridge: Marine Geology, v. 132, p. 151-164.

Ali-Zade, A., Shnyokov, E., Grigorianz, B., Aliev, A., and Rahmanov, R., 1984, Geotectonic conditions of mud volcano manifestation on the Earth and their significance for oil and gas prospects: Proc. 27th World Geol. Congr. C, v. 13, p. 166-172.

Allen, R.C., Gavish, E., Friedman, G.M., and Sanders, J.E., 1969, Aragonite-cemented sandstone from outer continental shelf off Delaware Bay: submarine lithification mechanism yields product resembling beachrock: Journal of Sedimentary Research, v. 39.

Arhangelski, A., 1932, Some words about genesis of mud volcanoes on the Apsheron peninsula and Kerch–Taman area: Bull. MOIP, Ser. Geol, v. 3, p. 269-285.

Artemov, Y.G., Egorov, V., Polikarpov, G., and Gulin, S., 2007, Methane emission to the hydro-and atmosphere by gas bubble streams in the Dnieper paleo-delta, the Black Sea.

Bagirov, E., Nadirov, R., and Lerche, I., 1996, Flaming eruptions and ejections from mud volcanoes in Azerbaijan: Statistical risk assessment from the historical records: Energy exploration & exploitation, v. 14, p. 535-583.

Barber, A., Tjokrosapoetro, S., and Charlton, T., 1986, Mud volcanoes, shale diapirs, wrench faults, and melanges in accretionary complexes, eastern Indonesia: AAPG Bulletin, v. 70, p. 1729-1741.

Bernard, B.B., Brooks, J.M., and Sackett, W.M., 1976, Natural gas seepage in the Gulf of Mexico: Earth and Planetary Science Letters, v. 31, p. 48-54.

Blinova, V., Ivanov, M., and Bohrmann, G., 2003, Hydrocarbon gases in deposits from mud volcanoes in the Sorokin Trough, north-eastern Black Sea: Geo-Marine Letters, v. 23, p. 250-257.

Blondel, P., 2009, The handbook of sidescan sonar, Springer.

Bohrmann, G., 2011a, R/V Maria S. Merian cruise report MSM15/2: Origin and structure of methane, gas hydrates and fluid flows in the Black Sea; MSM15, leg 2a and b, Istanbul-Piraeus, 10 May-02 June 2010, DFG-

Forschungszentrum MARUM, Universität Bremen.

Bohrmann, G., 2011b, R/V METEOR Cruise Report M84/2: Origin and Distribution of Methane and Methane Hydrates in the Black Sea: M84, Leg 2, Istanbul-Istanbul, 26 February-02 April, 2011, DFG-Forschungszentrum MARUM, Universität Bremen.

Bohrmann, G., Ivanov, M., Foucher, J.-P., Spiess, V., Bialas, J., Greinert, J., Weinrebe, W., Abegg, F., Aloisi, G., and Artemov, Y., 2003, Mud volcanoes and gas hydrates in the Black Sea: new data from Dvurechenskii and Odessa mud volcanoes: Geo-Marine Letters, v. 23, p. 239-249.

Bohrmann, G., and Pape, T., 2007, Cruise participants (2007) Report and preliminary results of R/V METEOR Cruise M72/3, Istanbul–Trabzon–Istanbul, 17 March–23 April, 2007. Marine gas hydrates of the Eastern Black Sea: Berichte, Fachbereich Geowissenschaften, Universität Bremen, p. 176.

Bohrmann, G., and Torres, M.E., 2006, Gas hydrates in marine sediments, Marine Geochemistry, Springer, p. 481-512.

Borowski, W.S., Paull, C.K., and Ussler, W., 1999, Global and local variations of interstitial sulfate gradients in deep-water, continental margin sediments: Sensitivity to underlying methane and gas hydrates: Marine Geology, v. 159, p. 131-154.

Branney, M.J., 1995, Downsag and extension at calderas: new perspectives on collapse geometries from ice-melt, mining, and volcanic subsidence: Bulletin of Volcanology, v. 57, p. 303-318.

Brooks, J., Kennicutt, M., Fay, R., McDonald, T., and Sassen, R., 1984, Thermogenic gas hydrates in the Gulf of Mexico: Science, v. 225, p. 409-411.

Brown, K.M., 1990, The nature and hydrogeologic significance of mud diapirs and diatremes for accretionary systems: Journal of Geophysical Research: Solid Earth (1978–2012), v. 95, p. 8969-8982.

Capozzi, R., and Picotti, V., 2002, Fluid migration and origin of a mud volcano in the Northern Apennines (Italy): the role of deeply rooted normal faults: Terra Nova, v. 14, p. 363-370.

Caress, D., and Chayes, D., 2001, Improved management of large swath mapping datasets in MB-System Version 5, AGU Fall Meeting Abstracts, Volume 1, p. 0373.

Caress, D.W., and Chayes, D.N., 1996, Improved processing of Hydrosweep DS multibeam data on the R/V Maurice Ewing: Marine Geophysical Researches, v. 18, p. 631-650.

Charlou, J., Donval, J., Fouquet, Y., Ondreas, H., Knoery, J., Cochonat, P., Levaché, D., Poirier, Y., Jean-Baptiste, P., and Fourré, E., 2004, Physical and chemical characterization of gas hydrates and associated methane plumes in the Congo–Angola Basin: Chemical Geology, v. 205, p. 405-425.

Cita, M.B., Ryan, W.F.B., and Paggi, L., 1981, Prometheus mud-breccia: An example of shale diapirism in the Western Mediterranean Ridge: Ann. Geol. Pays Hell.,

v. 30, p. 543– 570.

Claypool, G.E., and Kaplan, I., 1974, The origin and distribution of methane in marine sediments, Natural gases in marine sediments, Springer, p. 99-139.

Collett, T.S., 2002, Energy resource potential of natural gas hydrates: AAPG Bulletin, v. 86, p. 1971-1992.

Davidson, D., El-Defrawy, M., Fuglem, M., and Judge, A., 1978, Natural gas hydrates in northern Canada.

Davies, R.J., Brumm, M., Manga, M., Rubiandini, R., Swarbrick, R., and Tingay, M., 2008, The East Java mud volcano (2006 to present): An earthquake or drilling trigger?: Earth and Planetary Science Letters, v. 272, p. 627-638.

De Angelis, M., Lilley, M., and Baross, J., 1993, Methane oxidation in deep-sea hydrothermal plumes of the Endeavour Segment of the Juan de Fuca Ridge: Deep Sea Research Part I: Oceanographic Research Papers, v. 40, p. 1169-1186.

De Beukelaer, S., MacDonald, I., Guinnasso Jr, N., and Murray, J., 2003, Distinct side-scan sonar, RADARSAT SAR, and acoustic profiler signatures of gas and oil seeps on the Gulf of Mexico slope: Geo-Marine Letters, v. 23, p. 177-186.

De Lange, G.J., and Brumsack, H., 1998, Pore-water indications for the occurrence of gas hydrates in eastern Mediterranean mud dom structures

Degens, E.T., and Ross, D.A., 1972, Chronology of the Black Sea over the last 25,000 years: Chemical Geology, v. 10, p. 1-16.

Delisle, G., Von Rad, U., Andruleit, H., Von Daniels, C., Tabrez, A., and Inam, A., 2002, Active mud volcanoes on-and offshore eastern Makran, Pakistan: International Journal of Earth Sciences, v. 91, p. 93-110.

Deville, E., Battani, A., Griboulard, R., Guerlais, S., Herbin, J., Houzay, J., Muller, C., and Prinzhofer, A., 2003, The origin and processes of mud volcanism: new insights from Trinidad: Geological Society, London, Special Publications, v. 216, p. 475-490.

Deville, E., and Guerlais, S.-H., 2009, Cyclic activity of mud volcanoes: evidences from Trinidad (SE Caribbean): Marine and Petroleum Geology, v. 26, p. 1681-1691.

Dickens, G.R., 2004, Global change: Hydrocarbon-driven warming: Nature, v. 429, p. 513-515.

Dickens, G.R., Castillo, M.M., and Walker, J.C., 1997, A blast of gas in the latest Paleocene: Simulating first-order effects of massive dissociation of oceanic methane hydrate: Geology, v. 25, p. 259-262.

Dickens, G.R., and Quinby-Hunt, M.S., 1994, Methane hydrate stability in seawater: Geophysical Research Letters, v. 21, p. 2115-2118.

Dimitrov, L.I., 2002, Mud volcanoes—the most important pathway for degassing deeply buried sediments: Earth-Science Reviews, v. 59, p. 49-76.

Dimitrov, L.I., 2003, Mud volcanoes—a significant source of atmospheric methane: Geo-Marine Letters, v. 23, p. 155-161.

Dupré, S., Buffet, G., Mascle, J., Foucher, J.-P., Gauger, S., Boetius, A., Marfia, C., Team, A.A., and Team, Q.R., 2008, High-resolution mapping of large gas emitting mud volcanoes on the Egyptian continental margin (Nile Deep Sea Fan) by AUV surveys: Marine Geophysical Researches, v. 29, p. 275-290.

El Naggar, S.E.D., Dieckmann, G., Haas, C., Schröder, M., and Spindler, M., 2007, The Expeditions ANTARKTIS-XXII/1 and XII/2 of the Research Vessel" Polarstern" in 2004/2005: Berichte zur Polar-und Meeresforschung (Reports on Polar and Marine Research), v. 551.

Etiope, G., Caracausi, A., Favara, R., Italiano, F., and Baciu, C., 2002, Methane emission from the mud volcanoes of Sicily (Italy): Geophysical Research Letters, v. 29, p. 56-1-56-4.

Evans, R.J., Stewart, S.A., and Davies, R.J., 2008, The structure and formation of mud volcano summit calderas: Journal of the Geological Society, v. 165, p. 769-780.

Feseker, T., Boetius, A., Wenzhöfer, F., Blandin, J., Olu, K., Yoerger, D.R., Camilli, R., German, C.R., and De Beer, D., 2014, Eruption of a deep-sea mud volcano triggers rapid sediment movement: Nature communications, v. 5.

Feseker, T., Foucher, J.-P., and Harmegnies, F., 2008, Fluid flow or mud eruptions? Sediment temperature distributions on Håkon Mosby mud volcano, SW Barents Sea slope: Marine Geology, v. 247, p. 194-207.

Feseker, T., Pape, T., Wallmann, K., Klapp, S., Schmidt-Schierhorn, F., and Bohrmann, G., 2009, The thermal structure of the Dvurechenskii mud volcano and its implications for gas hydrate stability and eruption dynamics: Marine and Petroleum Geology, v. 26, p. 1812-1823.

Flecker, R., and Kopf, A., 1996, Data report: Clast and grain-size analysis of sediment recovered from the Napoli and Milano mud volcanoes, eastern Mediterranean, Proceedings of the Ocean Drilling Program. Initial reports, Volume 160, Ocean Drilling Program, p. 529-532.

Foucher, J.-P., Dupré, S., Scalabrin, C., Feseker, T., Harmegnies, F., and Nouzé, H., 2010, Changes in seabed morphology, mud temperature and free gas venting at the Håkon Mosby mud volcano, offshore northern Norway, over the time period 2003 - 2006: Geo-Marine Letters, v. 30, p. 157-167.

Friedman, G.M., Sanders, J.E., Gavish, E., and Allen, R.C., 1971, Marine lithification mechanism yields rock resembling beachrock: Carbonate Cements, Johns Hopkins University, Studies in Geology, p. 50-53.

Gerchow, P., 2009, PARASOUND-AWI-PANGAEA Data Storage and Management Version 1.1: Polarstern. 8.2009 ANT-XXV/5., v. 24.

Ginsburg, G., Guseynov, R., Dadashev, A., Ivanova, G., Kazantsev, S., Solov'yev, V., Telepnev, E., Askeri-Nasirov, R.Y., Yesikov, A., and Mal'tseva, V., 1992, Gas hydrates of the southern Caspian: International Geology Review, v. 34, p. 765-782.

Ginsburg, G., Kremlev, A., Grigor'ev, M., Larkin, G., Pavlenkin, A., and Saltykova, N., 1990, Filtrogenic gas hydrates in the Black Sea: Soviet Geology and

Geophysics, v. 31, p. 8-16.

Ginsburg, G., Milkov, A., Soloviev, V., Egorov, A., Cherkashev, G., Vogt, P., Crane, K., Lorenson, T., and Khutorskoy, M., 1999, Gas hydrate accumulation at the Haakon Mosby mud volcano: Geo-Marine Letters, v. 19, p. 57-67.

Ginsburg, G., and Soloviev, V., 1994, Mud volcano gas hydrates in the Caspian Sea: Bulletin of the Geological Society of Denmark, v. 41, p. 100.

Ginsburg, G., Soloviev, V., Cranston, R., Lorenson, T., and Kvenvolden, K., 1993, Gas hydrates from the continental slope, offshore Sakhalin Island, Okhotsk Sea: Geo-Marine Letters, v. 13, p. 41-48.

Görür, N., 1988, Timing of opening of the Black Sea basin: Tectonophysics, v. 147, p. 247-262.

Graue, K., 2000, Mud volcanoes in deepwater Nigeria: Marine and Petroleum Geology, v. 17, p. 959-974.

Greinert, J., Artemov, Y., Egorov, V., De Batist, M., and McGinnis, D., 2006, 1300-m-high rising bubbles from mud volcanoes at 2080m in the Black Sea: Hydroacoustic characteristics and temporal variability: Earth and Planetary Science Letters, v. 244, p. 1-15.

Greinert, J., and Nützel, B., 2004, Hydroacoustic experiments to establish a method for the determination of methane bubble fluxes at cold seeps: Geo-Marine Letters, v. 24, p. 75-85.

Gubkin, I., and Feodorov, S., 1940, Mud volcanoes of the USSR in connection with oil and gas prospects: Proc 27th Int Geology Congr, Moscow, part, v. 4, p. 33-67.

Guliyev, I., Feizullayev, A., Jevanshir, R.D., and Akademiĭasy, A.j.E., 1996, All about mud volcanoes, Geology Institute, Azerbaijan Academy of Sciences.

Hedberg, H.D., 1974, Relation of methane generation to undercompacted shales, shale diapirs, and mud volcanoes: AAPG Bulletin, v. 58, p. 661-673.

Heeschen, K.U., Tréhu, A.M., Collier, R.W., Suess, E., and Rehder, G., 2003, Distribution and height of methane bubble plumes on the Cascadia Margin characterized by acoustic imaging: Geophysical Research Letters, v. 30.

Higgins, G., and Saunders, J.B., 1974, Mud volcanoes: their nature and origin, publisher not identified.

Holland, C.W., Etiope, G., Milkov, A.V., Michelozzi, E., and Favali, P., 2003, Mud volcanoes discovered offshore Sicily: Marine Geology, v. 199, p. 1-6.

Hovland, M., Hill, A., and Stokes, D., 1997, The structure and geomorphology of the Dashgil mud volcano, Azerbaijan: Geomorphology, v. 21, p. 1-15.

Humphrey, W.E., 1963, Sedimentary volcanism in eastern Mexico and northern Colombia: Geological Society of America Bulletin, v. 74, p. 125-128.

Huseynov, D.A., and Guliyev, I.S., 2004, Mud volcanic natural phenomena in the South Caspian Basin: geology, fluid dynamics and environmental impact: Environmental Geology, v. 46, p. 1012-1023.

Ivanov, M., Limonov, A., and Van Weering, T.C., 1996, Comparative characteristics of

the Black Sea and Mediterranean Ridge mud volcanoes: Marine geology, v. 132, p. 253-271.

Ivanov, M., Limonov, A., and Woodside, J., 1998, Extensive deep fluid flux through the sea floor on the Crimean continental margin (Black Sea): Geological Society, London, Special Publications, v. 137, p. 195-213.

Ivanov, M., Pimenov, N., Rusanov, I., and Lein, A.Y., 2002, Microbial processes of the methane cycle at the north-western shelf of the Black Sea: Estuarine, Coastal and Shelf Science, v. 54, p. 589-599.

Jackson, M., and Vendeville, B., 1994, Regional extension as a geologic trigger for diapirism: Geological society of America bulletin, v. 106, p. 57-73.

Johnsen, S., and Sosik, H., 2004, Shedding light on light in the ocean: Oceanus Magazine, v. 43, p. 1-5.

Judd, A., 2005, Gas emissions from mud volcanoes, Mud Volcanoes, Geodynamics and Seismicity, Springer, p. 147-157.

Judd, A., Hovland, M., Dimitrov, L., Garcia Gil, S., and Jukes, V., 2002, The geological methane budget at continental margins and its influence on climate change: Geofluids, v. 2, p. 109-126.

Kessler, J., Reeburgh, W., Southon, J., Seifert, R., Michaelis, W., and Tyler, S., 2006, Basin-wide estimates of the input of methane from seeps and clathrates to the Black Sea: Earth and Planetary Science Letters, v. 243, p. 366-375.

Kideys, A.E., 2002, Fall and rise of the Black Sea ecosystem: Science, v. 297, p. 1482-1484.

Klaucke, I., Sahling, H., Weinrebe, W., Blinova, V., Bürk, D., Lursmanashvili, N., and Bohrmann, G., 2006, Acoustic investigation of cold seeps offshore Georgia, eastern Black Sea: Marine Geology, v. 231, p. 51-67.

Kopf, A., 1999, Fate of sediment during plate convergence at the Mediterranean Ridge accretionary complex: Volume balance of mud extrusion versus subduction and/or accretion: Geology, v. 27, p. 87-90.

Kopf, A., Klaeschen, D., and Mascle, J., 2001, Extreme efficiency of mud volcanism in dewatering accretionary prisms: Earth and Planetary Science Letters, v. 189, p. 295-313.

Kopf, A., Robertson, A., Clennell, M., and Flecker, R., 1998, Mechanisms of mud extrusion on the Mediterranean Ridge Accretionary Complex: Geo-Marine Letters, v. 18, p. 97-114.

Kopf, A.J., 2002, Significance of mud volcanism: Reviews of Geophysics, v. 40, p. 2-1-2-52.

Kopf, A.J., 2003, Global methane emission through mud volcanoes and its past and present impact on the Earth's climate: International Journal of Earth Sciences, v. 92, p. 806-816.

Kopf, A.J., 2008, Volcanoes: making calderas from mud: Nature Geoscience, v. 1, p. 500-501.

Korotaev, G., Oguz, T., Nikiforov, A., and Koblinsky, C., 2003, Seasonal, interannual,

and mesoscale variability of the Black Sea upper layer circulation derived from altimeter data: Journal of Geophysical Research: Oceans (1978-2012), v. 108.

Krastel, S., Spiess, V., Ivanov, M., Weinrebe, W., Bohrmann, G., Shashkin, P., and Heidersdorf, F., 2003, Acoustic investigations of mud volcanoes in the Sorokin Trough, Black Sea: Geo-Marine Letters, v. 23, p. 230-238.

Kvenvolden, K.A., 1985, Gas hydrate of the Middle American Trench deep sea drilling project leg 841.

Kvenvolden, K.A., 1993, Gas hydrates as a potential energy resource-a review of their methane content: United States Geological Survey, Professional Paper;(United States), v. 1570.

Kvenvolden, K.A., 1995, A review of the geochemistry of methane in natural gas hydrate: Organic Geochemistry, v. 23, p. 997-1008.

Kvenvolden, K.A., 2002, Methane hydrate in the global organic carbon cycle: Terra Nova, v. 14, p. 302-306.

Kvenvolden, K.A., and Lorenson, T.D., 2001, The global occurrence of natural gas hydrate, Wiley Online Library.

Lance, S., Henry, P., Le Pichon, X., Lallemant, S., Chamley, H., Rostek, F., Faugères, J.-C., Gonthier, E., and Olu, K., 1998, Submersible study of mud volcanoes seaward of the Barbados accretionary wedge: sedimentology, structure and rheology: Marine Geology, v. 145, p. 255-292.

Lashof, D.A., and Ahuja, D.R., 1990, Relative contributions of greenhouse gas emissions to global warming.

Leifer, I., and Patro, R.K., 2002, The bubble mechanism for methane transport from the shallow sea bed to the surface: A review and sensitivity study: Continental Shelf Research, v. 22, p. 2409-2428.

Letouzey, J., Biju-Duval, B., Dorkel, A., Gonnard, R., Kristchev, K., Montadert, L., and Sungurlu, O., 1977, The Black Sea: a marginal basin; geophysical and geological data, International Symposium on the Structural History of the Mediterranean Basins, Editions Technip Paris, p. 363-376.

Limonov, A., Van Weering, T.C., Kenyon, N., Ivanov, M., and Meisner, L., 1997, Seabed morphology and gas venting in the Black Sea mudvolcano area: observations with the MAK-1 deep-tow sidescan sonar and bottom profiler: Marine Geology, v. 137, p. 121-136.

Limonov, A., Woodside, J., Cita, M., and Ivanov, M., 1996, The Mediterranean Ridge and related mud diapirism: a background: Marine Geology, v. 132, p. 7-19.

Limonov, A., Woodside, J., and Ivanov, M., 1994, Mud Volcanism in the Mediterranean and Black Seas and Shallow Structure of the Eratosthenes Seamount: Initial Results of the Geological and Geophysical Investigations During the Third UNESCO-ESF" Training-through-Research" Cruise of RV Gelendzhik (June-July 1993).

Lu, H., Seo, Y.-t., Lee, J.-w., Moudrakovski, I., Ripmeester, J.A., Chapman, N.R.,

Coffin, R.B., Gardner, G., and Pohlman, J., 2007, Complex gas hydrate from the Cascadia margin: Nature, v. 445, p. 303-306.

Lüdmann, T., Wong, H.K., Konerding, P., Zillmer, M., Petersen, J., and Flüh, E., 2004, Heat flow and quantity of methane deduced from a gas hydrate field in the vicinity of the Dnieper Canyon, northwestern Black Sea: Geo-Marine Letters, v. 24, p. 182-193.

MacDonald, I., Leifer, I., Sassen, R., Stine, P., Mitchell, R., and Guinasso, N., 2002, Transfer of hydrocarbons from natural seeps to the water column and atmosphere: Geofluids, v. 2, p. 95-107.

MacDonald, I.R., Buthman, D.B., Sager, W.W., Peccini, M.B., and Guinasso, N.L., 2000, Pulsed oil discharge from a mud volcano: Geology, v. 28, p. 907-910.

MacDonald, I.R., Sager, W.W., and Peccini, M.B., 2003, Gas hydrate and chemosynthetic biota in mounded bathymetry at mid-slope hydrocarbon seeps: Northern Gulf of Mexico: Marine Geology, v. 198, p. 133-158.

Manga, M., Brumm, M., and Rudolph, M.L., 2009, Earthquake triggering of mud volcanoes: Marine and Petroleum Geology, v. 26, p. 1785-1798.

Marcon, Y., 2014, LAPMv2: An improved tool for underwater large-area photo-mosaicking, Oceans-St. John's, 2014, IEEE, p. 1-10.

Marcon, Y., Ondréas, H., Sahling, H., Bohrmann, G., and Olu, K., 2014, Fluid flow regimes and growth of a giant pockmark: Geology, v. 42, p. 63-66.

Marcon, Y., Sahling, H., and Bohrmann, G., 2013, LAPM: a tool for underwater Large-Area Photo-Mosaicking: Geoscientific Instrumentation, Methods and Data Systems Discussions, v. 3, p. 127-156.

Martin, J.B., Kastner, M., Henry, P., Le Pichon, X., and Lallement, S., 1996, Chemical and isotopic evidence for sources of fluids in a mud volcano field seaward of the Barbados accretionary wedge: Journal of Geophysical Research: Solid Earth (1978–2012), v. 101, p. 20325-20345.

Martinelli, G., and Judd, A., 2004, Mud volcanoes of Italy: Geological Journal, v. 39, p. 49-61.

Martinelli, G., and Panahi, B., 2006, Mud Volcanoes, Geodynamics and Seismicity: Proceedings of the NATO Advanced Research Workshop on Mud Volcanism, Geodynamics and Seismicity, Baku, Azerbaijan, from 20 to 22 May 2003, Springer Science & Business Media.

Max, M.D., 2003, Natural gas hydrate in oceanic and permafrost environments, Springer.

Mazurenko, L., Soloviev, V., Belenkaya, I., Ivanov, M., and Pinheiro, L., 2002, Mud volcano gas hydrates in the Gulf of Cadiz: Terra Nova, v. 14, p. 321-329.

Mazzini, A., Poludetkina, E., Mehrabi, B., Krueger, M., Inguaggiato, S., and Etiope, G., 2014, Mud Volcanism in the South East Caspian, Gorgon Plane, Iran, AGU Fall Meeting Abstracts, Volume 1, p. 1118.

McGinnis, D.F., Greinert, J., Artemov, Y., Beaubien, S., and Wüest, A., 2006, Fate of rising methane bubbles in stratified waters: How much methane reaches the

atmosphere?: Journal of Geophysical Research: Oceans (1978–2012), v. 111.

Medialdea, T., Somoza, L., Pinheiro, L.M., Fernández-Puga, M., Vázquez, J., León, R., Ivanov, M., Magalhaes, V., Díaz-del-Río, V., and Vegas, R., 2009, Tectonics and mud volcano development in the Gulf of Cádiz: Marine Geology, v. 261, p. 48-63.

Mellors, R., Kilb, D., Aliyev, A., Gasanov, A., and Yetirmishli, G., 2007, Correlations between earthquakes and large mud volcano eruptions: Journal of Geophysical Research: Solid Earth (1978–2012), v. 112.

Milkov, A., 2000, Worldwide distribution of submarine mud volcanoes and associated gas hydrates: Marine Geology, v. 167, p. 29-42.

Milkov, A.V., and Etiope, G., 2005, Global methane emission through mud volcanoes and its past and present impact on the the Earth's climate: International Journal of Earth Sciences, v. 94, p. 490-492.

Milkov, A.V., Sassen, R., Apanasovich, T.V., and Dadashev, F.G., 2003, Global gas flux from mud volcanoes: a significant source of fossil methane in the atmosphere and the ocean: Geophysical Research Letters, v. 30.

Mottl, M., 1992, Pore waters from serpentinite seamounts in the Mariana and Izu-Bonin forearcs, Leg 125: Evidence for volatiles from the subducting slab, Proc. Ocean Drill. Program Sci. Results, Volume 125, p. 373-385.

Motyka, R.J., Poreda, R.J., and Jeffrey, A.W., 1989, Geochemistry, isotopic composition, and origin of fluids emanating from mud volcanoes in the Copper River basin, Alaska: Geochimica et Cosmochimica Acta, v. 53, p. 29-41.

Naudts, L., Greinert, J., Artemov, Y., Staelens, P., Poort, J., Van Rensbergen, P., and De Batist, M., 2006, Geological and morphological setting of 2778 methane seeps in the Dnepr paleo-delta, northwestern Black Sea: Marine Geology, v. 227, p. 177-199.

Neurauter, T., and Roberts, H., 1994, Three generations of mud volcanoes on the Louisiana continental slope: Geo-Marine Letters, v. 14, p. 120-125.

Nikishin, A.M., Korotaev, M.V., Ershov, A.V., and Brunet, M.-F., 2003, The Black Sea basin: tectonic history and Neogene–Quaternary rapid subsidence modelling: Sedimentary Geology, v. 156, p. 149-168.

Nikolovska, A., Sahling, H., and Bohrmann, G., 2008, Hydroacoustic methodology for detection, localization, and quantification of gas bubbles rising from the seafloor at gas seeps from the eastern Black Sea: Geochemistry, Geophysics, Geosystems, v. 9.

Oguz, T., Malanotte-Rizzoli, P., and Aubrey, D., 1995, Wind and thermohaline circulation of the Black Sea driven by yearly mean climatological forcing: Journal of Geophysical Research: Oceans (1978-2012), v. 100, p. 6845-6863.

Okay, A.I., Şengör, A.C., and Görür, N., 1994, Kinematic history of the opening of the Black Sea and its effect on the surrounding regions: Geology, v. 22, p. 267-270.

Olu, K., Lance, S., Sibuet, M., Henry, P., Fiala-Médioni, A., and Dinet, A., 1997, Cold

seep communities as indicators of fluid expulsion patterns through mud volcanoes seaward of the Barbados accretionary prism: Deep Sea Research Part I: Oceanographic Research Papers, v. 44, p. 811-841.

Olu, K., Sibuet, M., Harmegnies, F., Foucher, J.-P., and Fiala-Medioni, A., 1996, Spatial distribution of diverse cold seep communities living on various diapiric structures of the southern Barbados prism: Progress in Oceanography, v. 38, p. 347-376.

Özsoy, E., and Ünlüata, Ü., 1997, Oceanography of the Black Sea: a review of some recent results: Earth-Science Reviews, v. 42, p. 231-272.

Paine, W.R., 1968, Recent peat diapirs in the Netherlands: A comparison with Gulf Coast salt structures.

Pape, T., Bahr, A., Rethemeyer, J., Kessler, J.D., Sahling, H., Hinrichs, K.-U., Klapp, S.A., Reeburgh, W.S., and Bohrmann, G., 2010a, Molecular and isotopic partitioning of low-molecular-weight hydrocarbons during migration and gas hydrate precipitation in deposits of a high-flux seepage site: Chemical Geology, v. 269, p. 350-363.

Pape, T., Blumenberg, M., Seifert, R., Bohrmann, G., and Michaelis, W., 2008, Marine methane biogeochemistry of the Black Sea: a review, Links Between Geological Processes, Microbial Activities&Evolution of Life, Springer, p. 281-311.

Pape, T., Feseker, T., Kasten, S., Fischer, D., and Bohrmann, G., 2011, Distribution and abundance of gas hydrates in near-surface deposits of the Håkon Mosby Mud Volcano, SW Barents Sea: Geochemistry, Geophysics, Geosystems, v. 12.

Pape, T., Geprägs, P., Hammerschmidt, S., Wintersteller, P., Wei, J., Fleischmann, T., Bohrmann, G., and Kopf, A.J., 2014, Hydrocarbon seepage and its sources at mud volcanoes of the Kumano forearc basin, Nankai Trough subduction zone: Geochemistry, Geophysics, Geosystems, v. 15, p. 2180-2194.

Pape, T., Kasten, S., Zabel, M., Bahr, A., Abegg, F., Hohnberg, H.-J., and Bohrmann, G., 2010b, Gas hydrates in shallow deposits of the Amsterdam mud volcano, Anaximander Mountains, Northeastern Mediterranean Sea: Geo-Marine Letters, v. 30, p. 187-206.

Park, K.H., 1990, A downsag caldera associated with the Chisulryoung Volcanic Formation, near Kyeongju city, southern Korea: Journal of the Geological Society of Korea, v. 26, p. 213-226.

Paull, C.K., Ussle, W., and Borowski, W.S., 1994, Sources of Biogenic Methane to Form Marine Gas Hydrates In Situ Production or Upward Migration? a: Annals of the New York Academy of Sciences, v. 715, p. 392-409.

Pérez-Belzuz, F., Alonso, B., and Ercilla, G., 1997, History of mud diapirism and trigger mechanisms in the Western Alboran Sea: Tectonophysics, v. 282, p. 399-422.

Planke, S., Svensen, H., Hovland, M., Banks, D., and Jamtveit, B., 2003, Mud and fluid migration in active mud volcanoes in Azerbaijan: Geo-Marine Letters, v.

23, p. 258-268.

Prior, D.B., Doyle, E.H., and Kaluza, M.J., 1989, Evidence for sediment eruption on deep sea floor, Gulf of Mexico: Science, v. 243, p. 517-519.

Rehder, G., Brewer, P.W., Peltzer, E.T., and Friederich, G., 2002, Enhanced lifetime of methane bubble streams within the deep ocean: Geophysical research letters, v. 29, p. 21-1-21-4.

Reilinger, R., McClusky, S., Souter, B., Hamburger, M., Prilepin, M., Mishin, A., Guseva, T., and Balassanian, S., 1997, Preliminary estimates of plate convergence in the Caucasus collision zone from global positioning system measurements: Geophysical Research Letters, v. 24, p. 1815-1818.

Rhakmanov, R., 1987, Mud volcanoes and their importance in forecasting of subsurface petroleum potential: Nedra, Moscow.

Ridd, M., 1970, Mud volcanoes in New Zealand: AAPG Bulletin, v. 54, p. 601-616.

Robertson, A., 1996, Mud volcanism on the Mediterranean Ridge: Initial results of Ocean Drilling Program Leg 160: Geology, v. 24, p. 239-242.

Robertson, A., and Dixon, J., 1984, Introduction: aspects of the geological evolution of the Eastern Mediterranean: Geological Society, London, Special Publications, v. 17, p. 1-74.

Robertson, A.H., and Kopf, A., 1998, Origin of clasts and matrix within the Milano and Napoli mud volcanoes, Mediterranean Ridge accretionary complex: Proceedings of the Ocean Drilling Program, Scientific Results, Vol. 160; Chapter 45.

Römer, M., Sahling, H., Pape, T., dos Santos Ferreira, C., Wenzhöfer, F., Boetius, A., and Bohrmann, G., 2014, Methane fluxes and carbonate deposits at a cold seep area of the Central Nile Deep Sea Fan, Eastern Mediterranean Sea: Marine Geology, v. 347, p. 27-42.

Ross, D.A., and Degens, E.T., 1974, Recent sediments of Black Sea: IN: THE BLACK SEA--GEOLOGY, CHEMISTRY, AND BIOLOGY.

Ross, D.A., Degens, E.T., and MacIlvaine, J., 1970, Black Sea: recent sedimentary history: Science, v. 170, p. 163-165.

Sahling, H., Bohrmann, G., Artemov, Y.G., Bahr, A., Brüning, M., Klapp, S.A., Klaucke, I., Kozlova, E., Nikolovska, A., and Pape, T., 2009, Vodyanitskii mud volcano, Sorokin trough, Black Sea: geological characterization and quantification of gas bubble streams: Marine and Petroleum Geology, v. 26, p. 1799-1811.

Sassen, R., and MacDonald, I.R., 1994, Evidence of structure H hydrate, Gulf of Mexico continental slope: Organic Geochemistry, v. 22, p. 1029-1032.

Sauter, E.J., Muyakshin, S.I., Charlou, J.-L., Schlüter, M., Boetius, A., Jerosch, K., Damm, E., Foucher, J.-P., and Klages, M., 2006, Methane discharge from a deep-sea submarine mud volcano into the upper water column by gas hydrate-coated methane bubbles: Earth and Planetary Science Letters, v. 243, p. 354-365.

Ser, M.E.P., 1996, Symbiosis between methane-oxidizing bacteria and a deep-sea carnivorous cladorhizid sponge.

Shakirov, R., Obzhirov, A., Suess, E., Salyuk, A., and Biebow, N., 2004, Mud volcanoes and gas vents in the Okhotsk Sea area: Geo-Marine Letters, v. 24, p. 140-149.

Shih, T., 1967, A survey of the active mud volcanoes in Taiwan and a study of their types and the character of the mud: Petrol. Geol. Taiwan, v. 5, p. 259-311.

Sirik, I., 1968, Oil and gas potential of the eastern slopes of the Western Sakhalin Mountain, Nauka, Moscow.

Slack, J.F., Turner, R.J., and Ware, P.L., 1998, Boron-rich mud volcanoes of the Black Sea region: Modern analogues to ancient sea-floor tourmalinites associated with Sullivan-type Pb-Zn deposits?: Geology, v. 26, p. 439-442.

Sloan, E., 1998, Physical/chemical properties of gas hydrates and application to world margin stability and climatic change: Geological Society, London, Special Publications, v. 137, p. 31-50.

Sloan, E.D., 2003, Fundamental principles and applications of natural gas hydrates: Nature, v. 426, p. 353-363.

Sloan Jr, E.D., and Koh, C., 2007, Clathrate hydrates of natural gases, CRC press.

Slope, L.C., 1998, Delineation of a Massive Seafloor Hydrocarbon Seep, Overpressured Aquifer Sands, and Shallow Gas Reservoirs, Louisiana Continental Slope, Proceedings-Offshore Technology Conference, Volume 1, Offshore Technology Conference., p. 37.

Söderberg, P., and Flodén, T., 1991, Pockmark developments along a deep crustal structure in the northern Stockholm Archipelago, Baltic Sea: Beiträge zur Meereskunde, v. 62, p. 79-102.

Söderberg, P., and Flodén, T., 1992, Gas seepages, gas eruptions and degassing structures in the seafloor along the Strömma tectonic lineament in the crystalline Stockholm Archipelago, east Sweden: Continental Shelf Research, v. 12, p. 1157-1171.

Somoza, L., Leon, R., Ivanov, M., Fernández-Puga, M., Gardner, J., Hernández-Molina, Pinheiro, L., Rodero, J., Lobato, A., and Maestro, A., 2003, Seabed morphology and hydrocarbon seepage in the Gulf of Cadiz mud volcano area: Acoustic imagery, multibeam and ultra-high resolution seismic data: Marine Geology, v. 195, p. 153-176.

Stewart, S.A., and Davies, R.J., 2006, Structure and emplacement of mud volcano systems in the South Caspian Basin: AAPG bulletin, v. 90, p. 771-786.

Suess, E., Torres, M., Bohrmann, G., Collier, R., Rickert, D., Goldfinger, C., Linke, P., Heuser, A., Sahling, H., and Heeschen, K., 2001, Sea floor methane hydrates at Hydrate Ridge, Cascadia margin: Natural gas hydrates: occurrence, distribution, and detection, p. 87-98.

Suess, E., and Whiticar, M., 1989, Methane-derived CO 2 in pore fluids expelled from the Oregon subduction zone: Palaeogeography, Palaeoclimatology,

Palaeoecology, v. 71, p. 119-136.

Sultan, N., Voisset, M., Marsset, T., Vernant, A.-M., Cauquil, E., Colliat, J., and Curinier, V., 2007, Detection of free gas and gas hydrate based on 3D seismic data and cone penetration testing: An example from the Nigerian Continental Slope: Marine Geology, v. 240, p. 235-255.

Takahashi, H., Yonezawa, T., and Takedomi, Y., 2001, Exploration for natural hydrate in Nankai-Trough wells offshore Japan, Offshore Technology Conference, Offshore Technology Conference.

Talley, L.D., Pickard, G.L., Emery, W.J., and Swift, J.H., 2011, Descriptive physical oceanography: an introduction, Academic press.

Talukder, A.R., Bialas, J., Klaeschen, D., Bürk, D., Brückmann, W., Reston, T., and Breitzke, M., 2007, High-resolution, deep tow, multichannel seismic and sidescan sonar survey of the submarine mounds and associated BSR off Nicaragua pacific margin: Marine Geology, v. 241, p. 33-43.

Tingay, M., Heidbach, O., Davies, R., and Swarbrick, R., 2008, Triggering of the Lusi mud eruption: Earthquake versus drilling initiation: Geology, v. 36, p. 639-642.

Tinivella, U., and Giustiniani, M., 2012, An overview of mud volcanoes associated to gas hydrate system, INTECH Open Access Publisher.

Tomkeieff, S.I., Walton, E.K., Randall, B., Battey, M., and Tomkeieff, O., 1983, Dictionary of petrology.

Tsunogai, U., Maegawa, K., Sato, S., Komatsu, D.D., Nakagawa, F., Toki, T., and Ashi, J., 2012, Coseimic massive methane release from a submarine mud volcano: Earth and Planetary Science Letters, v. 341, p. 79-85.

Tugolesov, D., Gorshkov, A., Meisner, L., Solov'ev, V., and Khakhalev, E., 1985, Tectonics of Mesozoic-Cenozoic deposits of the Black Sea basin: Nedra, Moscow, p. 215.

Van Rensbergen, P., Depreiter, D., Pannemans, B., Moerkerke, G., Van Rooij, D., Marsset, B., Akhmanov, G., Blinova, V., Ivanov, M., and Rachidi, M., 2005, The El Arraiche mud volcano field at the Moroccan Atlantic slope, Gulf of Cadiz: Marine Geology, v. 219, p. 1-17.

Veloso, M., Greinert, J., Mienert, J., and De Batist, M., 2015, A new methodology for quantifying bubble flow rates in deep water using splitbeam echosounders: Examples from the Arctic offshore NW-Svalbard: Limnology and Oceanography: Methods, p. n/a-n/a.

Vogt, P., Cherkashev, G., Ginsburg, G., Ivanov, G., Milkov, A., Crane, K., Sundvor, A., Pimenov, N., and Egorov, A., 1997, Haakon Mosby mud volcano provides unusual example of venting: EOS, Transactions American Geophysical Union, v. 78, p. 549-557.

Volgin, A.V., and Woodside, J.M., 1996, Sidescan sonar images of mud volcanoes from the Mediterranean Ridge: possible causes of variations in backscatter intensity: Marine Geology, v. 132, p. 39-53.

Wallmann, K., Drews, M., Aloisi, G., and Bohrmann, G., 2006, Methane discharge

into the Black Sea and the global ocean via fluid flow through submarine mud volcanoes: Earth and Planetary Science Letters, v. 248, p. 545-560.

Wei, J., Pape, T., Sultan, N., Colliat, J.-L., Himmler, T., Ruffine, L., De Prunelé, A., Dennielou, B., Garziglia, S., and Marsset, T., 2015, Gas hydrate distributions in sediments of pockmarks from the Nigerian margin-Results and interpretation from shallow drilling: Marine and Petroleum Geology, v. 59, p. 359-370.

White, D.E., 1955, Violent mud-volcano eruption of Lake City hot springs, northeastern California: Geological Society of America Bulletin, v. 66, p. 1109-1130.

Whiticar, M.J., 1999, Carbon and hydrogen isotope systematics of bacterial formation and oxidation of methane: Chemical Geology, v. 161, p. 291-314.

Williams, P., Pigram, C., and Dow, D., 1984, Melange production and the importance of shale diapirism in accretionary terrains.

Woodside, J., Ivanov, M., and Limonov, A., 1997, Neotectonics and fluid flow through seafloor sediments in the Eastern Mediterranean and Black Seas(preliminary results of geological and geophysical investigations during the ANAXIPROBE/TTR-6 cruise of R/V Gelendzhik, July-August 1996. Part I, Eastern Mediterranean Sea): Série technique- Unesco, Commission océanographique intergouvernementale.

Woodside, J., Ivanov, M., and Limonov, A., 1998, Shallow gas and gas hydrates in the Anaximander Mountains region, eastern Mediterranean Sea: Geological Society, London, Special Publications, v. 137, p. 177-193.

Yakubov, A., Ali-Zade, A., and Zeinalov, M., 1971, Mud volcanoes of the Azerbaijan SSR: Atlas: Azerbaijan Academy of Sciences, Baku.

Yang, T.F., Yeh, G.-H., Fu, C.-C., Wang, C.-C., Lan, T.-F., Lee, H.-F., Chen, C.-H., Walia, V., and Sung, Q.-C., 2004, Composition and exhalation flux of gases from mud volcanoes in Taiwan: Environmental Geology, v. 46, p. 1003-1011.

Yassir, N., 2003, The role of shear stress in mobilizing deep-seated mud volcanoes: geological and geomechanical evidence from Trinidad and Taiwan: Geological Society, London, Special Publications, v. 216, p. 461-474.

Zatsepina, O.Y., and Buffett, B.A., 1997, Phase equilibrium of gas hydrate: implications for the formation of hydrate in the deep sea floor: Geophysical Research Letters, v. 24, p. 1567-1570.

Zillmer, M., Flueh, E.R., and Petersen, J., 2005, Seismic investigation of a bottom simulating reflector and quantification of gas hydrate in the Black Sea: Geophysical Journal International, v. 161, p. 662-678.

Name: Tingting Wu
Datum : 2015-07-24
Anschrift : Luisental 29A 4-206, 28359, Bremen

Erklärung

Erklärung gemäß § 6 Abs. 5 der Promotionsordnung der Universität Bremen für die mathematischen, natur- und ingenieurwissenschaftlichen Fachbereiche. Hiermit versichere ich, dass ich

1. die vorliegende Arbeit ohne unerlaubte fremde Hilfe angefertigt habe,
2. keine anderen als die von mir angegebenen Quellen und Hilfsmittel benutzt habe,
3. die den benutzen Werken wörtlich oder inhaltlich entnommenen Stellen als solche kenntlich gemacht habe.

_____, den_____

_____
(Unterschrift)